Università degli Studi di Ferrara

DOCTORAL COURSE IN
EARTH AND MARINE SCIENCE

CYCLE XXXVII

COORDINATOR Prof. Paolo Ciavola

Quantitative Mineralogy: Sorting and Recycling of Construction and Demolition Waste

Scientific/Disciplinary Sector (SDS) GEO/06

Candidate
Dott. Bisciotti Andrea

_____
(signature)

Supervisor
Prof. Cruciani Giuseppe

_____
(signature)

Year 2021/2024

Table of contents

Abstract

Every year, nearly 700 million tons of construction and demolition waste (CDW) are generated globally from end-of-life buildings, representing approximately 30% of all global solid waste. As most residential areas and infrastructure in Western countries were constructed during the mid-20st century, the volume of CDW produced is expected to soar in the upcoming decades. Additionally, the construction of new buildings, following deconstruction of the old ones, demands vast quantities of nonrenewable mineral resources and is linked to significant CO_2 emissions. This doctoral thesis explores key topics aimed at driving the circular transition within this sector, facilitating the safe and efficient reuse of CDW in the development of more sustainable buildings. The circular pathway for CDW begins with the formal cessation of its waste classification, enabling its reintroduction as secondary raw material after undergoing recycling treatments. In line with the new Italian End-of-Waste regulation (D.M. n. 127/2024), legal threshold values have been established to determine whether CDW, following leaching tests, is potentially harmful or safe for reuse. To enhance and accelerate this protocol, a novel machine learning approach has been developed, allowing for the prediction of leachate concentrations based directly on CDW bulk chemical composition. Nowadays, most recycled aggregates (RAs) from CDW are used as sub-bases and bases for pavements/roads and highways. While the expansion of road infrastructure is slowing, concrete remains the second most consumed material globally, following only drinking water. The lack of adoption of RAs in high-grade applications (i.e., structural concrete) comes from the composite nature and the high heterogeneity of these secondary raw materials, which result in uneven interactions with cementitious binders. Indeed, RAs are typically affected by the presence of leftover attached mortar (AM) clinging to their surface. This characteristic is considered the primary obstacle preventing the use of RAs in new structural high-grade concrete. Thus, utilizing a novel mineralogical model based on X-ray Powder Diffraction (XRPD), the volume of AM has been reconstructed. These data are then combined with image analysis performed on a large dataset of CDW samples. To overcome the bottleneck associated with image processing, we further incorporate a deep learning model to automate the determination of the mortar volume, which enables high-throughput screening of CDW in real production. The model shows an impressive 90% recall rate in correctly distinguishing clean RAs from those with a considerable amount of superficial AM. This result shows that a portion of high-quality secondary raw materials can be extracted from the CDW stream using an optical-based sorting plant that employs artificial intelligence. Furthermore, the detrimental effects associated with the presence of AM were also investigated at the microscale level using lab-based X-ray computed tomography, along with optical and scanning electron microscopy. The observed decline trend in

various concrete properties with increasing AM content highlights the importance of monitoring this critical parameter and demonstrates the practicality of adopting the proposed XRPD-based approach for testing RAs. In conclusion, this doctoral thesis explores essential aspects of CDW circularity, spanning from the initial End-of-Waste declaration to the latest advancements in sorting technologies and optimal reuse practices. The objective is to promote CDW upcycling by integrating conventional laboratory techniques with innovative machine learning approaches, ultimately presenting scalable solutions to drive innovation in the construction and building materials industries.

Glossary

AM: Attached Mortar
CDW: Construction and Demolition Waste
EC: European Commission
EU: European Union
IC: Ion chromatography
ICP-MS: Inductive Coupled Plasma Mass Spectroscopy
Micro-CT: X-ray computed microtomography
NAs: Natural Aggregates
QPA: Quantitative Phase Analysis
RAs: Recycled Aggregates
SCMs: Supplementary Cementitious Materials
QPA: Quantitative Phase Analysis
XRPD: X-ray Powder Diffraction
XRF: X-ray Fluorescence

Cement chemistry notation

C: CaO (lime)
S: SiO_2 (silica)
H: H2O (water)
A: Al_2O_3 (alumina)
F: Fe_2O_3 (ferric oxide)
S: SO_3 (sulfate)
C_3S: Tricalcium Silicate (alite)
C_2S: Dicalcium Silicate (belite)
C_3A: Tricalcium Aluminate (aluminate)
C_4AF: Calcium Aluminoferrite (ferrite)
C-S-H: Calcium Silicate Hydrate
CH: Calcium Hydroxide (Porlandite)

1. Introduction

1.1. Building materials: life cycle and socio-environmental impacts

Globally, the building and construction sector represents the single most important source of human natural resource consumption (Caro et al., 2024). After drinkable water, concrete is the most used material worldwide, with three tons used annually per person on earth (Gagg, 2014). This production has experienced great popularity across the world due to its low cost and ease of use. Concrete represents a relatively cheap, performant and durable material which production employs large amounts of sand and gravel, cement and steel rebars. Especially the latter two man-made materials are strongly linked with CO_2 emissions (Chaturvedi & Ochsendorf, 2004), the greenhouse gas contributing most to the climate change. In 2022, the buildings and construction sector accounted for about 37% of global energy and process-related CO_2 emissions, translating to nearly 10 Gtons of CO_2 annually (UNEP, 2024). Due to high demand and consumption in concrete make up, cement production generates significant CO_2 emissions, coming from two key production aspects: (1) burning fossil fuels to operate high-temperature kilns (0.4 ± 0.2 kg CO_2/kg cement), and (2) mineral-derived CO_2 emissions from lime-stone decarbonation (0.25 ± 0.1 kg CO_2/kg cement), also known as calcination, where the limestone, which is the primary raw material for cement production, is converted from $CaCO_3$ to $CaO + CO_2$ (Van Roijen et al., 2024).
Nowadays, although there are alternative supplementary cementitious materials (SCMs) (Ndahirwa et al., 2022) the superior hydraulic property of Ordinary Portland cement, together with its historical reliability, gives this material an advantage over other binding products. It is important to highlight that Ordinary Portland cement has been used in construction for more than 200 years (Blezard, 1998) whereas SCMs are relatively novel. Nevertheless, combined use of SCMs and Ordinary Portland cement represents one of the most viable strategies to reduce building materials CO_2 footprint. SCMs are soluble siliceous, alumino-siliceous, or calcium alumino-siliceous powders with latent or active hydraulic behavior comparable to Ordinary Portland cement (Juenger et al., 2019). However, it is important to note that the global supply of SCMs may decrease in the future if net-zero emission pathways are followed (Brinkman & Miller, 2021). This expectation stems from the fact that these are industrial by-products, such as coal fly ash and granulated blast furnace slag, from high-emission industries like coal and steel production, which are expected to be limited in the upcoming years. The European Union (EU) has established the European Green Deal aiming to achieve zero carbon emissions (carbon neutrality) by 2050 and

decoupling economic growth from resource utilization. A similar strategy was also enacted by the Chinese government, which stated that carbon neutrality will be attained by 2060. The change in supply availability may necessitate the use of alternative waste materials as SCMs in order to avoid increased use of natural minerals or increased transportation distances (Frías et al., 2021).

The global cement production has soared over the past 20 years due to urbanization and population growth in emerging countries, where the demand for infrastructure and modern housing is constantly rising. China is currently leading the global trends, accounting for 56% of worldwide cement production (4.1 Gtons in 2019; USGS, 2024) followed by India (8%), the EU countries (4.5%) and the USA (2.2%).

The embodied CO_2 for cement is 0.73-0.99 kg CO_2/kg whereas concrete ranges between 0.04 kg CO_2/kg and 0.11 kg CO_2/kg, depending on the material design and operating conditions of manufacturing, in fact, steel rebars are much higher, ranging from 1.22 kg CO_2/kg to 1.66 kg CO_2/kg (Oh et al., 2017). The net proportions are influenced by the quantity of materials used in building projects, with concrete and cement employed in almost every construction phase whereas steel bars are mainly used for structural strengthening of the former. At the same time, due to spontaneous aging of concrete namely, the carbonation process, part of the emitted CO_2 is resorbed. For a typical building in an urban environment with a 64-year lifespan, it is found that ~0.05 kg CO2/ kg cement, or roughly 12% of calcination emissions, are re-absorbed during use (Van Roijen et al., 2024). Subsequently, the cement and building materials industry is one of the most challenging sectors to innovate towards the net-zero pathways projected for 2050 and 2060 worldwide.

The cement reaction starts with water addition, which is usually drinkable water. Therefore, concrete production is also responsible globally for 9% of industrial water withdrawals (2 Gtons in 2012; FAO, 2016), which is approximately 1.7% of total drinkable water consumption. It is expected that in 2050, 75% of the water demand for concrete production will likely occur in regions that are expected to experience water stress (Miller et al., 2018). Only recently have the aspects linked with aggregate consumption been getting more attention in the scientific community (Bendixen, 2019). Sand and gravel make up the most worldwide extracted group of materials, from 32 to 50 Gtons used each year, even exceeding fossil fuels (Torres et al., 2017). Most of these materials are employed again in the construction sector. These values are already exceeding the pace of natural renewal such that by mid-century, demand might outstrip supply. The majority of angular sand suitable for concrete production comes from rivers and from quarry mining. The extraction of sand and gravel has far-reaching consequences for ecology, landscape and the livelihoods of entire

ecosystems (Best, 2019). At the mining site, the work environment has serious impacts on the health and well-being of workers and the people within the vicinity. Sand extractors are positioned as external actors, and the activity is often portrayed as illegal and associated with violence and to 'sand mafias' in many developing countries (Hougaard, 2023). The process is also usually high in primary energy consumption due to the high-level use of machinery, and this energy is usually considered a part of the initial embodied energy of the extracted materials (Ding, 2014). There are additional harmful scenarios to consider related to the logistical aspects. Motor transportation is used for raw material and product delivery, starting from the manufacturer and arriving at each specific site for production (D. Song et al., 2016). In most cases, heavy diesel trucks are employed causing severe air pollution associated with lung pathologies. Packaging for distribution to the project represents a significant waste of resources and has serious impacts on landfills, as there are few packaging material options that are biodegradable or can be safely burnt (Pešta et al., 2020). When reaching the end of their life cycle, building materials and construction rubble continue to represent a burden to the environment, accounting for 35% of global waste disposed of in landfills (OECD, 2019). Construction and demolition waste (CDW) is usually defined as the waste coming from construction operations, reconstruction, alteration, extension, maintenance, and demolition of buildings and other infrastructure (EC, 2017). The average CDW average composition includes mainly natural sand, gravel, concrete, metal, plastic, ceramic, and glass (**Figure 1**).

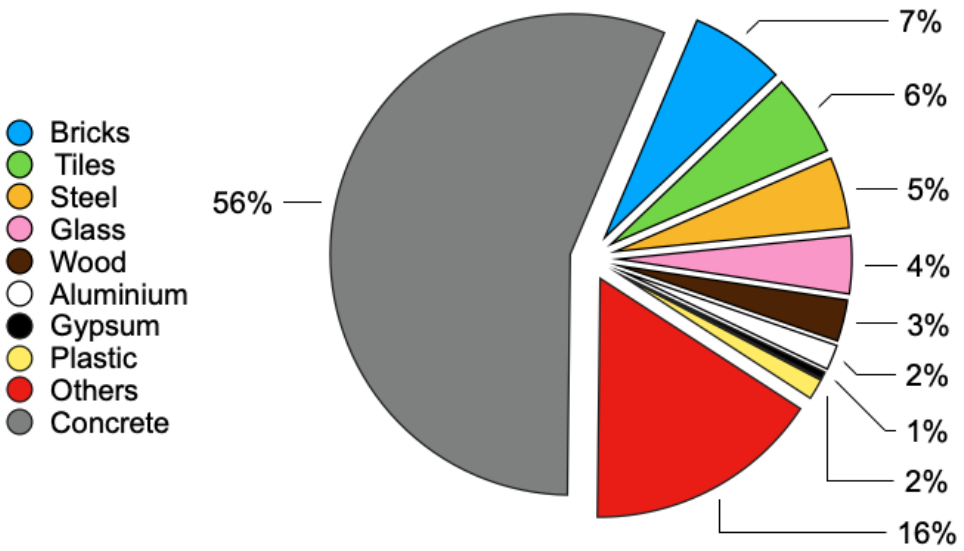

***Figure 1**. Bar chart for the average CDW composition in the EU Countries data from Damgaard et al., 2022.*

The inert non-biodegradable fraction of waste accounts for 40-85% of total CDW volume, excluding excavation soils and woods. It is commonly known that the quantity and makeup of CDW can differ greatly depending on the regions in which they are produced based on historical contest, geology, population, regional planning, legislation, and construction materials and technologies (Galderisi et al., 2023). The current global urbanization trend is constantly accompanied by an increase in CDW production. The three largest economies - China, the US, and the EU - are the largest global producers with 1704 Mtons, 600 Mtons, and 372 Mtons, respectively (C. Zhang et al., 2022). Furthermore, in the Western world, constructions undertaken during the economic growth of the 1950s will reach their end of life in the upcoming decade(s). As such, the generation of CDW is expected to rise rapidly, especially in Europe. The projections indicate that between 2020 and 2050, the overall outflow is predicted to more than double (Damgaard et al., 2022). Within the EU framework, the situation is analogous, with the most industrialized countries producing the highest quantities of waste. In 2022, France occupies the top of the list with 252 Mtons of CDW generated, followed by Germany with 201 Mtons, the UK with 145 Mtons and Italy with 56 Mtons **(Figure 2a**). At the same time, the situation is quite different if we take into account the pro-capite CDW generation in the same EU countries (**Figure 2b**). Here, at the top of the ranking we have Luxembourg with 7.85 tons/capita, followed by Austria with 5.50 and Finland with 4.28, whereas Italy has a per capita value of 0.95 tons of CDW.

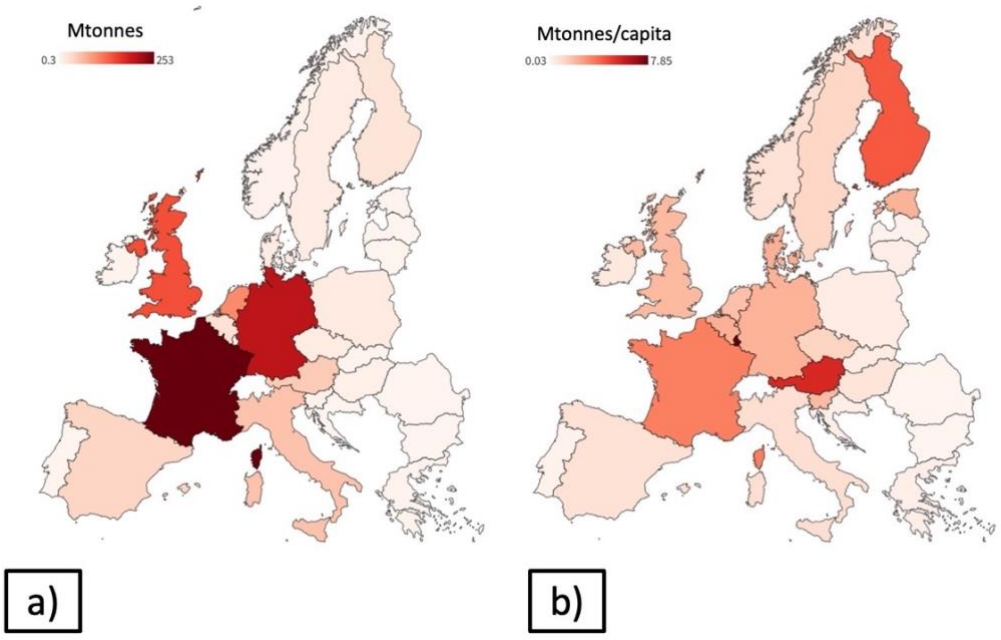

***Figure 2**. European countries and the CDW produced: a) total value in Mtons, b) tons/capita, data from Damgaard et al., 2022.*

In the upcoming years, the largest outflow of materials will be from Western EU countries (reaching a peak of 300 Mtons) in 2050, followed by Southern (100 Mtons), Eastern (30 Mtons), and Northern Europe (5 Mtons). When CDW is disposed of in landfill or reused in construction as recycled aggregates, rainwater, surface water, or groundwater may come into contact with it and leach hazardous elements, representing a potential threat to the environment (Saca et al., 2017). Hence, the environmental impact is not determined by the total amount of pollutants on the bulk materials, but by the amount that water can dissolve into the soil, reaching the surface and/or underground water (Prieto-Espinoza et al., 2022). It is therefore necessary to assess the environmental risk of CDW with respect to the release of potential pollutants (Diotti et al., 2020). At the same time, potential leachate is a direct product of the interaction between water and the bulk chemical and crystalline assemblage of the solid waste, and therefore different degrees of impact should be expected depending on the composition of the latter (López & Lobo, 2014).

Even though the specific hazard is low if compared to other waste streams, the associated environmental impacts of such a high volume of products are an important concern, mostly derived from its logistics and land occupation (Gálvez-Martos et al., 2018a). The disposal of CDW in landfill is a concern in many countries, necessitating the use of enormous extents, which may even encompass farmlands and cultivated areas. The scarcity of landfill space might also have additional effects, such as a rapid spike in the costs for disposal and serious environmental and social issues (Zheng et al., 2017). In fact, this material is not inert at all, since a few chemical reactions, especially the carbonation process of the hydrated cement paste, continue to occur throughout the whole Life cycle, even during deconstruction and disposal. It is known that an extra 0.12 kg CO_2/kg cement, or 30% of the total calcination emissions, is re-absorbed if the old cement paste is crushed to a particle size of 1-40 mm and exposed to air for about 3.5 months (the global average exposure length) in air (Xi et al., 2016). However, it has been highlighted that the energy necessary for breaking discarded concrete down to this size results in around 0.1 kg CO_2/kg cement, practically eliminating the advantages of carbon uptake occurring at this time (Van Roijen et al., 2024).

Prior to deconstructing and demolishing, buildings and infrastructure should be evaluated to assess aging and physical conditions, as well as the potential materials value (e.g., high-cost metals, well-conserved wood, marbles and/or decorative stones). As a result, before beginning any deconstruction, a thorough inventory should be completed (van den Berg et al., 2020). In most cases, selective demolition would be the ideal approach, with the aim of gathering sorted waste directly on the site, allowing an increased production of high-quality secondary raw materials from ca. 17% (traditional demolition) to ca. 53% (selective

demolition) (Lavagna et al., 2018). The majority of stakeholders, however, believe that this strategy is time-consuming and operationally and financially inconvenient (Coelho & De Brito, 2011). Therefore, the non-selective demolition approach is currently still the most predominant. In non-selective demolition, the entire building or structure is demolished in a way that combines all materials, such as wood, metal, concrete, and glass, into a single waste stream. This approach is often faster and less expensive than selective demolition, but it typically results in lower quality of waste with fewer opportunities for recycling or reuse. All building activities, such as construction, renovation, remodeling and especially deconstruction generate CDW that must be disposed of and treated in legit landfills and recycling plants. Here, the recovery and/or disposal practices usually vary within the EU countries depending on the national regulation and on the secondary raw-materials market availability. Eventually, illegal dumping or unauthorized waste disposal is still not completely overcome, which represents the act of disposing of waste materials in an unauthorized or inappropriate location, rather than using official and legal waste disposal facilities. This practice is illegal and can have significant negative impacts on the environment, public health, and local communities (Bianchini et al., 2020).

Prior to effective recycling and reuse, CDW needs to be cleaned and separated from foreign elements, such as plumbing, bituminous materials, insulation and gypsum panels which could have serious detrimental effects following the reuse (Butera et al., 2014). This operation should be conducted during the preliminary phase of deconstruction although is still mostly conducted manually by operators at the recycling plant.

When disposed of at an authorized landfill or recycling plant, CDW normally goes through a conventional recovery process that includes many phases. When dealing with a heterogenous waste form, the first stage is the acceptance and pre-sorting audit, in which the CDW is weighed and visually inspected upon arrival. Only specific materials are accepted accordingly to the CER classification, EWC – European Waste Catalogue (Council Directive 75/442, 1975) and the European List of Waste (European List of Waste 2000/532/EC, 2000), which provides a comprehensive list of waste types, each identified by a unique six-digit code. The first two digits indicate the waste's origin or sector (e.g., 01 for wastes from mineral extraction). The next two digits specify the sub-sector (e.g., 01 01 for wastes from mineral extraction, specifically from mineral excavation). The final two digits describe the particular waste type within that sub-sector (e.g., 01 01 01 for wastes from mineral excavation, like waste sand or clay). The EWC helps ensure compliance with EU waste management laws, facilitates waste sorting and recycling, and supports the circular economy by clearly categorizing waste streams. In this regard, attention needs to be paid to the

presence of asbestos-containing building materials, which are classified as hazardous special waste and cannot be treated together with CDW (Stevulova et al., 2022).

This initial step may involve manual or mechanical separation of large materials, like wood, metal, and pipes. This helps streamline subsequent stages and reduces contamination. Large and unwanted items, such as hazardous materials or oversized debris, are removed manually to avoid damaging the processing equipment. Afterwards, industrial magnets are commonly adopted together with clamshell buckets in order to separate metal components, mostly resulting from the rebars (Barbudo et al., 2020). In modern operating plants this step is often conducted in conjunction with the crushing process to improve the efficiency of sorting.

The second and crucial recycling step is the crushing and screening stage using either jaw or impact crushers. The first break up the particles by shearing across the main tension plane of compression while the latter employs rotating and impact plates until the required size fraction is reached (Ulsen et al., 2019). The pipeline of a modern sorting plant (**Figure 3**) typically starts with a first step of comminution through a jaw crusher that achieves a mean size below 100 mm. Most of the unwanted fractions that were still present within the CDW are rejected by the bypass conveyor and excluded after the first comminution operation. Light unwanted residues like plastics, wood and papers are also removed through air jigs that directly blow on the granulate stream to push away these fractions during crushing. Nevertheless, a minor percentage of unwanted fraction is unavoidable as no available process is 100% efficient (Skocek et al., 2024). Within the whole portion of inert mineral waste that is comminuted, fine fractions (<4 mm) and coarse fractions (<50/60 mm), and big blocks (>60 mm) can be found together. The size reduction is focused on maximizing the yield of the coarse fraction to decrease the production of fines that are later difficult to valorize. To finalize the size decreasing of the big blocks, the whole material is sent to feeding hopper 2, where a cone crusher (or other types of impact crusher) reduces the mean size of CDW below 60 mm. Lastly, with the aim to separate and obtain coarse and fine secondary raw-materials like sand and gravel, the crushed components are subsequently sieved using a vibrating screen (Gebremariam et al., 2020). Specific conveyor belts transport the sorted products in distinct stockpiles. Additional equipment, such as float-sink tanks or air tables, may be used to separate materials based on density. This step can further purify specific fractions, such as aggregates or glass. In some advanced sorting plants, optical sensors are used to identify and separate materials based on color or composition (W. Lu & Chen, 2022). For example, they can distinguish between different types of plastic or sort out specific contaminants (Serranti et al., 2023).

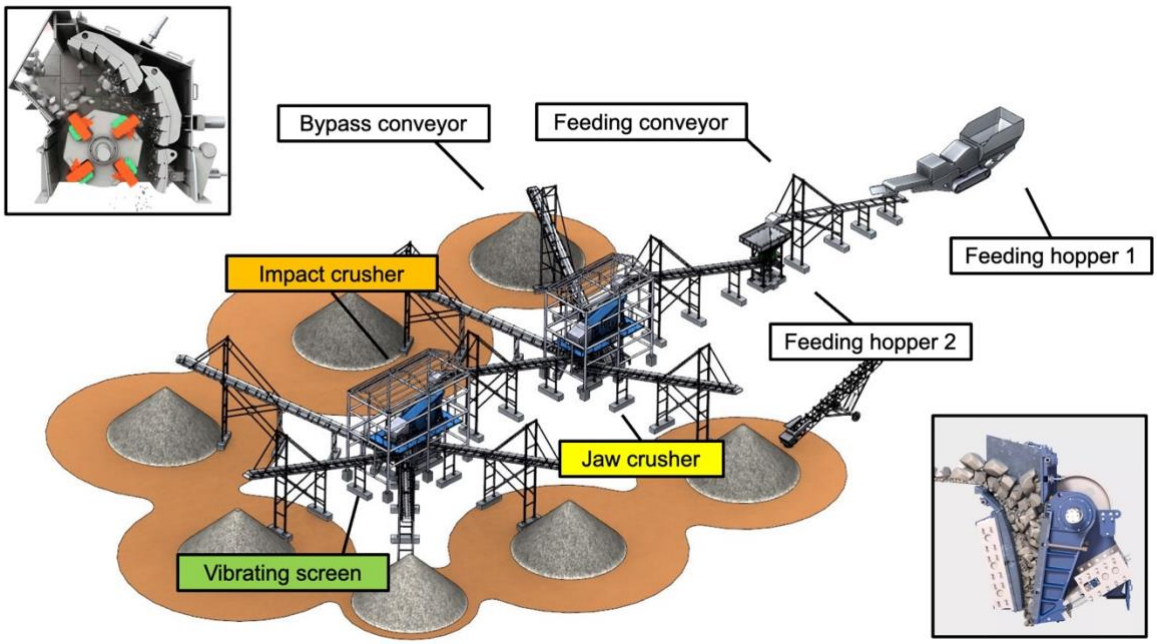

Figure 3. *Schematic representation of a modern recycling plant for CDW.*

The inert mineral secondary raw materials obtained from recycling processes—such as coarse gravel and sand—often exhibit a broad and variable chemical and mineralogical composition. These materials are typically derived from composite by-products like crushed concrete, ceramics, residual mortars, and tiles. Due to the presence of these mixed-origin materials, they frequently contain pollutants, including both legacy chemicals and contaminants introduced through inadequate separation. This situation largely results from the limited adoption of selective demolition practices by construction companies, as well as a shortage of advanced sorting facilities equipped with optical sensors and other technologies capable of precisely sorting materials based on their composition. Improving these processes is essential to enhance material separability and to reduce contamination, thus supporting more sustainable reuse in construction projects. In conclusion, depending on the original source, CDW properties fluctuate over time, affecting the potential reuse of this abundant resource and limiting the confidence of the stakeholders willing to re-introduce them in a circular economy. Nevertheless, the available numbers on CDW recycling in the various EU countries are surprisingly positive (EUROSTAT, 2023). The average recycling rate is 82.8%, with 5.6% backfilling, 11% landfilling, and 0.6% energy recovery treatment. The Netherlands has the highest CDW recycling rate in the EU, at 100%, followed by Slovenia (97.6%) and Italy (97.4%), where also most of the other EU countries have values around 70% (**Figure 4a**). When considering the landfill rate instead, Slovakia is found at the bottom of the list with 46.6%, followed by Cyprus (42.8%) and Norway (31.4%) even though the situation in the remaining countries appears very positive (**Figure 4b**).

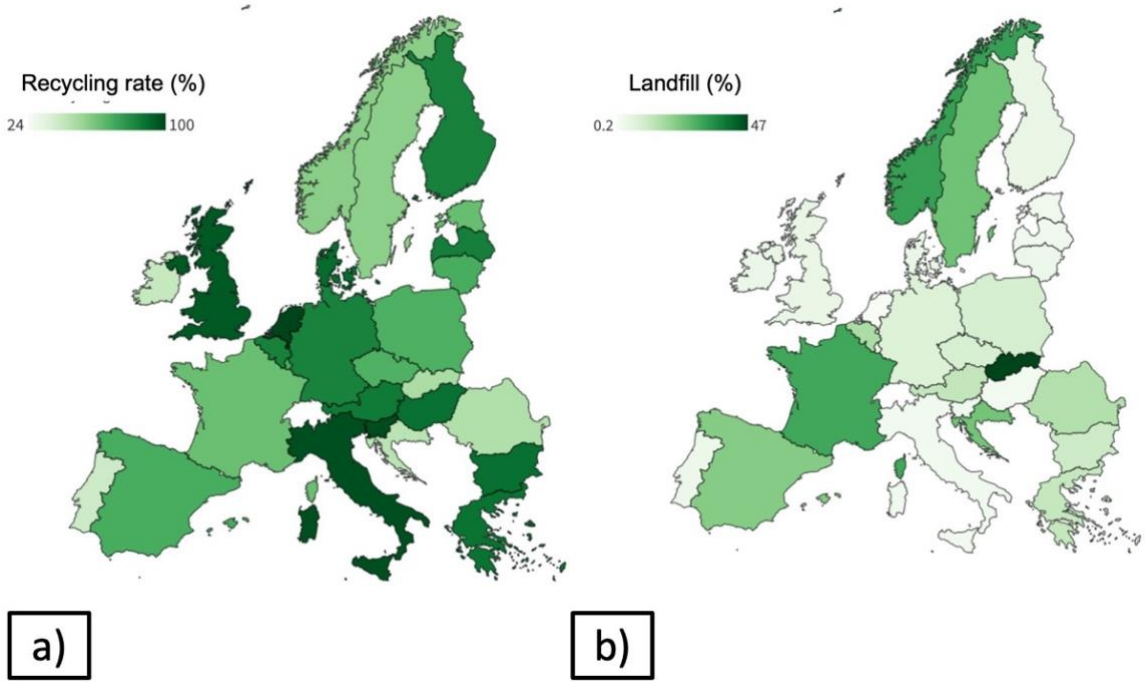

***Figure 4**. European Countries and the CDW treated: a) recycling rate (%); b) landfill (%) data from EUROSTAT, 2023.*

Official statistics are hampered, nevertheless, by a variety of factors, including a sizable amount of illegal dumping and a diverse secondary raw-material market in some areas (Bianchini et al., 2020). Although a common model for calculation methods exists across EU states, the definition of "recovery" for CDW is highly susceptible to varying interpretations and considerations by each nation. As a result, it is difficult to accurately compare values between different countries, or even within the same country (Galán et al., 2019). Recovery rates published by EUROSTAT are calculated on the basis of waste treatment data of non-hazardous mineral CDW, generated according to the EU Waste Statistics Regulation. Limiting factors like non-unified methods of data collection, different waste coding systems and misinterpretations of the term 'backfilling' impede a cross-country comparison of the published EU recovery rates (Moschen-Schimek et al., 2023). Currently, the recovery rate is measured from the contribution of downcycling and upcycling operations. Downcycling processes involve backfilling activities of CDW, used in esplanades or as sub-bases and bases of pavements/roads and highways where it is used in unbound layers and in low-grade concretes (C. Zhang et al., 2020). Upcycling operations, on the other hand, include the reuse in the production of high-grade concrete, mortars, cement manufacturing, secondary raw materials for the ceramic industry, CO_2 capture and storage and any other application where the final value of the recovered materials is equivalent to or even greater than that of the natural raw materials. Eventually, the actual

recovery rate should rely only on upcycling operations, whilst nowadays downcycling is the most common practice in the EU, and the difference between the two is not clearly shown in statistical monitoring.

The shortcoming of upcycling rises from poor communication, conflict management, lack of financial incentives (i.e., carbon emission trading), and inadequate knowledge of waste management strategies and laws. Other related obstacles encompass sub-standard quality of recycled products and production chain development costs (i.e., advanced sorting plants purchase). The economic barriers include high transportation and recycling costs, and financial losses from exporting waste for recycling. In terms of the economic value, CDW secondary raw materials are currently sold for an average of 8€/tonne in Italy (N = 30), depending on impurity content. In the same area, the average price for natural sand and gravel is nearly double, at around 16€/tonne, depending on diameter size and physical properties (N = 21). Therefore, since there could be a good margin of profit, the biggest limitation in this sector is the confidence of the stakeholders in the adoption of recycled materials in construction projects (Barbudo et al., 2020). In accordance with the (EU Construction & Demolition Waste Management Protocol, 2016), to increase the upcycling of CDW it is necessary to work on different aspects:

i) Waste identification, source separation and collection through pre-demolition audits and by conducting on-site sorting and processing, from controlled deconstruction and demolition with the aim of side-streams separation.

ii) Logistics, from the traceability and conformity with transport requirements.

iii) Processing, in the fields of landfilling (only hazardous waste), backfilling (selectively), re-use (cleaning and processing), recycling (approval/rejection processes), and recovery (energy recovery).

iv) Quality management, in the EU-wide quality assurance is required from labels (certificates and audit) and in compliance with End of Waste criteria. On the worksite, qualified workers and appropriate equipment are mandatory.

v) Policy and framework conditions, involve landfilling restriction, the regulation and enforcement of CDW management regulations, followed by public procurement and sector involvement by the central administration.

Eventually, the CDW management, particularly the recycling and upcycling of this waste, represents an integral part of achieving a circular economy in the construction sector and towards 2050.

1.2 – The EU and Italian waste framework for CDW

1.2.1 The European Union regulation

The notion of circular economy dates back to the 1960s, when increasing evidence of global-scale environmental threats such as ozone depletion, climate change, biodiversity loss, and nitrogen cycle disruption emerged (Kirchherr et al., 2017). These risks have been systematically investigated, raising questions about whether current prosperity trends can be sustained in the future due to limited supply of natural resources, their uneven spatial distribution and appropriation, and the implications of the assimilative capacities of ecosystems over economic growth (Geissdoerfer et al., 2017). A new type of economic system was finally theorized to re-design the traditional "take-make-dispose" linear path of production and consumption toward a circular conjunction which foresees reducing, alternatively reusing, recycling and recovering materials (Kiser, 2016). Transition toward a circular economy is a process of re-configuration and adaptation driven by technological innovation, with the aim of accomplishing sustainable development, thus simultaneously creating environmental quality, economic prosperity and social equity, to the benefit of current and future generations. Even when circular economy solutions are already technically feasible, their practical implementation is often limited by economic and market limitations. Public agencies have a crucial role in institutional framing, from infrastructures to legal set-ups (de Jesus & Mendonça, 2018). One of the EU's primary concerns is environmental protection, which includes waste legislation. Over the past 20 years, a number of waste-related EU directives have been updated. In general, these policies must be incorporated into each country's national legislation, and Member States must be accountable for waste management in accordance with the waste hierarchy principles. Since the 1970s, when the Environmental Action Programmes (EAP) were established, European institutions have begun to respond proactively to accumulating data on global-scale environmental dangers associated with irreversible ecological degradation and natural resource depletion (Thieffry & Nahmias, 1991). This commission's work resulted in the 1975 Waste Directive (ECC, 1975), which included a first definition of "waste" and three principles: (i) preventive efforts, (ii) control/rectification at the source, and (iii) the "polluter pays" principle. These principles were considered "innovative regulatory approaches to environmental policymaking" and are currently at the heart of European environmental policymaking (Duquennoi & Martinez, 2022). Before 1990, no binding obligation on how to treat waste was introduced by the EU, apart from refining waste oil. From 1990 to 2008,

numerous recycling initiatives and targets were implemented through various directives, including packaging waste (1994), vehicles (2000), electrical and electronic equipment (2002), batteries and accumulators (2006) and eventually the Waste Framework Directive (WFD). The WFD (Directive 2008/98/EC, 2008) encourages the reuse of products, addressing also CDW for the first time. This directive establishes the legal framework for waste management across EU member states, aiming to protect the environment and human health by preventing or reducing the adverse impacts of waste generation and management. At its core, the directive introduces a waste hierarchy, which encourages the prioritization of waste prevention over other actions. Where prevention is not possible, it advocates for measures that prepare waste for reuse, followed by recycling and recovery, with disposal as the last and least preferable option. This hierarchy helps direct waste management strategies toward sustainability and resource efficiency. Directive 2008/98/EC also emphasizes the importance of producer responsibility, encouraging member states to implement policies where producers are accountable for their products throughout the product lifecycle. This responsibility extends from the design phase, encouraging eco-friendly and sustainable product designs, to the end-of-life phase, where producers may be involved in the collection, recycling, or disposal of their products. Additionally, the directive requires that EU member states create comprehensive waste management plans and waste prevention programs. These plans are designed to address the entire waste cycle, from collection and treatment to final disposal, and aim to ensure that waste is managed in a way that minimizes risks to human health and the environment. The directive sets out clear targets for recycling, including an ambitious goal of recycling at least half of household waste and achieving a 70% recycling rate for construction and demolition waste by 2020. These targets aim to foster the development of a circular economy, where resources are kept in use for as long as possible, extracting maximum value before finally being recovered or recycled at the end of their life cycle. Another important aspect of Directive 2008/98/EC is the introduction of end-of-waste criteria. These criteria define specific conditions under which waste can be deemed no longer waste and may be used as a secondary resource. By setting these criteria, the directive encourages the safe and effective reuse of materials, supporting a circular economy and reducing the demand for virgin resources. The directive also places special focus on hazardous waste, establishing strict guidelines to ensure it is managed safely. This includes proper labeling, handling, and treatment procedures to protect public health and prevent environmental contamination.

Following the WFD, the EU has also set three other guidelines regarding CDW. First, in September 2016, the EU Construction & Demolition Waste Management Protocol was

published (EU Construction & Demolition Waste Management Protocol, 2016), which consists of five sections, all of which contribute to the overall aim (Waste identification, source separation and collection; Waste logistics; Waste processing; Quality management; Policy and framework conditions). Additionally, the protocol provides guidelines and best practices for stakeholders, including construction companies, waste managers, and local authorities, emphasizing collaboration and knowledge sharing. It underscores the importance of monitoring and reporting waste management activities to ensure transparency and track progress. Training and capacity building for industry professionals are also highlighted, ensuring that they have the necessary skills to implement effective waste management strategies. By promoting alignment with national and regional regulations, the protocol seeks to create a supportive legal framework for sustainable CDW management.

Lastly, in 2018, "Guidelines for audits before demolition of building" and a review of the "Implementation of EU waste legislation" have been published. The implementation review begins with the development of national waste management plans and programs that align with EU objectives. These plans typically include strategies for waste prevention, recycling, and recovery, along with measures to improve infrastructure and public awareness. Member states are also expected to set specific targets for waste reduction and recycling, as mandated by various directives. The European Commission and member states engage in regular assessments to track progress toward meeting waste management targets. Member states must provide data on waste generation, recycling rates, and the management of hazardous waste, ensuring transparency and accountability in their waste management practices. Furthermore, the EU supports member states through funding, guidance, and technical assistance, helping them develop effective waste management systems. The Commission may also initiate infringement procedures against member states that fail to comply with EU waste legislation, ensuring adherence to established regulations and standards. The EU encourages collaboration among various stakeholders, including local authorities, industry representatives, and civil society organizations, to foster a culture of sustainability and promote responsible waste management practices. In recent years, the EU has further strengthened its waste legislation through amendments and new directives, including the Circular Economy Action Plan. This plan aims to create a more sustainable and circular economy by setting ambitious targets for waste reduction, recycling, and resource efficiency. Overall, the implementation of EU waste legislation is a dynamic and multifaceted process that seeks to enhance environmental protection, promote sustainable resource use, and support the transition toward a circular economy.

1.2.2 The Italian regulation

The regulation of solid waste collection and transportation in Italy has evolved significantly over the years, starting with D.L. 20 Marzo 1941 n. 366, which primarily focused on hygiene and urban decorum. In 1982, a new regulation was introduced to implement European Directive 75/442 (ECC, 1975); however, this update did not significantly modernize waste management practices. The 1982 regulation continued to emphasize disposal without adequately addressing prevention and recovery processes. It established a distinction between municipal, special, and toxic-hazardous waste, with inert materials from construction and demolition waste (CDW) categorized as special waste. The framework changed with the introduction of the "Ronchi Decree" in 1997, which marked the first comprehensive legislation for waste management in Italy. This decree aimed to prevent and reduce waste generation, enhance recovery efforts, minimize landfill disposal, and promote separate collection to ensure high-quality recycling. It broadened the concept of waste management by incorporating all related operations, including collection, transportation, and recycling, thereby moving beyond the limitations of previous regulations. Subsequently, the DM 5/02/1998 established technical standards to define types of non-hazardous special waste and provided initial guidelines for recycling methods, including those applicable to CDW. The materials categorized as CDW encompass bricks, plaster, concrete, ceramic materials, metal fractions, wood, plastic, paper, and insulators, with asbestos explicitly excluded. The recovery activities outlined in this decree include processes such as crushing and screening, which allow for the separation of metals and unwanted fractions to produce an inert fraction with appropriate granulometry.

Following the Directive 2008/98/EC of the European Parliament, the D.L 3/12/2010 n. 205 was established to align with the EU guidelines. This law represents an important legislative step in Italy's efforts to enhance environmental protection, reflecting the country's alignment with EU directives and its commitment to fostering a sustainable and circular economy. One of the key objectives of D.L. 205/2010 is to improve the management of waste and to reinforce the principles established in earlier regulations, such as the "Ronchi Decree." The decree emphasizes the importance of waste prevention, reuse, and recycling, aiming to reduce the overall environmental impact of waste generation and management. It also introduced new measures to promote separate waste collection, thereby facilitating higher recycling rates and resource recovery. The decree further aims to streamline waste management procedures and enhance the responsibilities of different stakeholders, including local authorities, waste operators, and producers. It sets out guidelines for the proper

treatment of various waste streams, including municipal solid waste, CDW, and hazardous waste. Additionally, D.L. 205/2010 lays the groundwork for developing a circular economy by promoting the recovery and recycling of materials and reducing reliance on landfills. This is in line with the EU's broader goals of fostering a more resource-efficient economy and minimizing waste generation.

With the D.M. 11/11/2017 the new minimum environmental criteria (CAM – "*Criteri Ambientali Minimi*") were also introduced for contracts related to the construction, renovation, maintenance, and energy upgrading of public buildings, as well as for site management. The document contains general guidelines for contracting authorities. The document defines "environmental standards" and sets out minimum criteria to ensure that environmental performances of the construction phases and of the building materials used are above a certain standard. Among the points of particular interest are listed specific criteria that involve the adoption of CDW:

(i) The content of recovered or recycled materials used in construction must be at least 15% of the total weight of all materials used.

(ii) The concrete used for the projects must contain at least 5% recycled material (dry weight) based on the weight of the product (as the sum of the individual components).

(iii) At least 50% of the weight of the building components and prefabricated elements must be selectively dismantled at the end of their life cycle and be recyclable or reusable. Of this percentage, at least 15% must consist of non-structural materials.

(iv) For bricks used in masonry and flooring, the content of recycled and/or reused materials (dry weight) must be at least 10% of the product's weight. For bricks used for roofing, flooring, and external masonry, the content of recycled and/or reused materials (dry weight) must be at least 5% of the product's weight.

Lastly, in September 2024, the decree no. 127/2024, issued by the Ministry of Ecological Transition, establishes the specific "End of Waste" criteria under which inert waste from CDW, and other inert mineral waste subjected to recovery operations, cease to be classified as waste. The new decree, composed of 8 articles and 3 annexes, specifies the composition of the CDW allowed to be recovered, the treatment protocols, the environmental criteria related to leaching of pollutants, and eventually, the new materials in which it is allowed to reuse them. The waste concerned CDW, including those corresponding to CER Codes 170101 (cement), 170102 (bricks), 170103 (tiles), 170107 (mixed waste made of cement, bricks, tiles), 170302 (bituminous fraction), 170504 (excavated soils), 170508 (railroad rocks), 170904 (mixed construction waste). Also, other natural mineral fractions are

included such as those from 010408 to 010410 and 191209 (natural sand and gravel), 010413 (by-products of rocks cutting), 101201, 101206, and 120117 comprising non thermally treated minerals, 101208 and 101311 thermally treated ceramic and cement by-products, and lastly 200301 which are the CDW abandoned in illegal dumping.

The controls on the waste permitted for the production of recovered aggregate include: i) examination of the documentation accompanying the incoming waste, ii) visual inspection, iii) any supplementary checks. To this end, the producer of the CDW recycling plant must have a waste acceptance procedure suitable for verifying that the waste corresponds to the characteristics stipulated in this regulation. The treatment and recovery process of inert waste from CDW, as well as other inert waste of mineral origin, occurs through mechanical phases, which include, for example only: crushing, screening/granulometric selection, and the separation of the metallic fraction and unwanted fractions. The recovery process, depending on the type of material, may simply involve checking the waste to verify whether it meets the defined criteria. However, recovery is considered to have occurred whenever, through the completion of all or some of the aforementioned phases, or other mechanical processes, compliance with the criteria set forth in this regulation is achieved.

Each produced batch of secondary raw material must undergo leaching tests to evaluate compliance with the concentration limits of the parameters identified. Batches of recovered aggregate produced for the formulation of concrete as per the NTC 2018 with a compressive strength class of C12/15 or greater are excluded from the leaching test. Batches of recovered raw materials intended for the production of clinker for cement and those intended for the production of cement are also excluded. The UNI 20802 standard and the method specified by the UNI EN 12457-2 are used for the determination of the leaching test.

The secondary raw materials obtained from CDW can be used for: a) the realization of environmental recoveries, fill materials, and embankments; b) the construction of the bodies of earthworks in civil engineering; c) the production of asphalt mixtures and road, railway, airport, and civil and industrial yard sub-bases; d) the construction of foundation layers for transport infrastructure and civil and industrial yards; e) the creation of accessory layers with functions such as capillary break, frost resistance, and drainage; f) the formulation of mixtures bound with hydraulic binders (such as, for example, cemented mixtures, concrete mixtures); g) the production of concrete; h) the production of clinker for cement; i) production of cement.

1.3. Toward the implementation of CDW circularity

Reusing CDW is a key aspect in sustainable construction practices, and it supports the principles of circular economy by reducing the need for virgin materials and minimizing landfill waste. Prior to recycling, it is critical to recognize that the composition of the CDW input cannot be drastically altered. As a result, certain types of debris must be considered more valuable than others. In this aspect, clean and well-sorted streams outperform mixed materials. It is worth mentioning that the majority of the CDW acquired via selected demolition has, from this point of view, a greater intrinsic value than that from unsorted destruction. Afterwards, all treatments performed to the waste—whether advanced sorting operations or recycling through industrial processes—increase the quality of the recovered material while raising its final cost. As a result, the average market price of basic goods serves as a key constraint, defining the feasible subsequent industrial treatments within the economic profit margins. However, if national and European entities do not provide economic assistance to stimulate the market for secondary raw resources, the gap between the two will remain difficult to overcome. Following this consideration, the simplest and cheapest way to reuse CDW is to convert it into recycled aggregates (RAs), which could replace natural aggregates in the production of concrete, mortars, and plasters, as well as for use as subbase for road construction or filling. Other potential applications have also been examined and evaluated, such as the manufacturing of supplemental cementitious materials (SCMs) and the use of CDW for CO_2 capture and storage (Auroy et al., 2018; Y. Li et al., 2020). Although both of these advanced recycling processes are feasible, they may require additional processing affecting the final costs. In this framework, the most common and direct strategy to employ large volumes of CDW in a circular economy is the adoption of RAs in concrete, which represents the world's second most consumed commodity after drinking water (Caro et al., 2024). Before RAs become eligible for the use in concrete production, their composition and physical characteristics should be established and satisfy specific quality standards. This will facilitate its certification and classify increasing confidence among stakeholders, while also enabling better knowledge of the material and its future performance.

As discussed in the **previous Chapter (1.2.2),** the Italian and European regulations require, prior to reusing CDW as RAs, to evaluate the chemical leaching of each batch produced accordingly to standardized protocols. In fact, when CDW is disposed of in landfill or reused in construction as RAs, rainwater, surface water, or groundwater may come into contact with them and leach hazardous elements (e.g., Cr, Cu, Ni, Pb, V), representing a potential threat

to the environment (Saca et al., 2017). Hence, the environmental impact is not determined by the total amount of pollutants on the bulk materials but by the amount that water can dissolve in the soil reaching the surface and/or underground water (Prieto-Espinoza et al., 2022). This first approach toward CDW recycling will be further investigated in the following **Chapter 2 "Geochemical analyses, leaching and risk-assessment of CDW based on multivariate statistical analysis and machine learning".** In agreement with the End of Waste criteria, if the leachates are below the threshold values, the materials are eligible to be reused as RAs. Still, the quality of this secondary raw materials has to be evaluated, in order to reuse them into concrete. The most crucial quality parameters have been identified and compared with the values for the natural aggregates (Martín-Morales et al., 2013). These standards and recommendations were examined and compared across 16 different nations; the majority of these classifications are drawn from the criteria in the European Standard EN 933-11 of 2009. As a result, the idea of a performance-based classification that could certify quality of the RAs obtained from CDW and expected mechanical performances of recycled aggregate concrete was introduced. Regardless of the size, kind, or source of the RAs, a prediction model that could represent a solid base for harmonized standard quality criteria was first established utilizing as parameters to the equation the bulk density, water absorption (WA24) and oven-dried density (ODD) relationship from Silva et al. (2015). Afterwards, in addition to these parameters, an improved model created by Gonzalez-Corominas et al. (2017) also introduced other variables related to the production techniques (pre-soaking RAs or air-dry RAs with additional water). It is important to note that most of the proposed methods contain a factor to address the water absorption effects resulting from the use of RAs. These effects mainly result from the presence of residual adhered mortar (AM), commonly found as a leftover layer of cement clinging to the surface of RAs following comminution practices. This characteristic is considered as the primary obstacle that prevents the use of RAs in new structural high-grade concrete (Tam et al., 2021; Verian et al., 2018). Compared to natural rocks, the presence of AM increases the average porosity and reduces the bulk density of such aggregates, which is a major reason for the observed declining trend in comparative studies on the fresh-mixing properties (Deng et al., 2023; Faleschini et al., 2014; B. Li et al., 2021), mechanical properties (Piccinali et al., 2022; B. Wang et al., 2021), and durability of recycled aggregate concrete (Guo et al., 2018). Furthermore, chloride penetration and thermal conductivity were also discovered to be predominantly influenced by the volume and distribution of the AM (Kang et al., 2024; W. Xu et al., 2024). Therefore, it is possible to state that the presence of AM represents one of the major burdens in limiting the

confidence of the stakeholders in adopting RAs in the mix design formulation of concrete. With the aim to improve model prediction and provide a more comprehensive model that integrates also the contribution from the AM content in modelling the mechanical properties of concrete with RAs the discussed equations have been further integrated with parameters like the Los Angeles (LA) coefficient and of micro-Deval coefficient (MDE) (X. Chen et al., 2022; Younis & Pilakoutas, 2013). These parameters provide an information on the resistance to impact and abrasion due to heavy and repetitive impacts, both in dry and water-saturated conditions, such as in wet environments. Being possible to separate the AM from the original aggregate through mechanical processing, these two parameters contain within their values an indirect measure of the first. For this reason, considering the importance of this feature in determining the quality of RAs a direct method to assess the content and volume of AM using XRPD and novel machine learning approach will be discussed in the **Chapter 3 "Advanced separation of CDW: estimating attached mortar paste on the surface of recycled aggregates based on machine learning and XRPD".** The proposed models rely mostly on physical parameters obtained from laboratory measurements (WA24, ODD, MDE, LA) that define the engineering properties of RAs. At the same time, data on the chemical and mineralogical composition of RAs are typically not fully considered. Even though concrete's mechanical behavior is directly affected by the composition of the RAs, either from the mineralogical composition of the secondary raw materials (i.e., concrete, natural aggregates, bricks, gypsum) or from the composite nature of the products (i.e., AM content). For instance, ceramic materials usually have negative effects due to their lower mechanical strength than leftover concrete and natural aggregates (J. Yang et al., 2011). Furthermore, when RAs are produced from a heterogeneous mixed waste source made up of a variety of components, poor selection and cleaning could also result in the presence of minor harmful components (such as asphalt, gypsum, glass, etc.) which may cause detrimental effects (expansions or alkali silica reactions). Lastly, as already discussed, the negative impact from AM content and composition needs to be directly considered. From the previous literature, it is well-known that the final mechanical properties of concrete (mechanical strength, durability) show a declining trend with the increase in the AM content (de Juan & Gutiérrez, 2009; J. Kim, 2022; Seo & Choi, 2014). In this regard, **Chapter 4. "CDW as coarse and fine recycled aggregates, evaluating their impact on the microstructure of concrete from X-ray powder diffraction and X-ray computed tomography"** will present a practical testing in the field of recycled concrete production and RAs quality control using XRPD. Different samples from coarse, fine, and ultra-fine RAs are used to substitute natural aggregates in a fixed proportion. A comparison is then

conducted between the obtained values and the macroscopical and microscopical features in the recycled aggregate concrete.

1.3.1. X-ray Powder Diffraction as a tool to leverage circularity

The information on the composition of CDW can be obtained using different approaches, at different scale levels, from the bulk chemical (typically using X-ray fluorescence analysis) to the petrographic description (from optical and electron microscopy) and also from the mineralogical point of view. From a mineralogical perspective, X-ray powder diffraction (XRPD) analysis is employed to identify the crystalline mineral phases within CDW. This technique provides essential information on the types of minerals present, which can influence the material's behavior in environmental and recycling contexts. XRPD data can be further refined through Quantitative Phase Analysis (QPA) using Rietveld refinement, a method that allows for precise quantification of the mineral phases. This level of analysis is especially valuable in assessing the CDW's suitability for reuse, as specific mineral constituents may impact the material's stability, reactivity, and environmental performance. The instrument used within the present thesis is a Bruker D8 Advance Da Vinci diffractometer manufactured by Bruker AXS GmbH (Karlsruhe, Germany), available at the Department of Physics and Earth Science of the University of Ferrara (**Figure 5**). The instrument works with a CuK X-ray tube source, a LynxEye XE 1D array detector, a Ni filter, and a Bragg-Brentano – configuration. The XRPD process begins with the collection of the X-ray diffraction pattern, all the data that will be discussed in the present thesis are collected in the 2θ range of 5-90° at room temperature. Within the goniometer range the measure is registered at each 0.02 step (θ) for a time of 2 or 3 seconds, depending on the expected resolution. The entire measurement takes from 2 hours to 3 hours to be completed. It is worth mentioning that for industrial purposes and practical applications which differ from research aims it is possible to achieve satisfactory results in less than half an hour. Furthermore, through the continuum developments of the hardware and software components this time is progressively reducing. The instrument used holds an automatic variable divergence slit which is an additional component that automatically controls the vertical width of the X-ray beam before it reaches the sample. The setting used is a fixed irradiated length mode, where the slit width is automatically adjusted to maintain a constant irradiated length of 15 mm on the sample surface as the 2θ angle increases. Variable slits help obtain high-quality diffraction patterns with reduced background from air scattering especially in the low 2θ angular range. This portion of the diffraction patterns provides

unique information on sometimes poorly crystalline mineral phases characterized by large *d*-spacings (e.g., clay minerals). As the X-rays interact with the crystal lattice of the sample, they are diffracted according to Bragg's Law ($2d \sin\theta = \lambda$), producing a series of peaks. Each peak corresponds to a specific set of crystallographic planes with given *d*-spacing, and the 2θ position (hence the *d*-spacing) and intensity of these peaks provide a unique fingerprint for each crystalline phase present in the material. After collecting the raw diffraction data, it is essential to process it before phase identification. The software integrated with the instrument automatically processes the raw data into a plot of intensity versus 2θ. The resulting clean pattern enables easier identification of peak positions. Each crystalline phase has a characteristic pattern of peaks that occur at specific angles and intensities. By carefully analyzing the pattern, it is possible to distinguish between various phases that might be present in the sample. Phase identification was carried out with DIFFRACT.EVA v. 6.0.0.7 suite utilizing the Powder Diffraction File (PDF-2) database maintained by the International Centre for Diffraction Data (ICDD).

Figure 5. *Bruker D8 Advanced da Vinci diffractometer.*

The Rietveld approach for QPA is a widely used method to determine the weight percentage of the crystalline phases present in a material using XRPD data. Named after the Dutch scientist Hugo Rietveld, this technique involves a least-squares fitting of an XRD pattern to a calculated pattern based on known crystal structures. The QPA method is particularly effective for multi-phase samples and allows for the precise quantification of each phase in a mixture. To conduct the Rietveld QPA, high-quality XRPD data is collected. This diffraction pattern consists of peaks corresponding to the crystalline phases in the material. Next, structural models of the anticipated phases, including atomic positions, unit cell

parameters, and space groups, are input into the Rietveld software. The one used in the present thesis is TOPAS 5.0. These models are typically sourced from crystal structure databases such as the Inorganic Crystal Structure Database (ICSD) or the Crystallography Open Database (COD). For each phase, a scaling factor $\boldsymbol{S}$ is refined, which is proportional to the amount (weight fraction) of that phase in the sample, provided that the mass absorption of the mixture (typically unknown) is taken into account. These scale factors are optimized during the least-squares reiterations to minimize the difference between the calculated and observed diffraction patterns. The scale factor for each phase is used to calculate its weight fraction relative to other phases. The weight fraction $\boldsymbol{W_k}$ of a phase **k** in a sample with multiple phases is determined using the following **Equation (1)**:

$$W_k = \frac{S_k Z_k M_k}{\sum S_i Z_i M_i} \quad (1)$$

Where:

- S_k is the scale factor for phase k.
- Z_k is the number of formula units per unit cell for phase k.
- M_k is the molecular weight of the formula unit of phase k.
- The summation in the denominator is carried out over all phases present in the sample.

The Rietveld method employs a least-squares fitting approach to refine the scale factors, along with other structural and instrumental parameters, to minimize the residual differences between the observed and calculated diffraction patterns. By iteratively adjusting parameters, the method ensures that the calculated diffraction pattern best matches the observed data, thus yielding reliable phase fractions. After completing the refinement process, the software calculates the relative quantities of each phase, expressed as weight fractions (wt. %). The quality of the fit is then evaluated using factors such as the R-factor and goodness-of-fit (GOF). Smaller residuals between the observed and calculated patterns indicate an accurate fit, suggesting reliable quantification. The Rietveld method has several advantages. It allows for precise quantification, can handle overlapping peaks, and can even estimate amorphous content by including an internal standard. It is also versatile, being useful across a wide range of fields, from cement analysis to mineralogy and pharmaceutical quality control. However, it does have some limitations. The technique depends on accurate structural models, and the quality of the XRD data and sample preparation can influence the reliability of the results. Moreover, the refinement process is computationally demanding, although modern software has streamlined this aspect considerably.

1.3.1. The introduction of the *pseudo-density* parameter

Following XRPD analysis and QPA analysis, the whole crystalline assemblage of RAs under analysis is defined. This fingerprinting framework enables the introduction of a novel parameter termed "pseudo-density." This parameter is derived from weighted, tabulated physical attributes of minerals and does not directly reflect the actual density of the RAs being analyzed. The proposed method employs the weight percentages (wt%) of identified crystalline phases, extracted from QPA and normalized to unity (unity ($wt_{(i)}$), as parameters for **Equation (2)**. The parameter is then calculated based on the weighted mean of tabulated densities of the crystalline phases found after XRPD for natural minerals, clinker minerals and cement hydration and ageing product, as reported in the literature (ρ_{tab}).

$$p_{pseudo} = \sum_{i=1}^{n} \frac{wt_{(i)} * \rho_{tab}}{N} \quad (2)$$

The p_{pseudo} parameter can be adopted to perform various possible model reconstructions of crucial macroscopical features of the RAs, which describe main impactful properties of these secondary raw materials. Although the calculated values differ from the measured densities of the RAs, the proposed parameter not only provides a single value representing the average mineralogical composition but also introduces information that accounts for the crystallochemistry of phases. In fact, the density of crystalline phases obtained from the literature are typically calculated from the unit cell dimensions from X-ray diffraction data (Balonis & Glasser, 2009). This is generally done following **Equation (3)**:

$$\rho_{tab} = \frac{Z \cdot M}{N_A \cdot V} \quad (3)$$

Where:

- Z is the number of formula units per unit cell
- M is the molar mass of the compound (g/mol)
- N_A is the Avogadro's number (6.022 x 10^{23} atoms/mol)
- V is the volume of the unit cell (cm^3), obtained from XRD data

Therefore, when conducting a weighted mean of the tabulated density obtained from a QPA, we also introduce the contribution of the molar mass of each crystalline compound, its unit cell volume, and of each chemical species present in the lattice.

The method has therefore been tested in different scenarios, which will be presented in detail in the following chapters, using various tailored mineralogical models designed to predict specific properties and ultimately improve the final design of building materials encompassing secondary raw materials obtained from CDW.

To briefly present and introduce the potential applications of the proposed parameter and its effectiveness in monitoring CDW properties, different p_{pseudo} values have been calculated from the QPA results made available in a previous study (Galderisi et al., 2023). The samples were manually sorted into six groups enriched in natural stones (NS), concrete (CO), tiles (TI), bricks (BR), perforated-bricks (PF), and roof-tiles (RT). The investigated CDW has a broad mineralogical composition, although it remains homogenous within the samples. Each CDW group was first washed to remove fines and impurities and then dried. Afterward, the six groups were used to prepare 13 different samples of RAs by combining 50 wt.% natural aggregates with 50 wt.% of each of the CDW sample, introducing also reference samples with 100% natural aggregates and 100% RAs. The obtained groups were then crushed and sorted to obtain a Fuller grain-size distribution. The same cement type (CEM I 42.5 R) was used to prepare 13 mortars specimens. The absolute and relative contents of aggregates, cement and water can be found in (Galderisi et al., 2023). The mortars have been then tested after 28 and 91 days for the compressive and flexural strengths, ultrasonic pulse velocity, electrical resistivity and dynamic modulus of elasticity. The values obtained of p_{pseudo} values were therefore correlated with the results of the physical and mechanical testing conducted on the mortars. The results show a good correlation with all the aforementioned properties, with R^2 values from 0.58 to 0.87 (**Figure 6**).

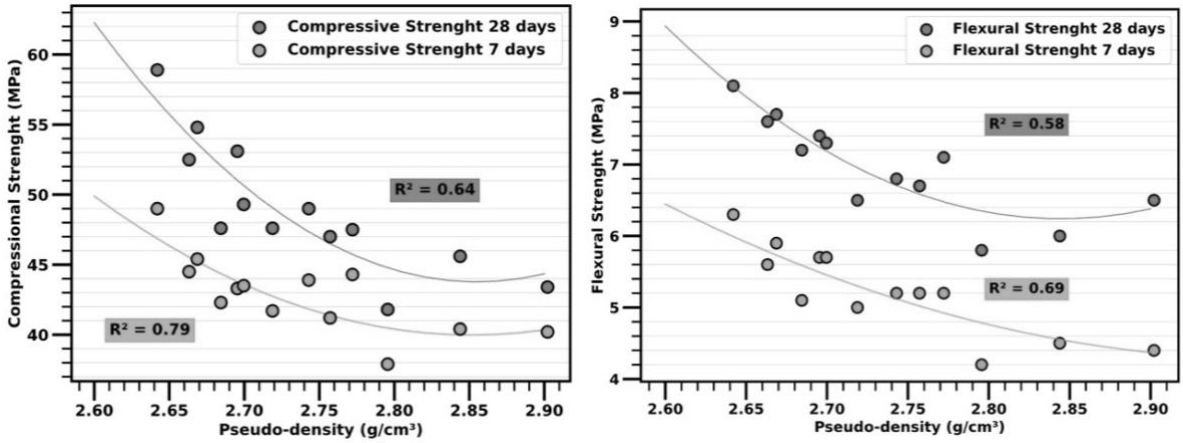

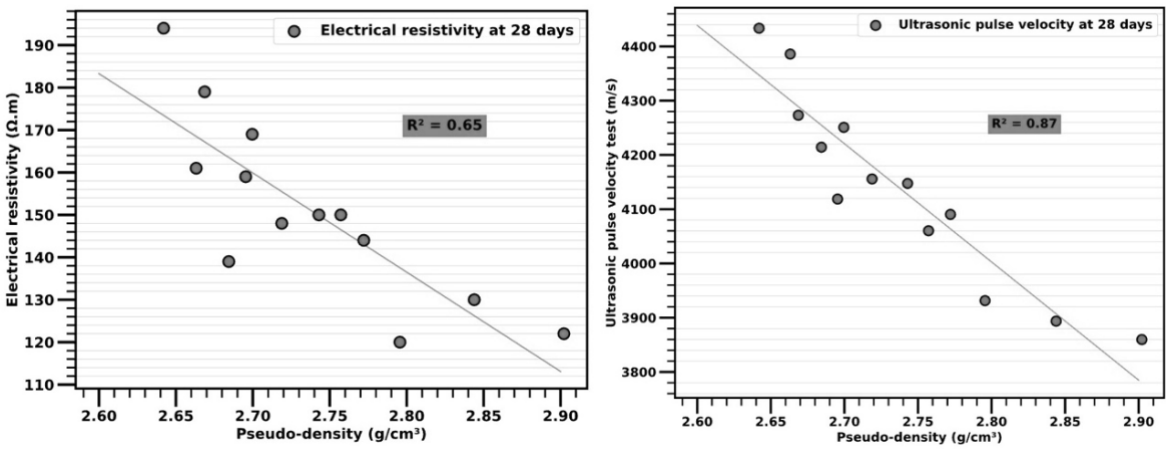

Figure 6. *Comparison of the pseudo-density parameters with the mortars' properties.*

A comparison is made between the measured density of the RAs, determined using a pycnometer, and the p_{pseudo} calculated for the same samples following QPA, as shown in (**Figure 7**). Although there is a strong correlation between the two measurements ($R^2 = 0.81$), an inverse relationship is observed. Specifically, as the measured density increases, the calculated pseudo-density tends to decrease.

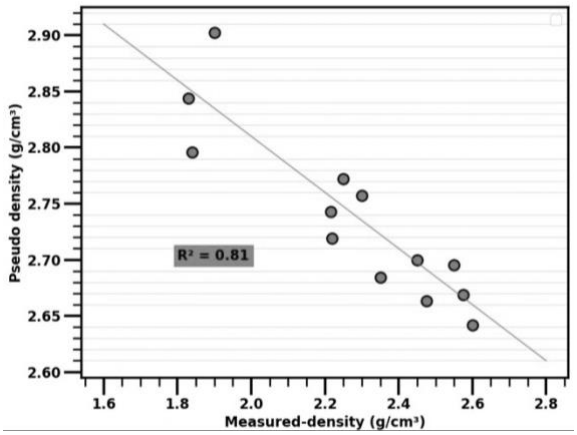

Figure 7. *Scatter plot of measured density vs pseudo-density of RAs.*

The measured density contains a physical information regarding the volume of solids, porosity and inter-particle volume. Instead, the p_{pseudo} relies only on the average crystallochemistry of the phases, without considering any physical constrain and amorphous content (**Figure 8**). Therefore, the results in **Figure 7** can be interpreted in light of this last condition. Materials with lower packing density have on the other hand a high average crystallochemistry density. At the same time the materials with higher-packing density have a lower average crystallochemistry density. The first group includes man-made minerals and building materials that have undergone sintering process. These products are often specifically designed to be light (less than 2.0 g/cm^3), but they also develop greater porosity

despite being composed of extremely heavy crystalline products (quartz 2.65 g/cm^3, mullite 2.7 g/cm^3, alumina 3.9 g/cm^3, zirconia 5.68 g/cm^3). In the same group, we also have pure clinker cement (anhydrous powder) which has a measured density of 1.44 g/cm^3 despite having an XRPD mineralogical composition mainly made of C_3S, C_2S, C_3A, C_4AF, with respective densities of 3.2, 2.98, 3.02, 3.70 g/cm^3 (ρ_{tab} from Balonis & Glasser, 2009). On the opposite end of the distribution, we have natural stones, whose measured density is very close to the p_{pseudo} value. In fact, the measured density for the gravel studied in Galderisi et. al (2023) is of 2.65 g/cm^3, and its mineralogical composition, consisting of silicates rock forming mineral is close to this value (quartz 2.65 g/cm^3, feldspar 2.56 g/cm^3, micas 2.7 g/cm^3). Between of these two end-members, we find concrete and mortars which are typically made from a combination of both groups. They have measured density ranging from 2.1 to 2.5 g/cm^3 mixed CDW. Depending on the amount of cement paste (which can range from 20 to 70% depending on the mix-design) they are distributed more or less toward the first group. In this conext, RAs and CDW can be described based on this condition, emphasizing that it does not respond directly to any physical density of the material. To conclude, p_{pseudo} represents a novel parameter, aiming to establish a tool derived from rapid XRPD screening. This parameter enables the swift classification of RAs materials, both pre- and post-recycling treatments, which can be used to model and describe various engineering properties and macroscopic features. By providing such insights, p_{pseudo} may contribute significantly to circular economy practices.

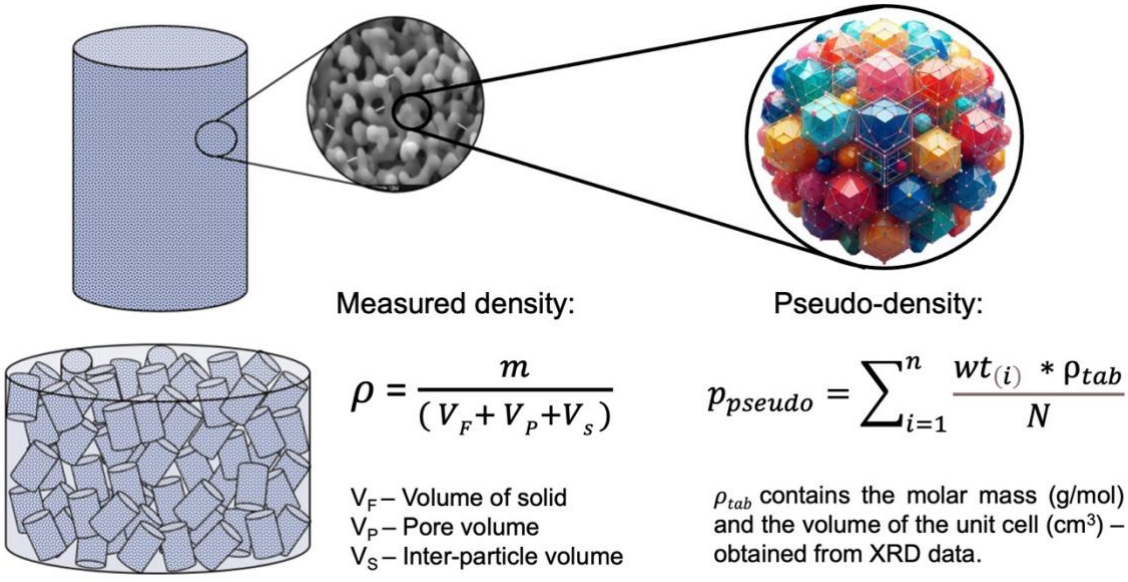

Figure 8. *Comparison of measured and pseudo-density.*

2. Geochemical analyses, leaching and risk-assessment of CDW based on multivariate statistical analysis and machine learning

Abstract

Managing construction and demolition waste (CDW) poses serious concerns regarding landfilling and recycling because of the potential release of hazardous elements after leaching. Ceramic materials such as bricks, tiles, and porcelain account for more than 70% of CDW. Fourteen samples of different CDW products from Ferrara (Northeast Italy) were subjected to geochemical analyses, including leaching tests, in accordance with UNI EN 12457-2. The interaction between ceramics and concrete was examined, highlighting the influence of mixed environments on the leaching behavior. Results were compared with an extensive database of more than 150 samples collected from the literature on different CDW types worldwide. Multivariate statistical analysis and machine learning were used to classify the CDW compositions based on the bulk chemical data. Various metrics—contaminant factors (Cf and Cd) and hazardous quotients (HQ and HQm)—were introduced to quantify the key environmental hazards of leachates. The results of this study underscore the potential of the proposed approaches in automating CDW classification and predicting Cf and HQ using only the starting bulk chemical composition. The findings enhance CDW management practices and support sustainability efforts in the construction industry.

Keywords: Construction and demolition waste; Ceramic; Leaching; PCA; Machine Learning.

The data contained in this chapter are part of a Full-Length Article under review in Waste Management, Elsevier (since 30th September 2024) – Manuscript Number: WM-24-2901:

"Classification and predictive leaching risk-assessment of construction and demolition waste (CDW) through multivariate statistical and machine learning analyses."

A. Bisciotti[a,*], V. Brombin[a], Y. Song[b], G. Bianchini[a], G. Cruciani[a]

[a] *Department of Physics and Earth Science, University of Ferrara, Via Saragat 1, 44122 Ferrara, Italy.*

[b] *Department of Civil and Environmental Engineering, Physics of AmoRphous and Inorganic Solids Lab (PARISlab), University of California Los Angeles, 520 Portola Plaza, Los Angeles, CA, 90095, USA.*

2.1. Introduction

European and Mediterranean countries frequently use considerable amounts of ceramic materials in construction projects (Caro et al., 2024). Ceramics in construction encompass a diverse array of materials and applications, each contributing to the efficiency, durability, and safety of building environments (Vidak Vasić et al., 2024). At the end of their life cycle, these building materials are typically demolished and collected together with other by-products such as concrete, wood, metals, glass, and plastics. The agglomerates of these materials are referred to as construction and demolition waste (CDW). Although CDW products are usually heterogeneous over time across space (Galderisi et al., 2022), they are usually composed of more than 70% mixed concrete and ceramic products (Gálvez-Martos et al., 2018b). At the same time, the proportions of these constituents and the different types of ceramics found may vary abundantly, with different potential impacts on the environment at the end of their life cycle. Because of the enormous quantity and intricate nature of CDW, achieving accurate and effective management of this waste poses major challenges (Hossain et al., 2017). When CDW is disposed of in landfills or reused in construction (as recycled aggregates), hazardous elements (*e.g.*, V, Cr, Cu, Ni, and Pb) following interaction with rainfall can leach out and pollute the surrounding aquifers, representing a potential threat to the environment (Saca et al., 2017). Hence, the environmental impact is determined not by the total amount of pollutants in the bulk materials but by the dissolvable portion that water can transport (Prieto-Espinoza et al., 2022). It is therefore necessary to assess the environmental risk of CDW with respect to the release of potential pollutants (Diotti et al., 2020). Nevertheless, different degrees of impact are expected from the interaction between solid waste and water, depending on the bulk chemical composition of the former (López and Lobo, 2014). The leaching behavior and contaminant release from CDW have been extensively studied (Abedin Khan et al., 2024; Diotti et al., 2021) with a focus on concrete-based materials (Engelsen et al., 2009, 2010a) or on mixed CDW products, including ceramic, bituminous, and other variable fractions (Barbudo et al., 2012; Butera et al., 2014). However, investigations into the individual leaching of the most common CDW ceramic constituent are still lacking. Standardized column leaching tests typically require different days of laboratory work to accurately evaluate the leaching behavior (Ershadi et al., 2023), thereby limiting the possibility of conducting a preliminary risk assessment and defining the most appropriate CDW management strategies on site.

The introduction of machine learning (ML) algorithms and artificial intelligence has the potential to address various challenges in waste management and drive significant

advancements in this field (Abdallah et al., 2020). Various models, such as artificial neural networks, convolutional neural networks, and support vector machines, can analyze and interpret massive volumes of data, including waste creation trends, project specifics, and environmental considerations (Lakhouit and Shaban, 2024). In the realm of CDW, ML is used in the following four primary areas: waste generation, on-site handling, transportation, and disposal practices (Gao et al., 2024). Waste generation focuses on predicting and estimating waste volume (Maged et al., 2024). On-site handling involves addressing automated identification, categorization, and recycling methods (Nežerka et al., 2024; Z. Wang et al., 2020). The transportation system establishes pathways and routes for the optimal movement of materials (Bi et al., 2022). Disposal practices determine the most beneficial disposal management options based on the success of recycling or, alternatively, landfill disposal (Sarc et al., 2019; Wu et al., 2023). In these areas, computer vision is the most explored technology because photographs are easy and inexpensive to collect and are suitable for analyses (Lu and Chen, 2022). However, the composition of CDW is complex and difficult to extrapolate through a "simple" visive approach. For this reason, we used the chemical composition as the input for ML to identify CDW. In this way, ML enables high-throughput screening of CDW, allowing authorities to proactively respond to waste creation and disposal concerns (Hossain et al., 2017; Imam et al., 2024). For example, ML can provide information about the potential release of contaminants from solid waste products, which is directly influenced by the chemical composition of the waste. The adoption of ML models for forecasting leaching values from municipal solid waste has only recently gained attention (Z. Liu et al., 2022; C. Zhang et al., 2023). Testing in the CDW sector could provide a faster and more efficient method with important practical implications for the management of waste and recycling materials (Ershadi et al., 2023).

In the present research, 14 samples of different CDW types were collected from a municipal landfill in Ferrara (Northeast Italy), covering the most common building materials (tiles, bricks, porcelain, stoneware). To expand the database and better highlight the influence of the mixed environment with residual cement, all samples were also tested after mixing with concrete waste. As an extension of the experimental investigation, the results of the in-deep geochemical characterization of the samples were compared with those of more than 100 individual CDW samples from the literature using traditional multivariate statistical analysis (principal component analysis [PCA]) and novel ML methods (t-distributed stochastic neighbor embedding [t-SNE]) to assess the most effective approach for classifying CDW. A leaching test was also performed on all the samples to measure the concentration of the released chemical species and compare the results with those from similar studies in the

literature. The results were used to train an artificial neural network to classify the samples according to their composition and predict their leaching behavior and risk assessment for the environment.

2.2. Materials

Fourteen samples of different CWD products were sampled from stockpiles of landfilled materials in authorized recycling facilities in Ferrara city (Northeast Italy; **Figure 9**). To encompass the most common products found in CDW, the sample set in this study includes the following: (i) seven different full brick samples (BR1–BR7); (ii) one sample of ceramic perforated brick (LF1); (iii) one sanitary ware porcelain (PO1); (iv) two tiles with inorganic painting pigments (TL1 and TL2); (v) one sample of stoneware (GR1); (vi) one roof tile (RF1); and (vii) one sample of concrete (CON). For each material, at least 20 kg was collected, following the standard UNE-EN 932-1 (1998). The samples were then homogenized and reduced using the quartering methods (UNE-EN 932-2, 2000). All materials were crushed into fine powder (<100 μm) for geochemical analyses and leaching tests to ensure adequate particle liberation. In addition, each sample was mixed (1:1) with CDW concrete powder to mimic composite samples and the mixed disposal conditions during landfilling. To create these composite samples, 1 g of each CDW sample was mixed with the same aliquot of concrete by automatic planetary ball milling to obtain a homogeneous sample.

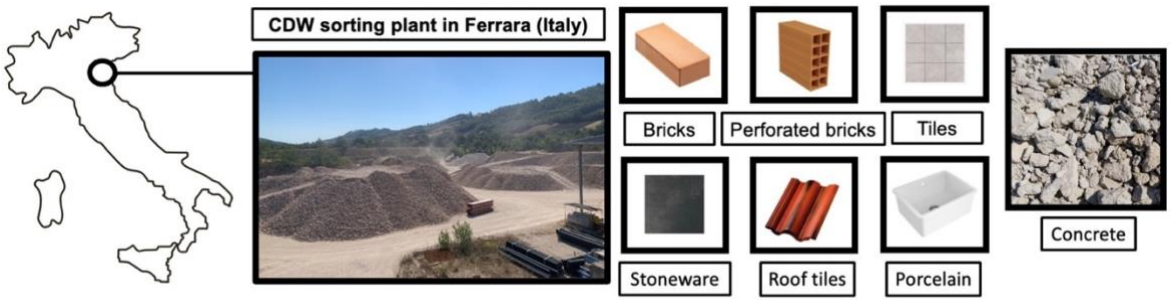

***Figure 9**. Provenance and types of CDW materials included in this study.*

2.3. Methods

2.3.1. Major and trace element characterization

Bulk major and trace (Ba, Co, Cr, Cu, Ga, Ni, Sc, V, and Zn) element concentrations of the collected and mixed samples were determined by wavelength-dispersive X-ray fluorescence spectrometry (XRF) on pressed powder pellets using an ARL Advant-XP+ spectrometer.

The concentrations of the aforementioned major and trace elements always exceeded 50 ppm, making the XRF determination fully reliable and not requiring further time-consuming inductively coupled plasma–mass spectrometry (ICP–MS) analyses with these elements. Volatile contents were determined as loss on ignition (LOI) at 1000°C. For the determination of other trace elements (Rb, Sr, Zr, Nb, Th, U, Li, Be, B, As, Se, Mo, Ag, Cd, Sn, Sb, Te, Tl, Pb, Bi, and other rare earth elements), sample powders were completely digested using a mixture of HF and HNO_3 and analyzed by ICP–MS using an iCAPTQ Thermo Fisher Scientific instrument.

2.3.2. Leaching procedure

Leaching tests were performed on the powder (<100 μm) of each CDW and mixed sample, following a leaching protocol modified from UNI EN 12457-Part 2 (2004) and reported by Bianchini et al. (2020) and Galderisi et al. (2022). Briefly, for each sample, 1 g of powder was soaked in 10 ml of deionized water for 24 h (Liquid–Solid ratio 10:1; L/S 10), during which the temperature and pH of the leachates were monitored. The mixtures were then centrifuged at 4000 rpm for 10 min to separate the solid particles and filtered at 45 μm (Minisart®NML syringe cellulose acetate filters). The major cations (Na, Mg, K, and Ca) and trace elements (Li, B, Al, P, Sc, Ti, Ba, V, Cr, Fe, Co, Ni, Cu, Ga, As, Se, Rb, Sr, and Mo) in the leachates were analyzed by ICP–MS using an iCAPTQ ThermoFisher Scientific instrument. The concentrations of major anions (Cl, NO_3, and SO_4) were measured using an isocratic dual-pump ion chromatography (IC) ICS-1000 Dionex equipped with an AS9-HC 4 × 250 mm anion column, AG9-HC 4 × 50 mm guard column, ADRS600 suppressor, and AS-40 autosampler. Accuracy and precision, based on the repeated analyses of standards and certified reference materials, were better than 10% for all the considered parameters.

2.3.3. Hazard and environmental threat assessment

Several distinct metrics were used to quantitatively evaluate the hazardous potential of the elements released into the environment. The contamination factor (C_f) provides a comparison of the leachate concentration and the concentration of the same species in an uncontaminated environment (Dong et al., 2021; Hakanson, 1980). C_f is calculated by dividing the concentration of each leachate by its background concentration in the uncontaminated water/sediment, as follows (Dong et al., 2021; Hakanson, 1980):

$$C_f = \frac{Conc.measured}{Conc.background} \quad \textbf{(4)}$$

In this study, we used the average concentration from a saline coastal aquifer in the Po River lowland (Italy), near Ferrara (Colombani et al., 2015), as the background concentration. The overall degree of pollution in the environment is indicated by the contamination degree (C_d), as defined by the Eq. (2) of Abrahim and Parker (2008), which was modified by Hakanson (1980) as follows:

$$C_d = \frac{\sum_{i=1}^{n} C_f^i}{n} \quad \textbf{(5)}$$

where C_f is the contamination factor calculated using Eq. 1 and n is the number of chemical species. The C_d values were categorized as follows: C_d 1.5–2 = low contamination; $2 < C_d < 4$ = moderate contamination, $4 < C_d < 8$ = high contamination; $8 < C_d < 16$ = very high contamination; and $C_d > 16$ = extremely high contamination.

The hazard quotient (HQ) compares the leachates with the leaching thresholds specified by specific laws or national legal limits (Ardit et al., 2022) and can be calculated using:

$$HQ = \frac{Conc.\ measured}{Conc.limit} \quad \textbf{(6)}$$

For the concentration limits, we employed the new Italian End of Waste decree (September 2024) for the reuse of recycled CDW materials (D.M. n. 127/2024). The permissible limit is exceeded when the HQ value exceeds unity. A similar approach to that adopted by Abrahim and Parker (2008) was used for HQ. Similar to C_d, the mean value is calculated to obtain HQ_m as follows:

$$HQ_m = \frac{\sum_{i=1}^{n} HQ_i}{n} \quad \textbf{(7)}$$

where n is the number of chemical species. If the calculated value exceeds the unitary value, the waste is not suitable for nonharmful waste classification.

2.3.4. Multivariate analysis for compositional data analysis

A matrix (N × M) with 165 samples (N; *i.e.*, 138 samples from the literature + 27 samples of this study) and 11 major oxide concentrations (M, in wt.%) from wavelength-dispersive

XRF was generated for multivariate analysis. The constant sum problem of the composition data was addressed using the Aitchison approach (Aitchison, 1990; Aitchison and Egozcue, 2005). Starting from raw data, the variables for the compositions were transformed into centered log ratio using CoDaPack 2.03 software (Comas and Thió-Henestrosa, 2011). The raw chemical dataset was then analyzed by PCA using Prism9 software as part of the GraphPad suite.

2.3.5. Machine learning t-distributed stochastic neighbor embedding

Using the tools provided by scikit-learn in Python (Pedregosa et al., 2011), t-SNE analysis was conducted to determine the major elemental compositions of the 165 samples. The t-SNE algorithm requires several input parameters, which are known as hyperparameters in ML. These parameters are set before learning; thus, they provide important control over the output. The most important parameter is perplexity (Van Der Maaten and Hinton, 2008), which represents the number of nearest neighbors considered by t-SNE when converting pairwise similarities (affinities) of data points into probabilities (Van Der Maaten and Hinton, 2012).

2.3.6. Machine learning prediction of the key leaching metrics

An artificial neural network model was used to estimate the concentrations of key leachates and associated leaching metrics to investigate the potential of ML in predicting the leaching characteristics of various CDW products. The neural network was selected because it can effectively manage complex datasets and map nonlinear relationships (Gevrey et al., 2003). The input to the model consisted of the bulk chemical compositions of the major elements. The neural network model was also separately trained to predict key leaching parameters, including Cu, Cr, Ni, and V concentrations, as well as the C_d and HQ_m. Following the removal of incomplete or unqualified samples from the raw dataset, the curated dataset comprised 51 samples, including the 27 newly measured samples in this study. To evaluate the model's prediction accuracy, six concrete samples with varying CDW contents were randomly selected from the study cohort for testing: BR5 + CON, BR7 + CON, LF1 + CON, PO1 + CON, TL2 + CON, and RF1 + CON. The remaining samples were used for model training. The six testing samples were specifically selected to (i) assess the model robustness in predicting the leaching behavior of CDW within recycled concrete and (ii) ensure no data leakage between the training and testing sets regarding compositional

information. The modeling process was executed using the PyTorch library (version 2.0.0) in the Python environment (version 3.10.10) (Paszke et al., 2019). Unless specified later in this section, the modeling pipeline generally followed those of previous neural network-based studies (Y. Song et al., 2021, 2022; Y. Song, Zhao, et al., 2024). Given the limited size of the curated dataset, a simple neural network architecture with a single hidden layer of four neurons was adopted for modeling. Functional layers—batch normalization followed by rectified linear unit nonlinear activation—were added before and after the hidden layer. In addition, an adaptive moment estimation (Adam) optimizer and mean square error loss were adopted to train the model. For each prediction target, three key hyperparameters were optimized to maximize accuracy. First, the number of training epochs was fixed at 300 to ensure smooth model convergence. Two other hyperparameters, the learning rate (which controls the model's update rate) and weight decay (a regularization term to prevent overfitting), were fine-tuned using a brute force search. This exploration involved testing various hyperparameter combinations, with the optimal set selected based on its performance on a validation set, which comprised 20% of the training samples. Wide search ranges (10^{-5} to 10^{2} for the learning rate and 10^{-6} to 10^{-1} for weight decay) were employed to ensure optimal selection. The root mean square error (RMSE) was used as the primary performance metric for model evaluation. After training the model, a SHapley Additive exPlanations (SHAP) analysis was employed to elucidate the composition–leaching patterns captured by the neural network. For more information on the application of SHAP in materials science, readers are referred to previous studies on ML-based materials research (Y. Song et al., 2022; Y. Song, Lu, et al., 2024; Y. Song, Zhao, et al., 2024).

2.4. Results and Discussions

2.4.1. Bulk chemical composition

Samples were labeled and divided into three main groups: (i) ceramic (CER), which included samples of full brick (BR1–BR7); ceramic perforated brick (LF1); sanitary ware porcelain (PO1); tile (TL1 and TL2), stoneware (GR1), and roof tile (RF1); (ii) concrete (CON), which included the cement sample; and iii) mixed waste (MRA), which included the CER samples mixed with the CON sample in a 1:1 ratio. The bulk chemical compositions of the collected samples and the obtained mixtures of CDW and concrete are reported in **SUPPLEMENTARY TABLE I & TABLE II** . The XRF analysis of the materials of this study displays a considerable degree of variability in major oxides composition, even more

if a comparison is conducted with previous literature investigating CER, CON, as well as MRA (Alexandridou et al., 2014; Bianchini et al., 2020; Favaretto et al., 2017; Frías et al., 2020; Galderisi et al., 2022; Komnitsas et al., 2015; Limbachiya et al., 2007; Moreno-Pérez et al., 2018; Sabai et al., 2016). Positive or negative correlations between oxides in binary diagrams indicate the dominant mineralogy of the CDW materials (**Figure 10**). The CER samples were primarily silicate-based (SiO_2: 50–70 wt.%) and mainly produced from quartz and feldspar-bearing sands, whereas the CON samples had a calcium-based chemical structure (CaO: 35–50 wt.%), resulting from Portland cement binders, lime, and gypsum (Moreno-Pérez et al., 2018) (**Figure 10a**). As expected, the MRA samples were mainly clustered between these two end-members. However, near the CON samples, a CER (TL2) sample and an MRA (TL2 + CON) sample were also found. The CER (TL2) sample was a tile made of cementitious matrix, known as "*veneziana*," which was extensively used throughout the 20th century in residential buildings in Italy. the MRA (TL2 + CON) sample was a 1:1 mixture of the same tile and another material. Although it has the appearance of a tile, our classification of TL2 in the CER group was evidently incorrect because of the high percentage of CaO (38.26 wt.%) in its composition. In general, the increasing presence of carbonate and leftover cement paste from CER to MRA to CON is indicated by the positive correlation between CaO and LOI (**Figure 10b**). Enrichments of Al_2O_3 (12–25 wt.%) and alkalis such as $K_2O + Na_2O$ (3.5–6.0 wt.%) (**Figure 10c**) are characteristic of CER products because bricks and tiles are made from clay-based minerals (Vidak Vasić et al., 2024). In addition, the Fe_2O_3 content was higher in the CER samples (above 4 wt.%) than in the other groups (1–4 wt.%), despite the absence of a linear trend (**Figure 10d**). The high Fe_2O_3 content is likely due to the presence of minerals such as iron oxides and iron-bearing minerals, including clays such as chlorites (Dzene et al., 2022). A more extended discussion of the bulk chemical assemblage, including trace elements, is provided in the **SUPPLEMENTARY**.

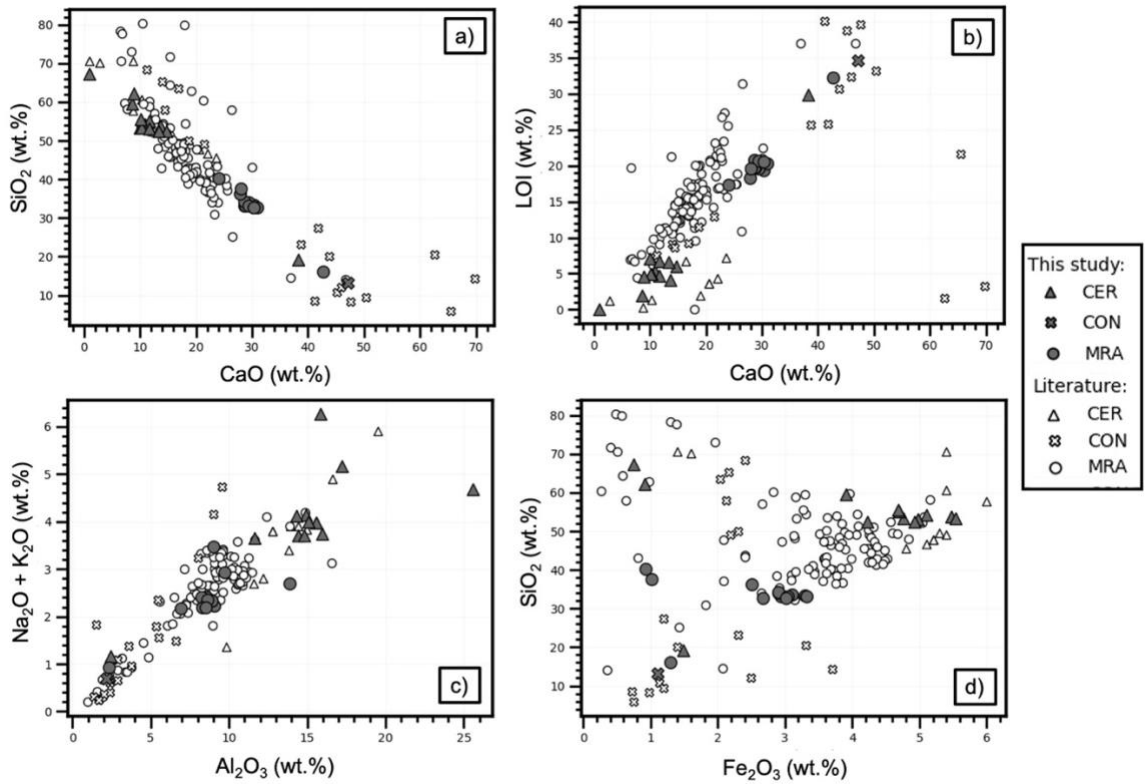

Figure 10. *Distribution of (a) CaO vs SiO_2, (b) CaO vs LOI, (c) Al_2O_3 vs K_2O + Na_2O and (d) SiO_2 vs Fe_2O_3 for the studied samples and for the data from the literature: Alexandridou et al., 2014; Bianchini et al., 2020; Favaretto et al., 2017; Frías et al., 2020; Galderisi et al., 2022; Komnitsas et al., 2015; Limbachiya et al., 2007; Moreno-Pérez et al., 2018; Sabai et al., 2016.*

The description conducted using the biplot in **Figure 10** can be summarized in the standard ternary plot diagram commonly used for geochemical data (**Figure 11**). It is noteworthy that similar patterns were observed when comparing the analyzed samples with the data from the literature. This suggests that CER and CON waste can typically be distinguished based on their bulk chemical composition, particularly the SiO_2-CaO-Al_2O_3 content (**Figure 11a**). Meanwhile, minor oxides, such as Na_2O + K_2O and Fe_2O_3 (**Figure 11b**), do not significantly contribute to the identification of the materials. Furthermore, it is evident that while this type of plot is effective for a general material description, it is not suitable for clearly distinguishing the MRA fraction, which commonly overlaps with the end-members. Additionally, it can be observed within the high-CaO field the presence of few outliers related to the MRA and CER samples (either from this study and from the literature). This condition may occur when composite construction materials, are attribute to an incorrect waste category (*i.e,* CER, CON, or MRA) due to their appearance rather than their chemical composition.

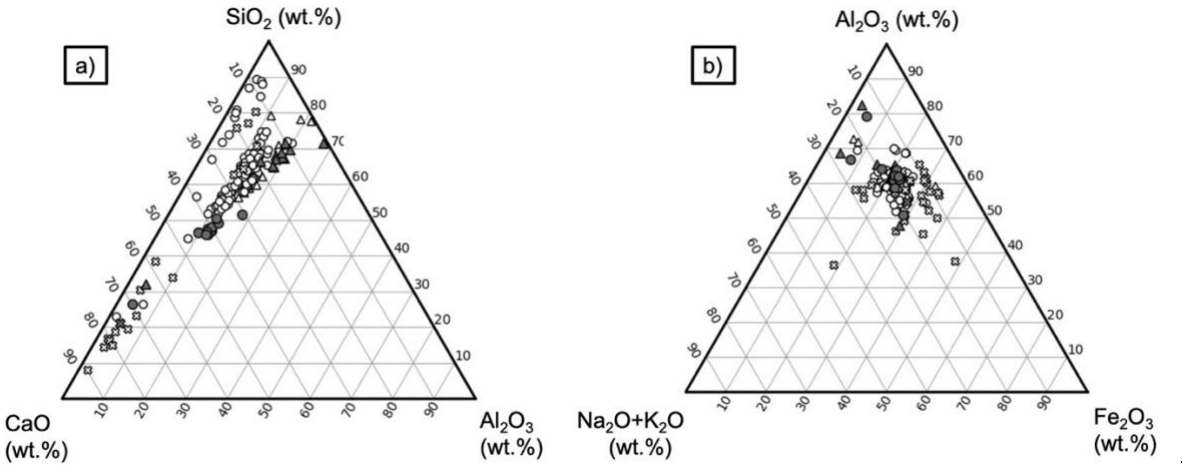

Figure 11. *Ternary plot for the CDW composition of samples of this study and from the literature, cited references, symbols and colors as in* ***Figure 10****.*

2.4.2. Trace elements composition

The trace element bulk composition of samples from this study are reported in **SUPPLEMENTARY TABLE I & TABLE II** and selected trace element (V, Cr, Co, and Ni) concentrations, typically contained in building materials and considered hazardous for human health, were plotted in **Figure 12**.

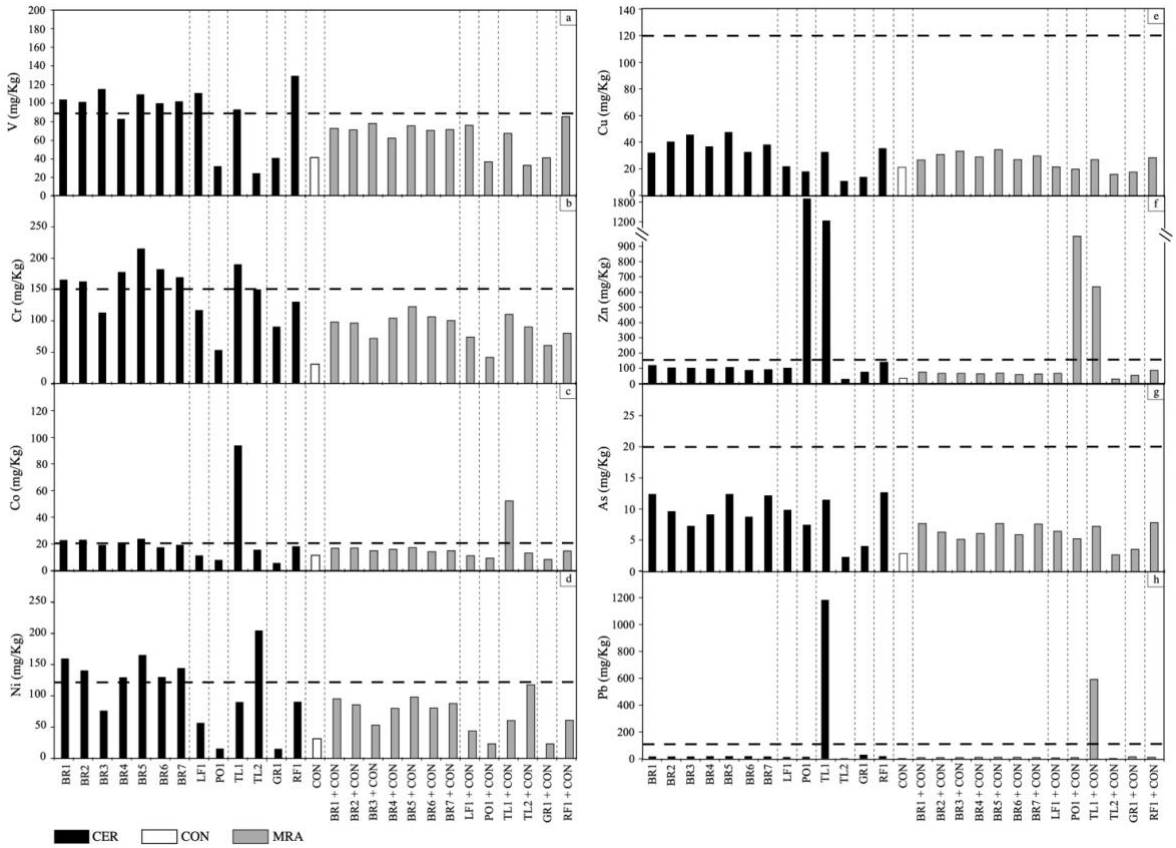

Figure 12. *Concentrations in mg/Kg of (a) V, (b) Cr, (c) Co, (d) Ni, I Cu, (f) Zn, (g) As, and (h) Pb of CER, CON, MRA leachates from this study. Dotted lines represent the Italian thresholds of the green areas (Italian Legislative Decree 152, 03/04/2006).*

Currently, there are no specific threshold values for solid waste. Therefore, to assess the potential risk posed by certain elements, their concentrations were compared with the Italian threshold values for soils in green areas intended for public and private residential use (Italian Legislative Decree 152, 03/04/2006). Most of the CER samples exceeded the Italian limits for vanadium (V), chromium (Cr), and nickel (Ni), indicating that these samples may pose a potential contamination risk. However, the high concentrations of V, Cr, and Ni do not necessarily indicate the presence of anthropogenic contaminants, as these elements naturally occur in the alluvial sediments of the Po River plain, which extends across Northern Italy, including the area around Ferrara. These sediments are rich in V, Cr, and Ni because the parent rocks in the Po River catchment contain mafic and ultramafic lithologies, which are naturally rich in heavy metals (Amorosi, 2012; Bianchini et al., 2012, 2013). These sediments are also used to produce raw materials in the region, potentially contributing to their presence in CDW. Additionally, painted tile sample TL1 exhibited particularly high concentrations of Co, Zn, and Pb, which were also recorded in the sample mixed with cement paste (TL1 + CON). The presence of Co and Pb in the tile sample can be explained by the use of artificial pigments rich in these elements (Bae et al., 2016; Maslennikova et al., 2006). Tile TL1 and porcelain sample PO1 are also rich in Zn, which is commonly used in tiles, sanitary ware, and decorative ceramics because it lowers firing temperatures and improves mechanical properties and surface quality (Mirhadi et al., 2012). However, it is important to note that these elevated concentrations represent only a potential risk to the environment and human health. The actual release of these elements depends on their mobility, which is why the concentrations of these elements were also analyzed in the leachates of the samples.

2.4.3. Principal Component Analysis

Following the PCA of the extended data, the contributions of PC1 (57.10%) and PC2 (13.61%) together account for >75% of the total variance within the dataset, where the lower acceptable value is usually >60% (Maćkiewicz and Ratajczak, 1993). The primary advantage of PCA, which is a linear dimensionality reduction technique, is that the variance between chemicals can highlight the enrichment of specific species. In fact, samples with high SiO_2 or CaO contents can be found at the extreme ends of the plots, providing an intuitive understanding of the chemical gradients. The PCA plot (**Figure 13a**) shows that the samples from this study are grouped into three main clusters within the entire literature data distribution. The three groups were associated with CON (upper left), MRA (central area),

and CER (lower right). The CaO and LOI variances affected the clustering of CON and cement-based CDW. Meanwhile, in the opposite direction, the second cluster was dominated by the SiO_2 variance of the CER materials. However, challenges arose when attempting to identify dominant chemical influences in the case of the MRA samples, where analysis was less definitive because of the compositional complexity associated with the remaining chemical species, which were scattered and distributed from a noisy central region of the plot. By including the contribution from PC3 (6.93%) in the PCA plot, the total proportion of variance was 82%. Therefore, it is necessary to also introduce a three-dimensional (3D) plot (**Figure 13b**), which provides a clearer representation of the sample distribution in Euclidean space. In this plot, the CON samples are located in the upper-back region, influenced by the CaO and LOI values, and are separated by a threshold around the value of 0 along PC3. The CER samples were directed from the center to the front right and controlled by SiO_2 and Al_2O_3. In addition, owing to the volumetric extension of the plot in the 3D space and the inclusion of the PC3 contribution, the MRA region (determined by the remaining chemical species) became more defined, substantially improving the clustering of the entire dataset, with CON and CER overlapping less.

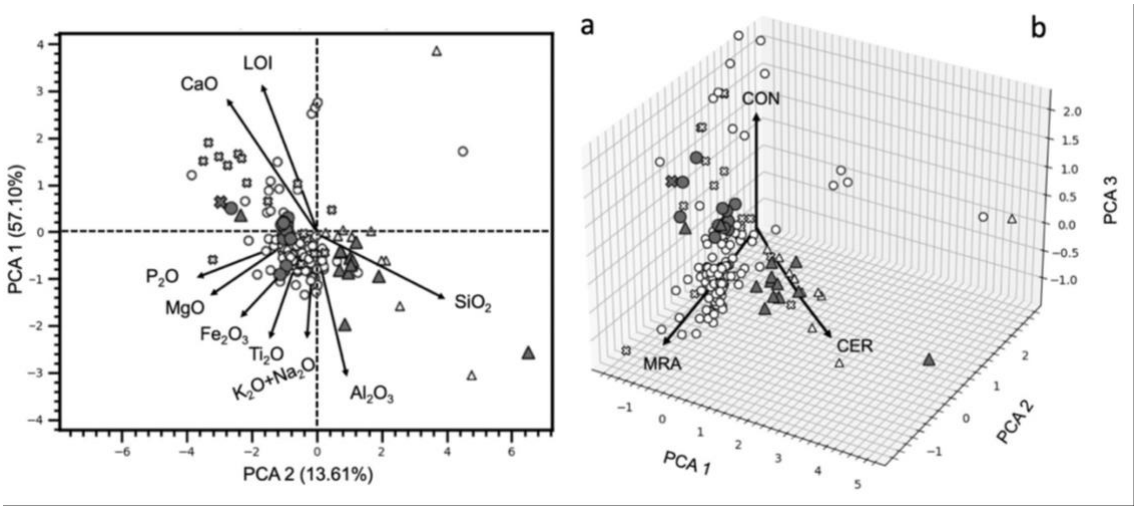

Figure 13. *Principal Component Analysis (a) 2D and (b) 3D plots of the CDW bulk composition of samples of this study and from literature. Cited references, symbols and colors as in* ***Figure 10****.*

2.4.4. t-SNE clustering

Similar to PCA and related multivariate data analysis techniques, t-SNE performs dimensionality reduction on an n-dimensional matrix using the bulk chemical composition of samples from this study and the literature. This allows the visualization of high-dimensional data in 2D space, which is represented by two variables simply termed t-SNE

variables 1 and 2. The stochastic nature of the t-SNE model means that multiple runs do not always produce the same pattern. However, for well-chosen input parameters, the resulting patterns are reproducible; thus, the t-SNE model yields robust results (Belkina et al., 2019). The approach was tested with different Perplexity (Perp) values (1, 5, 10 15, 30, and 50), which substantially changed the t-SNE visualization patterns (Wattenberg et al., 2016). The t-SNE performance was fairly robust to changes in Perp, with typical values ranging from 5 to 50 (Van Der Maaten and Hinton, 2008). The complete results are presented in the **Supplementary Information**. These results show that for Perp values in the range of 10–15, similar patterns were observed in the t-SNE visualizations. When Perp was <10, local variations within each cluster were dominant, and too many clusters were returned. Conversely, for Perp >15, the samples could not be separated into distinct clusters. A small Perp value should be used when the sample size is small. For the 165 CDW samples, a good Perp value should be 15 (**Figure 14)**. For Perp < 10, local variations within each cluster dominated, and too many clusters are returned. For Perp > 15, the samples could not be separated into distinct clusters. A small Perp value should be assigned when sample size is small. For the 166 samples of CDW, a good Perp value should be below 15.

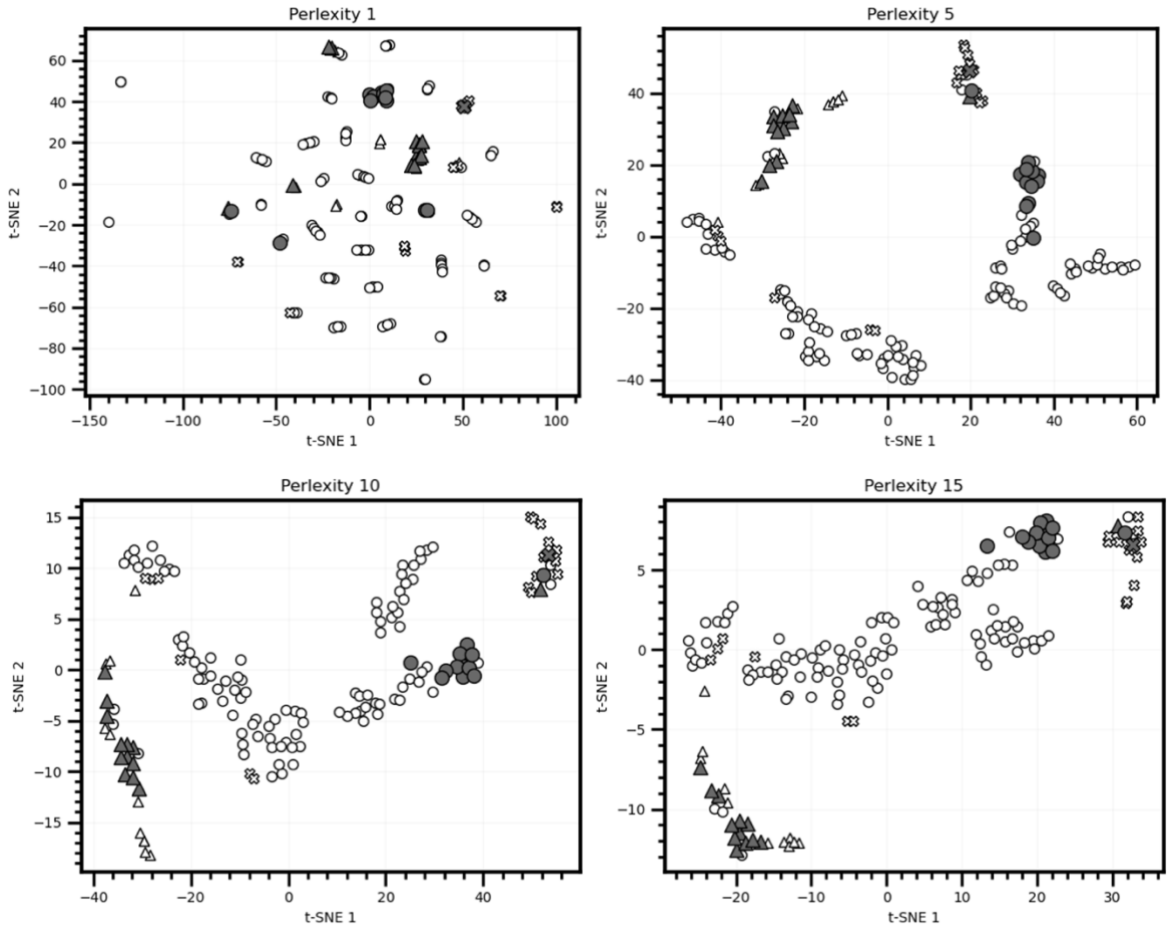

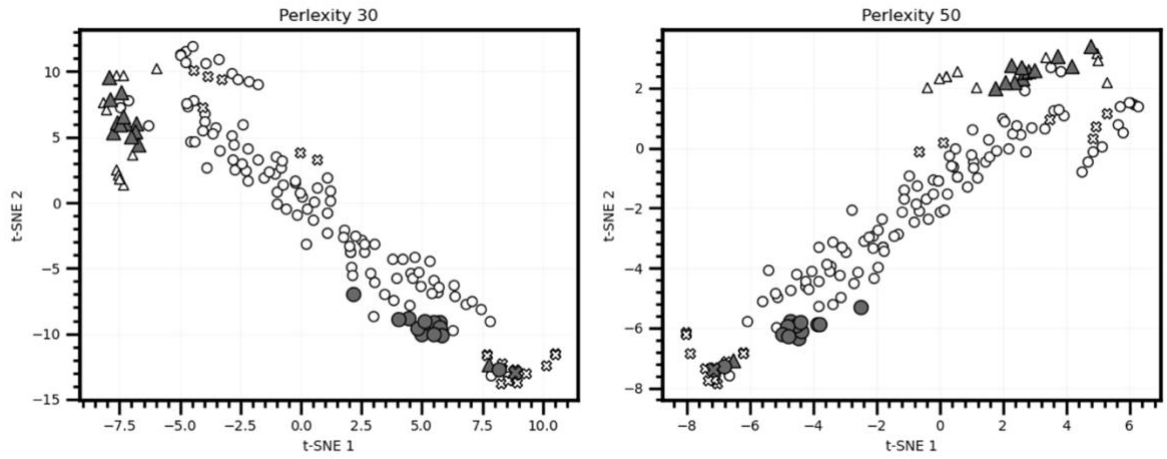

Figure 14. *t-SNE clustering of the chemical database with different perplexity factors of samples of this study and from literature, cited references, symbols and colors as in* ***Figure 10****.*

To obtain additional separation or details that might be missed in 2D projections, the t-SNE dimensionality was increased to three variables, thereby allowing for a 3D visualization. The Perp value was kept at 15, which was identified as the most performant. Clustering in 3D (***Figure 15***) facilitated the accurate separation of samples into distinct classes of CER, MRA, and CON. The first class is characterized by a well-delineated cluster of samples (upper left), all of which are related to the same species, with only a few outliers from the literature data. Most of the MRA samples are located in the center of the plot.

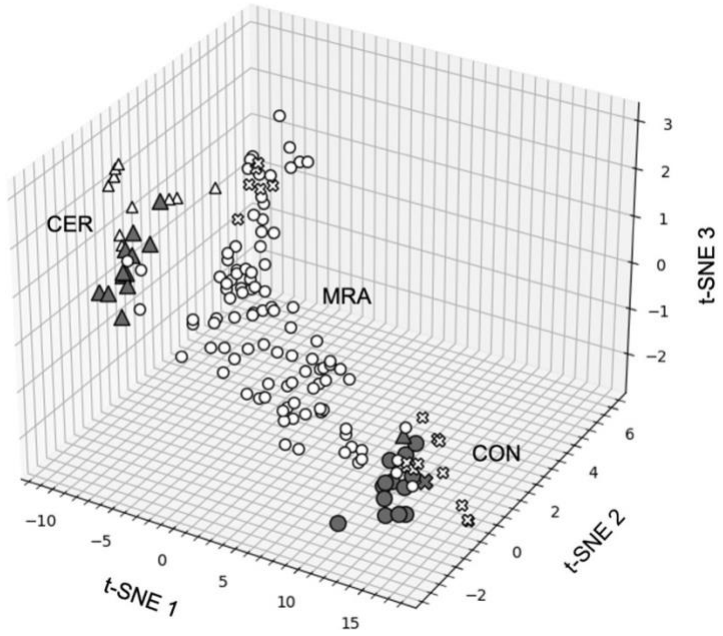

Figure 15. *3D t-SNE clustering using Perp. 15 factor of samples of this study and from literature, cited references, symbols and colors as in* ***Figure 10****.*

No outliers were found in this region outside the selected group. The lower-right portion of the plot shows CON- and high-grade cement-based materials. In this context, the MRA samples used in this study were categorized with the pure CON sample to ensure the correct interpretation of the data. Lastly, in the opposite direction (*i.e.,* in the upper-central portion of the plot), a group of CON samples from a previous study can be noted together with other MRA materials from the literature. A possible interpretation is that these products, although primarily made of CON, contain a low amount of leftover cement paste and are instead rich in natural aggregates (which usually accounts for 70% of total concrete volume). These aggregates have a silico-aluminate composition (*e.g.*, feldspars and quartz), resulting in a composition more similar to that of CER materials than to standard CON waste. Unlike PCA, t-SNE distinguished the CER and CON samples and isolated MRA outliers, suggesting that these outliers represent waste with high residual cement content. The t-SNE approach also accurately identified CER outliers, such as cement-based tiles, as evidenced in this study.

3.4.5. Leaching measurements

The size of CDW materials in landfills is highly variable, ranging from entire blocks to fine powder created by erosion due to prolonged exposure of CDW to atmospheric agents. It is well known that the release of potential contaminant elements is inversely proportional to the granulometry of materials. However, we investigated the worst-case scenario to assess the maximum potential release of chemical species (Diotti et al., 2021). Therefore, 24-h leaching tests of the 28 CDW samples were performed on powder (<100 μm). During the test, the pH values of the leachates were monitored (**Figure 16**). The CON stream was characterized by pH >10.5 (except for the cement-based tile *veneziana* sample), with the pH reaching 11.2 after 24 h. The CER materials had pH <10 (ranging from 7.8 to 9.6) and decreased after 24 h of leaching. The mixed CDW streams often recorded pH values higher than those of pure CER components and sometimes above those of the pure CON sample. The measured values ranged from 10.7 to 11.4, which could represent a serious hazard for humans and the environment because they enhance the mobilization of traces (Abedin Khan et al., 2024).

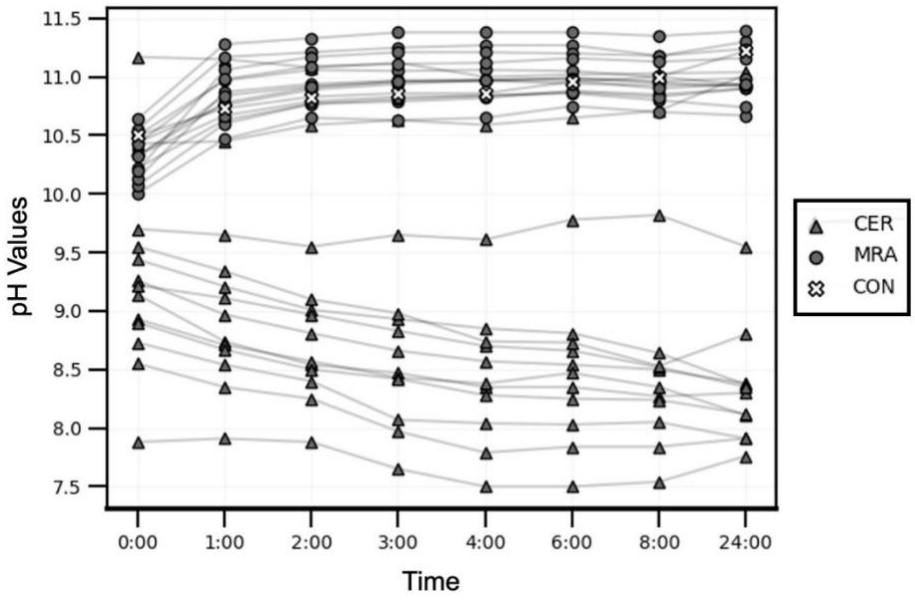

***Figure 16**. pH values of samples of this study monitored over 24 hours of leaching test*

Building materials contain trace elements that pose potential hazards to both the environment and human health. According to the data presented in **SUPPLEMENTARY TABLE III & TABLE IV & TABLE V** and **Figure 17** the CER samples showed the highest levels of Cr, Ni, and V, whereas the painted tiles, such as TL1, exhibited elevated concentrations of Co and Pb, which can be attributed to the use of artificial pigments. Although investigating the concentrations and sources of these trace elements is crucial, it is essential to note that these elevated concentrations only represent a potential risk to the environment and human health. The actual release of these elements depends on their mobility, which is why their concentrations were also analyzed in the leachates. After 24 h of leaching, the leachates were analyzed for the eventual release of elements from the solid phase to the liquid phase. The results show that a different scenario occurred in the MRA and pure CER environments, where the released amounts of elements were considerably lower at high alkaline pH, likely due to the interactions with the intact cement hydrate phases of the CON sample, as previously observed by Engelsen et al. (2009). The results show that most of the V and Ni concentrations in the CER leachates were below the limits established by the End of Waste criteria (D.M. n. 127/2024), indicating that these elements had low mobility. For Cr, although fewer CER samples exceeded the threshold, many MRA leachates exhibited higher Cr concentrations. This increase was attributed to the presence of cement paste (CON), which elevated the Cr concentration, often exceeding the legal limit of 50 µg/L. This increase was primarily due to the direct contribution of Cr, rather than being induced by pH changes. In the leachates of some bricks, nitrites and sulfates also require attention because their concentrations exceeded the legal limits. However, the high concentrations of V, Cr, and Ni

do not necessarily indicate the presence of anthropogenic contaminants, as these elements naturally occur in the alluvial sediments of the Po River plain, which extends across Northern Italy, including the area around Ferrara. These sediments are rich in V, Cr, and Ni because the parent rocks in the Po River catchment contain mafic and ultramafic lithologies, which are naturally rich in heavy metals (Amorosi, 2012; Bianchini et al., 2012, 2013). These sediments are also used to produce raw materials in the region, potentially contributing to their presence in CDW.

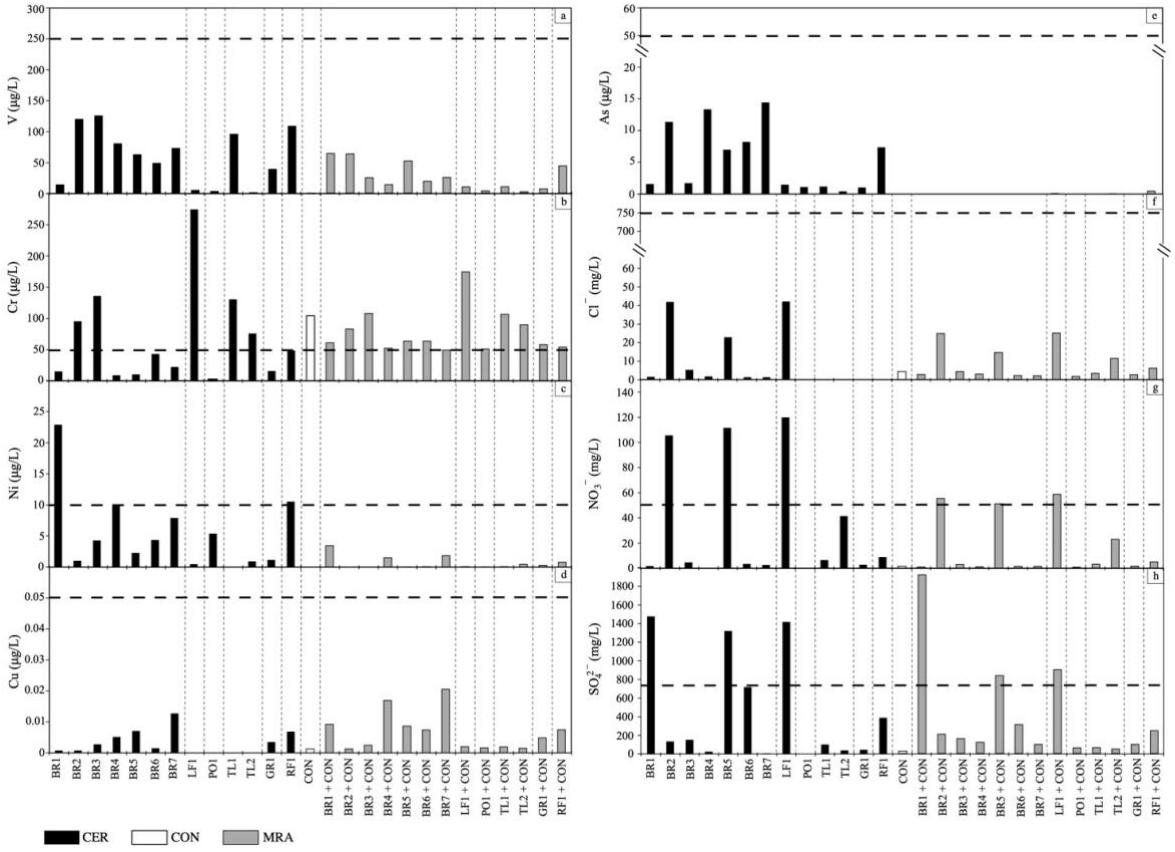

Figure 17. *Concentrations in µg/L of (a) V, (b) Cr, (c) Ni, (d) Cu, I As, (f) Cl-, (g) NO32-, and (h) SO42- of CER, CON, MRA leachates from this study. Dotted lines represent the Italian thresholds of the End of Waste (D.M. n. 127/2024) decree.*

To obtain an overview of the leaching behavior, a comparison was made with data from the literature, focusing on species that frequently exceed the legal limit (i.e., V, Cr, Ni, Cu, and SO_4) (**Figure 18**).

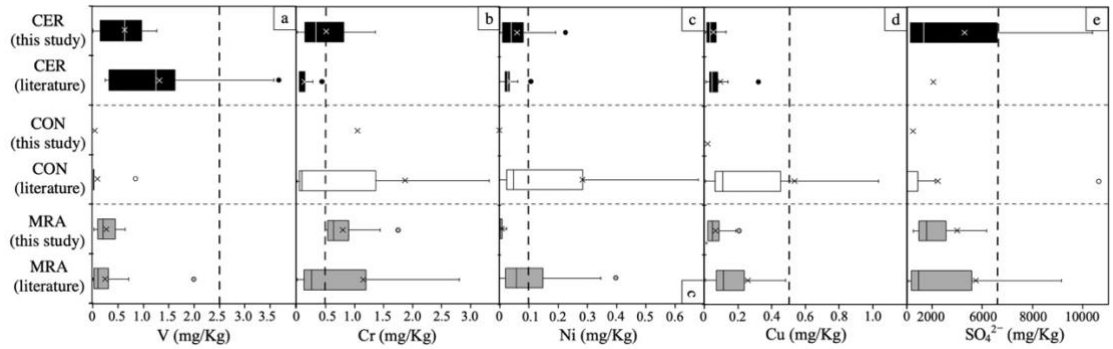

Figure 18. Concentrations in mg/Kg of (a) V, (b) Cr, (c) Ni, (d) Cu, and I SO_4^{2-} of CER, CON, MRA leachates from this study and from literature (Barbudo et al., 2012; Bianchini et al., 2020; Butera et al., 2014; Coudray et al., 2017; Diotti et al., 2020; Engelsen et al., 2010b; Galderisi et al., 2022; Galvín et al., 2013; Strufe et al., 2006; Susset & Grathwohl, 2011). Dotted lines represent the Italian thresholds of the End of Waste (D.M. n. 127/2024) decree. As some literature studies used L/S 2:1 instead of L/S 10:1, the concentration values of all samples, as well as the Italian threshold values, were normalized.

It is immediately possible to observe a lack of data on pure CER materials in the literature. Only Galderisi et al. (2022) and Strufe et al. (2006) provided relevant information. In contrast, abundant data are available on CON and MRA waste. As shown in the plot **Figure 18**, it is clear that the leaching of V is characteristic of CER products, likely due to the original addition during production as a pigment for coloring or for catalytic purposes. A high Cr content is commonly found in cement paste, which constitutes a significant portion of the CON waste (Butera et al., 2015). Strategies such as material substitution or treatment technologies specifically designed for Cr removal may be necessary to mitigate its leaching potential. In addition, the elevated concentrations of V, Cr, and Ni, especially in the CER and MRA samples in this study, could have a geogenic nature as already explained. If sediments rich in V, Cr, and Ni are used as raw materials in building materials, it is not surprising that CDW is anomalously enriched in Cr and Ni, as suggested by Bianchini et al. (2020) in a similar work investigating the CDW of the North Macedonia. Meanwhile, the Cu content, which often exceeds that of CON products, typically originates from systems that involve electrical, plumbing, and mechanical installations, which could contaminate the CON source during the deconstruction and demolishing of buildings (Caro et al., 2024). Lastly, sulfates are the primary products of CER. The flux can originate from various sources, including construction materials such as gypsum (Barbudo et al., 2012), which is often associated with binders (plasters) used for installing floor and wall tiles and other CER products, such as sanitaryware.

2.4.6. Contaminant Factors and Hazard Quotients

To estimate the potential hazard posed by the CDW studied in the Ferrara environment, contaminant factors (C_f and C_d) and hazard quotients (HQ and HQ_m) were calculated for selected chemical species of interest. These calculations considered the possible environmental and human health impacts of their release (Prasad et al., 2021; Verma et al., 2023). The C_f and C_d values were determined for Cr, Ni, Cu, and V because these species most frequently exceeded the legal limits in the leaching tests. The results are presented in **SUPPLEMENTARY TABLE VI & TABLE VII**. The C_f values for the studied samples were calculated using the composition of the water aquifer near Ferrara as the uncontaminated background concentrations, based on a study by Colombani et al. (2015), determined only the composition of the trace elements. The results in **Figure 19a** indicate that Cr and V pose the highest risk, with mean values of >1, indicating potential threats to the site. However, the C_d parameter (**Figure 19b**), which assesses the degree of environmental pollution, had mean values of 0.5 and 0.7 for CER and MRA, respectively, both below the low contamination threshold (1.5). In addition, the HQ values were also calculated for the leachates in this study in accordance with the End of Waste Italian decree (D.M. n. 127/2024). Accordingly, 11 critical chemical species were identified (Cr, Ni, Cu, V, Se, Ba, As, Cl, Li, NO_3, and SO_4) as the most harmful and most likely to exceed the legal limits set by the aforementioned decree (Verma et al., 2023). Similar to the C_d value, a weighted mean parameter, namely HQ_m, was also introduced to assess the overall potential risk of each sample studied. Among the studied materials, only two samples (BR5 and LF1) had HQ_m values >1, indicating they do not qualify for nonharmful waste classification according to the Italian legal limits (D.M. n. 127/2024) (**Figure 19c)**. Within the studied materials only two samples have a value higher than 1 (BR5 and LF1) which are then not suitable for a non-harmful waste classification accordingly to the Italian legal limits (D.M. n. 127/2024).

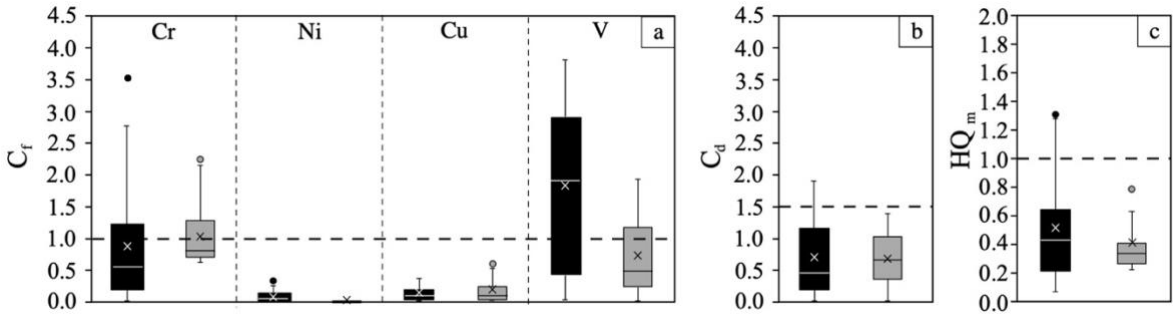

Figure 19. *Box plot representing the Cf (a) of Cr, Ni, Cu, and V, as well as (b) Cd and (c) HQm calculated for CER (in black), CON and MRA (in grey). The dotted lines represent an indication of the degree of pollution in the environment (see text for details).*

2.4.7. Predicting the potential environmental impact

The results obtained using the bulk chemical concentration to predict the leaching values of Cu, V, Cr, and Ni, based on their respective RMSEs, reflect varying levels of model accuracy (**Figure 20**).

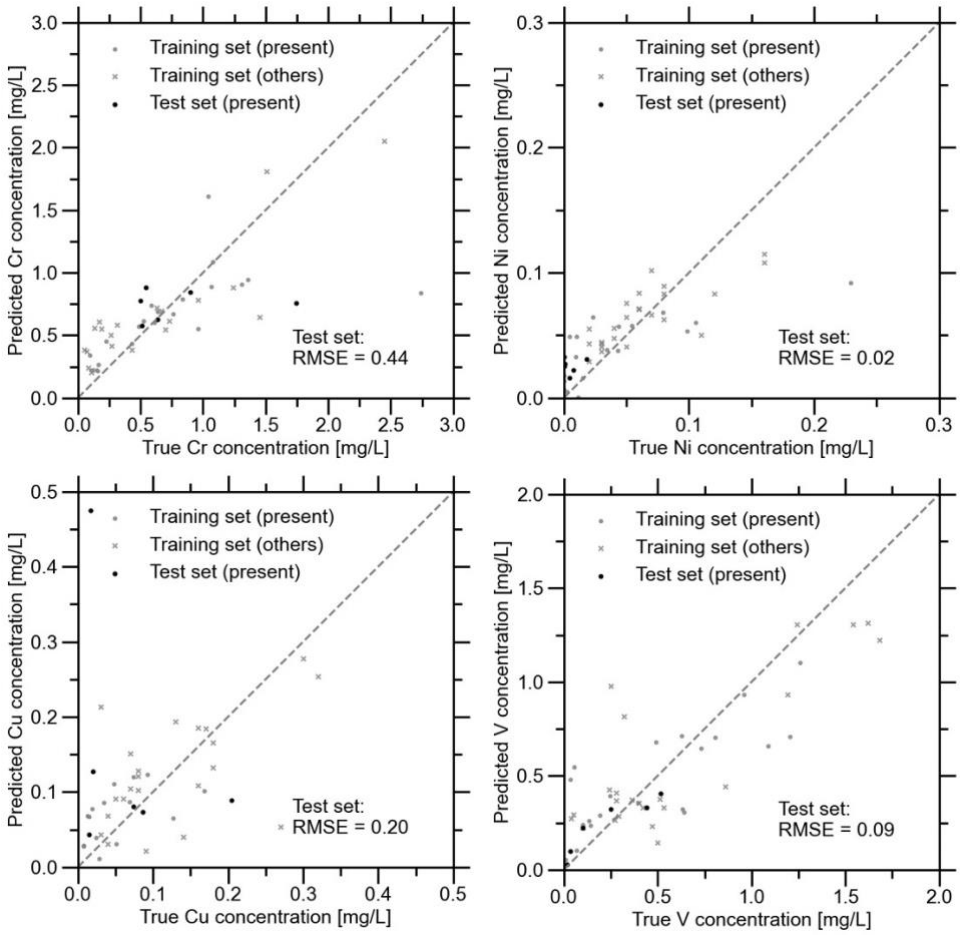

Figure 20. *Prediction of the leachate concentrations for Cr, Ni, Cu and V. The light grey dots correspond to the training set for the materials analyzed in this study, the cross for the cited literature and the dark dots for test set. Cited literature as in* ***Figure 18***

To explore the potential of ML in predicting the leaching characteristics of various CDW materials, we used a neural network to predict the leaching behavior of the CDW samples from this study, along with the associated contaminant factors and hazard quotients. The results obtained using the bulk chemical concentration to predict the leaching values of Cu, V, Cr, and Ni reflect varying levels of model accuracy based on their respective RMSEs.

The highest RMSE (0.44) was observed for Cr, indicating that the model struggled to accurately predict leaching. This suggests that important factors influencing Cr leaching were not fully captured even though the Cr concentration was reasonably predicted. Because Cr is predominantly released from CON in mixed environments with CER, in which the presence of leftover cement paste may vary (Bisciotti et al., 2024), the mobility of Cr in leachates can be unpredictable and is linked to the pH of the environment. In contrast, Ni showed the highest predictive levels (RMSE ~0.02) indicating that the model effectively captured the variables influencing Ni leaching. Meanwhile, Cu had a moderate RMSE of 0.20, indicating reasonably accurate predictions although there is some room for improvement. The complexity of factors influencing Cu leaching, such as electrical, plumbing, and mechanical installation contamination, may account for this moderate error. Finally, V also exhibited a low RMSE (0.99), indicating high prediction accuracy. Because this species is predominantly released from CER materials with a peculiar bulk chemical composition, the model effectively captured the most consistent factors influencing the leaching, making predictions for V highly reliable. Using the bulk chemical concentrations of the major oxides, the C_d and HQ_m values were successfully predicted for the entire dataset. The results for C_d yielded an RMSE of 0.09 (**Figure 23**). The low RMSE indicates high accuracy in the ML model's predictions. The relative impact of the different bulk major oxides on the C_d prediction were higher for CaO and SiO_2, both with a relative impact of ±3 (based on the SHAP analysis; Section 2.7). These results suggest that these two oxides play key roles in determining C_d. The result can be explained in terms of the impact, described previously in **2.3.1.**, of these two chemical species in differentiating the CON waste from the CER waste, which were eventually characterized by distinguished and homogenous leaching behaviors. Fe_2O_3 and Al_2O_3 exhibited moderate or intermediate influence on the prediction because they achieved a relative impact of ±1. These oxides are characteristic of CER products, although their relative impact has less weight than that of CaO and SiO_2. In fact, according to **Figure 21**, the contributions of these chemical species in distinguishing among CER and CON were relative. The remaining chemical species (TiO_2, P_2O_5, Na_2O, K_2O, MgO, and MnO) had an impact factor <1, suggesting a minimal role in determining the degree of contamination. Although present, these species likely do not contribute as

significantly to the leaching behavior of contaminants in CDW as expected. Finally, the C_d parameter is directly influenced by the waste type and can be effectively predicted based solely on the bulk chemical composition. In predicting HQ_m, an RMSE of 0.17 was achieved (**Figure 22**), which is a less accurate prediction than that of the C_d, although it is still considerably high. The most significant impacts on the HQ_m predictions are those of Al_2O_3, SiO_2, CaO, Na_2O, and Fe_2O_3, each with a relative impact value of ±1. The influence of CaO, Al_2O_3, and SiO_2 can be further explained by the different material source compositions of the CDW. At the same time, the sensible effects of Na_2O and Fe_2O_3 are somewhat unexpected. In this case, this can be explained by the CER chemical composition, in which specific types of products particularly enriched in the latter oxides (similar to the BR samples) are more likely to exceed the legal limit thresholds. Ultimately, further in-depth examination is required to highlight this aspect.

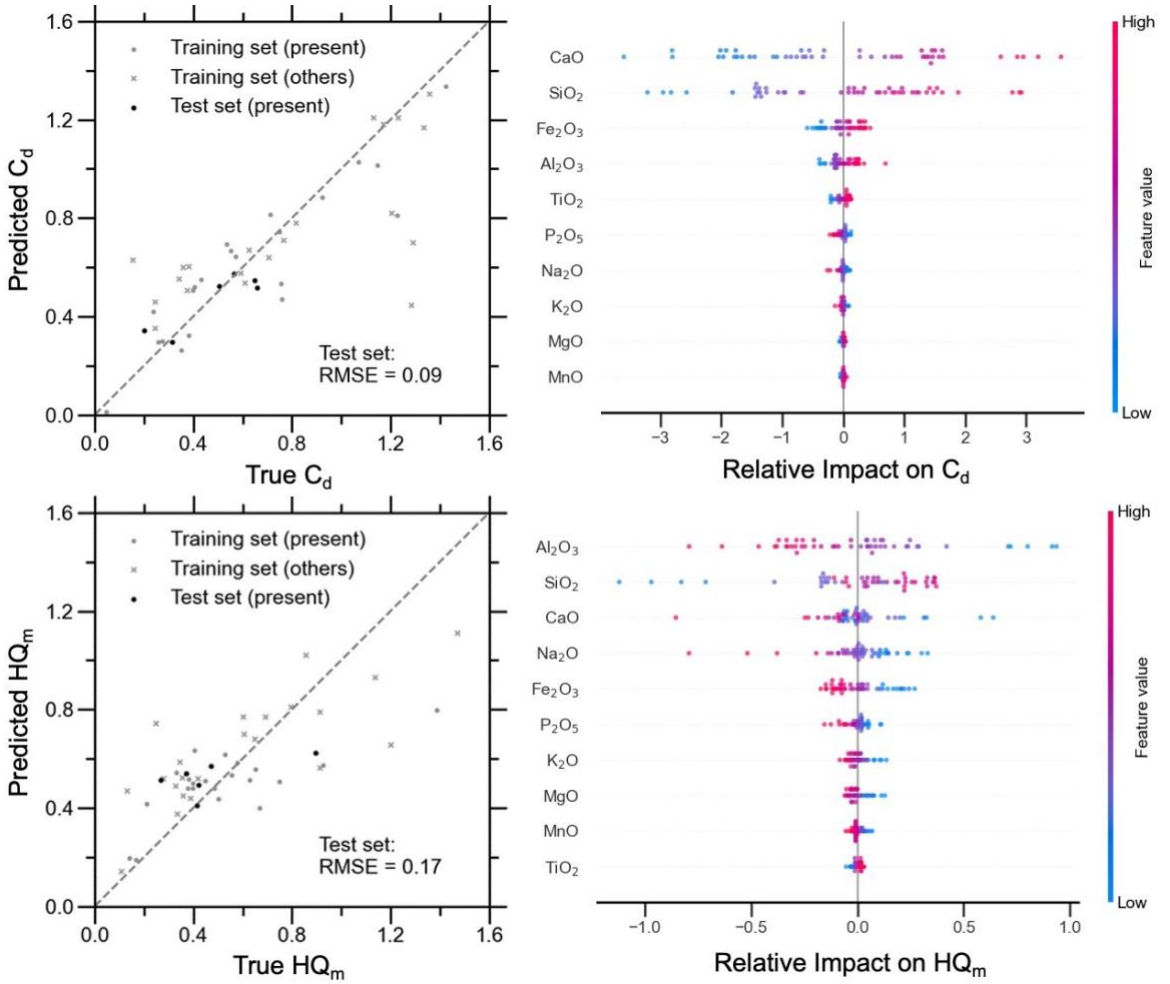

Figure 23. *Prediction of C_d and HQ_m. The light grey dots correspond to the training set for the materials analyzed in this study, the cross for the cited literature and the dark dots for test set. Cited literature as in*

2.5. Conclusions

Improving the sorting and classification of CDW requires innovative methods. Current practices rely heavily on the expertise of landfill workers and computer vision systems, both of which face challenges in accurately identifying materials. For this purpose, in the present study, different ceramic (CER) samples, including bricks, tiles, roof tiles, porcelain, and stoneware, were studied, either as-is or mixed with pure concrete (CON) in a ratio of 1:1 (MRA) in the laboratory. The materials were geochemically characterized in terms of their bulk major and trace element compositions. Based on the results, an automated clustering and classification was performed using PCA and t-SNE via ML. The results support the evidence that key major chemical species can be used to rapidly distinguish clusters of waste with similar composition and that the automated t-SNE method can be fine-tuned (using the perplexity value) to achieve accurate waste classification without human supervision. In addition, a 24-h leaching test was performed on the same sample, and the results were used to calculate the contaminant factors (C_f and C_d) and hazard quotients (HQ and HQ_m), which were used to assess the CDW risk in the Ferrara landfill. Although Cr, Ni, and V were found as the primary concerns owing to their elevated levels, C_d and HQ_m showed that the site is still classifiable as "low contaminated." To support the development of non-supervised real-time risk-assessment tools for CDW management, we proposed for the first time an artificial neural network model to predict the concentrations of key leachates directly from the bulk chemical composition, as well as the C_d and HQ_m factors. The leaching values obtained align with the variation of the same key major chemical species identified (SiO_2, CaO, Fe_2O_3, and Al_2O_3). Consequently, the risk assessment of this waste can be effectively performed using ML models that are driven by the waste's composition. In addition, these models can be used to predict contaminant leaching and environmental hazards. Further refinement is required to more effectively address the hazards associated with complex materials such as MRA. In this context, components such as TiO_2, P_2O_5, Na_2O, K_2O, MnO, and other minor species show significant potential for advancing this process.

3. Advanced separation of CDW: estimating attached mortar paste on the surface of recycled aggregates based on machine learning and XRPD

Abstract

Recycled aggregates, obtained from construction and demolition waste (CDW), are currently underutilized in the production of new concrete given the incidence of widespread leftover mortar paste adhering to the surface. CDW sorting facilities based on optical technology can be developed and applied on an industrial scale, improving the overall quality of this secondary raw material. In this study, we present a novel approach based on image analysis and mineralogical laboratory methods to determine the residual attached mortar volume. Through clustering analysis, we classify CDW samples with a comparable cement content determined by the image analysis. The attached mortar paste from these CDW classes is mechanically extracted and examined using X-ray Powder Diffraction and Rietveld refinement. To estimate the attached mortar volume and the carbonation of the cement paste, we present a novel mathematical model based on the mineralogical data. To overcome the bottleneck associate with the image analysis, we further incorporate a deep learning model to automate the determination of the mortar volume, which enables high-throughput screening of CDW in real production.

Keywords: Recycled Aggregates, Attached Mortar, CDW, Machine Learning, X-ray Diffraction

The data contained in this chapter are published in a Full-Length Article in Cleaner Materials, Elsevier (March 2024) - https://doi.org/10.1016/j.clema.2023.100215.

Estimating attached mortar paste on the surface of recycled aggregates based on deep learning and mineralogical models

A. Bisciotti[a,*], Y. Song[b] , D. Jiang[b], G. Cruciani[a]

[a] *Department of Physics and Earth Science, University of Ferrara, Via Saragat 1, 44122 Ferrara, Italy.*

[b] *Department of Civil and Environmental Engineering, Physics of AmoRphous and Inorganic Solids Lab (PARISlab), University of California Los Angeles, 520 Portola Plaza, Los Angeles, CA, 90095, USA.*

3.1. Introduction

One of the most important steps toward achieving the circular economy in the construction industry is recycling and reusing construction and demolition waste (CDW) in the production of new concrete and new building materials. Recent literature identified at least two different types of recycled aggregates (RAs) which can be recovered from CDW (Silva et al., 2014): (1) Mixed Recycled Aggregates, and (2) Recycled Concrete Aggregates. The latter is directly derived from the comminution of CDW containing more than 90% of concrete. It is commonly acknowledged that recycled aggregates (RAs) made from CDW crushed concrete have the potential to substitute natural aggregates (NAs) in construction projects (Fan et al., 2016; Wang et al., 2021). This latter, compared to NAs, can be often distinguished by the presence of residual cement paste bound to their surface. Because of its chemical composition, the attached mortar (AM) interacts with cementitious binders forming in the area of surface contact a thin layer known as interfacial transition zone. As a result of this effect, when RAs are integrated instead of NA, based on the amount of AM inferior mechanical performances and reduced workability are often observed in the new concrete (Bai et al., 2020; H. Zhang et al., 2022). The addition of fibers (fiber-reinforced recycled aggregate concrete) represents a viable solution to inhibit the coalescence of the weak areas of the interface transition zone, at the same time their use is not always suitable in every engineering application due to costs and operating conditions (C. Wang, Wu, et al., 2022; C. Wang, Xiao, et al., 2022). Besides the pure content of residual cement paste attached to the CDW aggregate, the bulk assemblage and composition of the residual cement itself has direct impact to define the correct and most efficient managing strategy to reuse RAs facing the AM impact. The composition of the attached mortar can be very diverse due to various aging, environmental circumstances during disposal, and the initial composition of the cement used. Mostly, the carbonation level of the residual paste attached has a significant impact on varying the mineralogical major phases (Georget et al., 2020; Shen et al., 2022). Therefore, the degree of carbonation of the layer itself also affects, together with the amount of AM, affects the possibility of reusing RAs in new cement paste (Lu et al., 2019; R. Wang et al., 2020). Because of the variability of the CDW properties, these secondary raw-materials are currently underutilized in the manufacturing of new concrete, whilst they are mostly used for esplanades or as sub-bases and bases of pavements/roads and highways. This can be labeled as downcycling and greatly hinders the industry's potential to transition to a circular economy since the net expansion of the road infrastructure is reducing and may eventually come to an end (C. Zhang et al., 2020). In the present scenario,

CDW concrete recycling relies mostly on industrial crushing and sieving techniques, often using jaw crushers and impact crushers in order to produce an unsorted granular product with the necessary size fractions (Ulsen et al., 2019). Mixed CDW streams will have to be separated and extensively cleaned up before comminution, in order to gain enough quality to reuse the different fractions. After conducing primary, and occasionally secondary crushing, an electromagnet is usually employed to remove any metallic components (such as rebars). Nevertheless, coarse RAs, obtained from recycled concrete, are often discharged because they still have residual cement paste clinging to the surface, despite being successfully sorted within CDW. A step forward in sorting strategies, has just recently been outlined and discussed for the fine CDW materials (< 4 mm) based on mechanical system for extracting the RAs separating the cement-based fractions (Gebremariam et al., 2020). The development of advanced separation process for CDW can improve the quality of this secondary raw material, reducing the overall heterogeneity, and enhancing the effectiveness of the reuse of these products in substitution to natural aggregates counterparts in concrete production. Optical sorting is one of the most advanced key technology for the coarse CDW fractions (≥ 4 mm), even if still not extensively adopted world-wide in CDW treatment plants (J. Li et al., 2022; Nežerka et al., 2024; Serranti et al., 2023). Therefore, to meet the efficient sorting of CDW in industrial plants, advanced sorting-machine can be used for screening high-quality RAs, based on AM content, using RGB optical sensors and hyper-spectral imaging cameras (Bonifazi et al., 2018; Trotta et al., 2021). In order to increase performance, this strategy also needs a significant contribution from machine learning, specifically deep neural networks (DNN), which classify the acquired data (RGB or hyper-spectral) in agreement with the material composition (Lau Hiu Hoong et al., 2020). The separation and further quantification of AM appears then as mandatory processes to assess the quality of RAs, and different methods have been proposed (mechanical, thermal, thermal–mechanical, chemical, microwave, ultra-sound) as summarized in (Braymand et al., 2017; Tam et al., 2021). In spite of those methods, an internationally standardized procedure has not been established yet. The quantification of AM based on image analysis methods (IAM) using digital cameras has been one of the early achievements in RA scientific researches (Abbas et al., 2009; Ulsen et al., 2022; Y. Wang et al., 2021). However, a bottleneck of the conventional IAM lies in the fact that this approach can be very sensitive to noise artifacts and blurring (A. Singh, 2015). In addition, segmenting the attached mortar in the image often requires constant human judgments (e.g., for readjusting the color threshold even when there is a slight change in the aggregate type or light conditions). Hence, despite the advances of conventional image analysis in recognizing the residue mortar, it is challenging to use this

approach to overcome the above limitations for fulfilling high-throughput screening of recycled aggregates in real engineering projects. Alternatively, recent advances in artificial intelligence (AI) and computer vision open up new opportunities to rely on a computer to accomplish vision-based tasks such as object recognition or image perception (Pan & Zhang, 2021; Szeliski, 2022). This approach has been demonstrated to be successful in multiple fields in civil engineering (Xu et al., 2021) including phase analysis for concrete materials (Das et al., 2022; Y. Song et al., 2020). The rationale behind this approach is that AI is good at capturing the correlation between the input data and the predicted target, including the explicit information that is utilized by the image analysis (e.g., color contrast) but also some implicit clues that may not be easily captured (e.g., material texture). To the best of our knowledge, however, the potential of AI has not been investigated for improving the detection of the residue mortar in recycled aggregates. To overcome the challenges associated with conventional image analysis, we leverage AI and computer vision techniques to enable a direct and robust inference of the residual mortar attached to the aggregate. To this end, a deep learning model is developed to leverage the advances of convolutional neural network (CNN) in recognition of the different phases in the aggregate image. In particular, our model is trained to predict the mass fraction of the AM on the recycled aggregate particles. In addition to determining the AM content, a quick, accurate, and repeatable method is provided to determine the RA's degree of carbonation in order to categorize the CDW and stimulate the final reuse. There are several methods for quickly evaluating the carbonation of concrete, but RAs specimens are unable to be utilized within the same measurements. To obtain accurate information on the carbonation front, laboratory tests are typically conducted (Georget et al., 2020; Tang et al., 2023) and usually combine scanning electron microscopy (SEM), XRPD, and thermogravimetric analysis. Even though they are highly accurate, these approaches are not appropriate for a quick evaluation of the carbonation degree. A novel mathematical model based on the outcomes of X-ray powder diffraction analysis is introduced for the first time in in order to categorize the RAs based on a bulk volume materials reconstruction. As parameters to the equation, we propose quantitative phase analysis outcome, which is based on Rietveld modeling of diffraction patterns together with tabular mineral phase density data. Such a method has the potential to be industrially applied to quality control, as it has already been proposed in the mining industry to estimate the main parameters of minerals grade ore deposits as a faster and cheaper alternative to traditional wet chemistry methods, ensuring reproducibility and accuracy of prediction even when the ore feeding the plant is changed. (Melo et al., 2020; Mulder et al., 2013). The Rietveld approach is already well-established in the field of cement

research for developing prediction models of newly-formed mineral assemblages in the kiln and in the hydration process. (Abzaev et al., 2019; Mulder et al., 2013). The contribution in the field of CDW is presented here for the first time. The identified hydrated minerals and anhydrous cement components, after only using XRPD, give a detailed in-deep description of the CDW and a direct evaluation of the carbonation level of the connected cement paste. The output consists of a 3D volume reconstruction of the associated AM and on a direct assessment of the degree of carbonation of the layer resulting from the bulk microscopic crystalline mineralogical assemblage. The output of the research represents an innovative approach to determining the most effective strategies for the reuse of concrete-based CDW based on the estimation of AM content and carbonation degree of the connected residual cement paste.

3.2. Materials

The CDW acquired from a precasting facility in Perugia (Umbria District, Italy) was jaw-crushed on an industrial scale to produce the RAs under analysis. The crusher's parameters were defined to produce aggregates with a diameter between 0 and 25 mm. For this reason, the jaw spacing was fixed at 22 mm for the jaw crusher, accordingly to a previous work (Hubert et al., 2023). The beginning CDW comprises more than 90% structural concrete (> 40 Mpa), resulting in a product that may be categorized as recycled concrete aggregates. (Silva et al., 2014). The collection of material samples followed the guidelines in standard UNE-EN 932-1, 1997. The RAs are homogenized and decreased in the lab using a quartering process according to UNE-EN 932-2, 1999. Following screening, an average of 70% of the material produced by industrial jaw-crushing of CDW is formed of the coarse fraction of RAs (≥ 4 mm), which is also the granulometric diameter with the greatest potential for recycling. (Pedro et al., 2017). This latter coarse RAs fraction is the selected portion of starting material which undergoes the following investigations.

3.3. Methods

3.3.1. Preliminary Image Analysis assessment of attached mortar

Using a ZEISS stereomicroscope (SteREO Discovery V12) with an Axiocam 208 color camera mounting a fixed light source (CL 6000 LED) and a magnification of x10, digital images for more than 300 unique coarse RA are acquired, being the most far-magnification feasible also by using high-resolution RGB camera. Following a first visual evaluation of the database, the population exhibits several forms of RAs (**Figure 24**) within clean aggregates, intermediate mortar-covered aggregates, and full mortar-based aggregates.

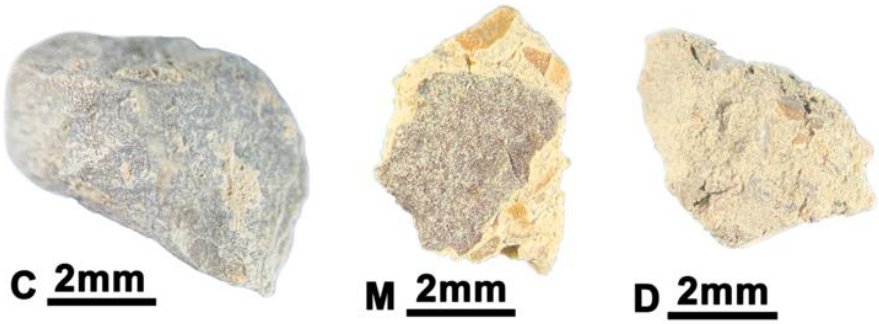

Figure 24. *Image taken with a high-resolution RGB camera of three distinct RA samples, where C means clean aggregate, M stays for mortar covered aggregate and D for mortar-based aggregate.*

The images collected from RAs are subjected to IAM using ImageJ Software (Schneider et al., 2012) following the method proposed by Y. Wang et al., 2021. Each sample's image was analyzed to yield an estimation of the surface covered (SC %) from the attached mortar (for the entire collection of RA images see Supplementary Materials). The initial stage of processing involves converting the RGB images to 8-bit grayscale, where each pixel is encoded using a grey scale from 0 to 255 (256 values), where 0 is black and 255 is white. ImageJ software allows to easily perform the 8-bit greyscale transformation of the starting database and also to define the correct scaling of the pixel/size ratio which has been fixed at 0.4 mm/pixel for the present application, same used in the cited work. The grayscale values, after Y. Wang et al., 2021, can be divided into three intervals, namely, 0–50, 50–175, and 175–255, respectively, corresponding to the pixel values of background, aggregates, and adhered mortar (**Figure 25**).

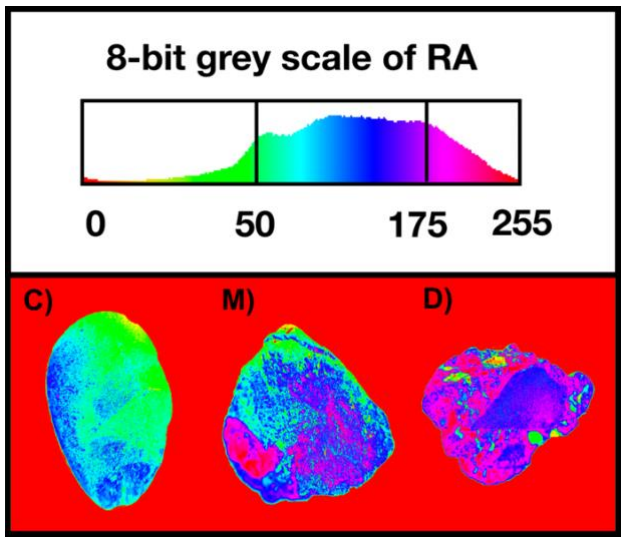

***Figure 25**. Spectrum of 8-bit colored greyscale intensity of three RA with different amount of AM on the surface (here again C stands for clean, M for mortar-covered and D for mortar-based aggregates).*

The process of IAM can be divided into three steps: (I) image segmentation transformation, (II) filtering and denoising, and (II) boundary treatment. Segmentation is then conducted with a first cutoff threshold of 160, resulting in the individual RA total area without the background. Furthermore, a consequent cutoff of 210 is applied to achieve a segmentation of the surface covered by AM. It is, afterwards, necessary to filter and denoise the greyscale image to remove impurity information in each region related to aggregate and adhered mortar after the segmental transformation of the grayscale image. Non-linear and component filters, such as median and opening filtering were used to deal with the grayscale image of RA (**Figure 26**). For an extended discussion of boundary treatment procedure and accuracy and precision of the used IAM see Y. Wang et al. 2021.

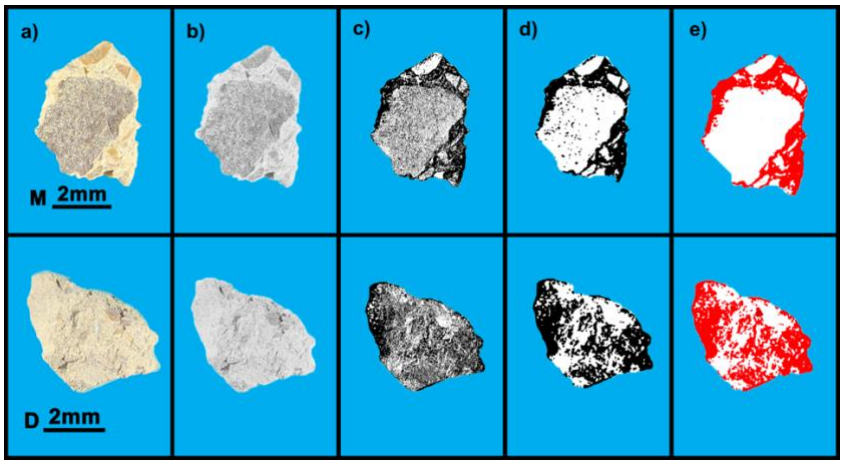

***Figure 26.** Examples for M and D aggregates classes of the different IAM steps conducted: a) Original data (RGB), b) 8-bit transformed data (greyscale), c) Threshold for the 210 value, d) Filtering result, e) Pixel counted (Analyze Particle).*

The quantitative information concerning 2D area is derived from pixel counting following the threshold of the 8-bit greyscale pictures. ImageJ's inbuilt tool "Analyze Particles" was used to carry out the measurements. Only regions larger than 1 mm^2 are tallied, and the minimum Area Size identified ($pixel^2$) is fixed at 50. Total Area (mm^2) is connected to the background's segmented surface, producing a figure for the bidimensional total area for each RA. Instead, the value of Area Covered (mm^2) results from the pixel count coming from the latter segmentation at 210, which is tied to the associated mortar. The parameter of Surface Covered Percentage (SC%) is then calculated using **Equation (8)**:

$$SC\% = \frac{Area\ Covered\ (mm^2)}{Total\ Area\ (mm^2)} * 100 \quad \textbf{(8)}$$

3.3.2. Gaussian Mixture Model clustering of samples

Exploratory clustering analysis is used to determine the presence of subgroups of samples within the results obtained after the IAM. The outputs of the IAM's Surface Covered Percentage (SC%) serves as a distinctive attribute for every single specimen in performing the analysis. Consequently, the initial RAs samples are divided into three distinct categories based on comparable AM content levels. The method of clustering chosen is the Gaussian Mixture Model (GMM), a parametric probability density function represented as a weighted sum of Gaussian component densities. GMM parameters are estimated with the iterative expectation-maximization (EM) algorithm using the Bayesian Information Criterion (BIC) for model selection (M. S. Yang et al., 2012). By employing BIC, we first establish K, which represents the total amount of Gaussian mixture components (Baudry et al., 2010). As a result, the best predicted model is displayed after a series of iterations. To explore the database, a starting model with two K components and full covariance is defined. In the end, clusters from the entirety of the population are fitted by independent Gaussian distributions.

3.3.3. Separation and quantification of attached mortar by mechanical treatments

The groups of samples resulting from GMM clustering were individually processed to precisely quantify AM average percentage in the bulk material within 10 RAs. The experimental method followed the protocol by Tam et al., 2021, involving mechanical treatments like impact and abrasion to remove AM layers from clast surfaces and determine the average AM mass ratio (AM wt.%). An autogenous cleaning technique was applied by

placing RAs samples in a rotating mill drum loaded to 33% and revolved at 1400 RPM for 20 minutes. The AM powder detached was then sieved at 5 µm and weighed, referred to as AM detached (g). These values, in combination with the total mass of RAs before processing, RAs total mass (g), were used to calculate accordingly to the **Equation (9)** the mass fraction wt.% of AM as follows:

$$\text{AM mass ratio (wt.\%)} = \frac{\text{AM detached (g)}}{\text{RAs total mass (g)}} * 100 \quad \textbf{(9)}$$

3.3.4. Computer-vision-based prediction of the attached mortar

To achieve a more accurate and robust analysis, AI is employed to replace conventional image analysis for predicting the amount of mortar attached to recycled aggregate particles. The pipeline of the AI analysis is illustrated in **Figure 27**, and all the relevant data processing and modeling work are programmed in Python.

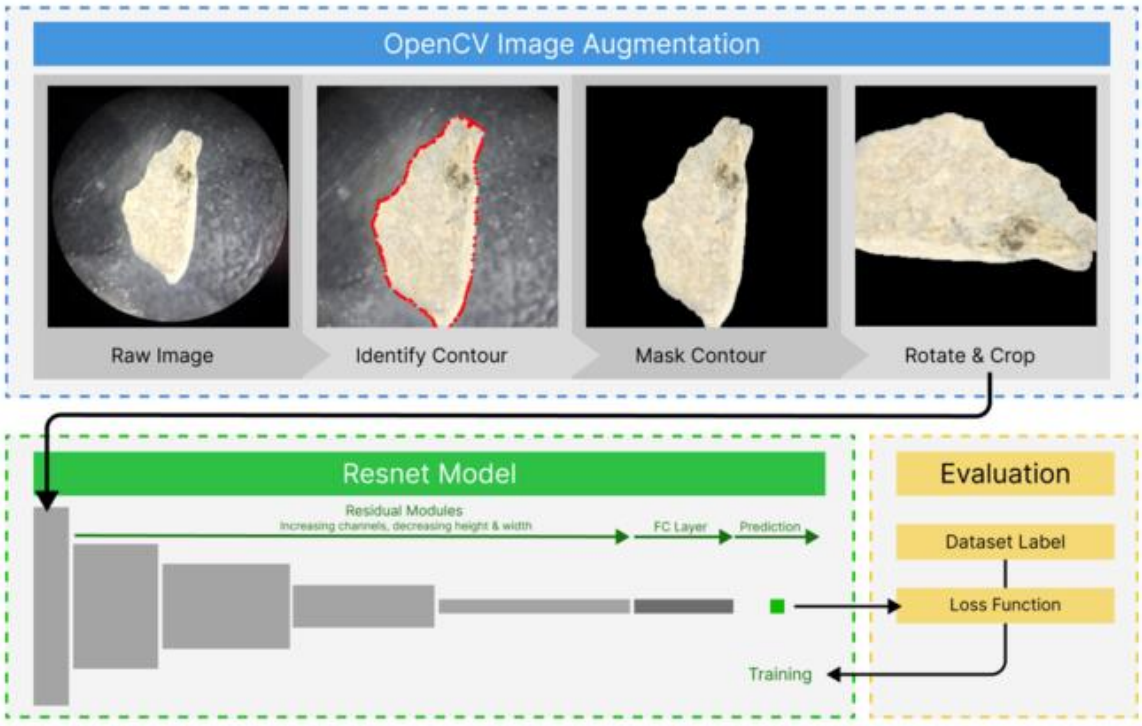

***Figure 27**. Illustration of the pipeline for training the AI model. During training, the model is regularized for good generalizability such that it can predict the mass fraction of the attached mortar for new aggregate images that are not involved in the model training.*

Herein, a deep learning model (convolutional neural network, CNN) is trained to infer the mass fraction of the AM, based on the same image of individual aggregate particles that is obtained from IAM. The CNN approach is selected because it is well-recognized for visual

imagery with its dominant superiority in accuracy and efficiency among all computer vision methods (Szeliski, 2022). Following the common practice, 80% of the images are used (i.e., training set) to train the model, while the remaining 20% of images (i.e., test set) are kept hidden for testing the prediction accuracy of the trained model. To avoid the bias related to randomness, it is adopted a stratified sampling for splitting the training and testing images (Y. Song et al., 2020). Prior to the model training, the raw aggregate image is pre-processed to mask the non-aggregate region. This step removes irrelevant information associated with the background, which essentially ensures that the model only learns to make predictions based on aggregate-related data. Otherwise, the model could fit irrelevant features appearing in the background. The background removal is done by filtering the raw image based on brightness, using basic functions in the OpenCV package—an open-source computer vision library (Bradski, 2000). The model training is driven by minimizing the mean squared error (MSE) loss between the predicted and true mass fractions of the attached mortar, with careful consideration of several settings. In order to facilitate a consistent learning process, a small learning rate of 0.0001 was adopted. This choice aimed to ensure gradual updates and prevent abrupt changes that may hinder convergence. Additionally, a weight decay of 0.0001 is implemented to effectively regulate the model's learning process and prevent overfitting on the training data. To sufficiently capture the underlying patterns and optimize the model's performance, the training was conducted over a total of 100 epochs, allowing for extensive iteration and refinement. To further improve the stability of the model prediction, the model training is repeated five times so as to obtain five individual models. Thus, the final prediction for a given input is based on the ensembled predictions yielded from the five individual models, by taking the average. The model predictions presented in the following sections are all based on the ensemble prediction. A common challenge faced by material studies lies in training machine learning models with a small number of samples (e.g., less than tens of thousands of images). This issue also applies to the present study, as the limited size of the aggregate image dataset does not allow training a deep learning model from scratch. To overcome this issue, special attention is paid to addressing this issue. First, the ResNet-18 is adopted as the backbone model (He et al., 2015). In comparison to other deep learning models that usually have much deeper and more complex networks, ResNet-18 is selected because it is relatively simple, and requires less data to achieve decent training outcomes. In addition to ResNet-18, the model is trained based on the pretrained model parameters from IMAGENET1k (Russakovsky et al., 2015). This approach, also known as transfer learning, is a popular technique in the field of computer vision for training deep learning models based on small datasets. The idea of transfer learning is that, while the

pretrained model parameters are originally optimized for other visual analysis tasks (e.g., recognizing different animals), some of them are generic for detecting shapes or patterns so that adopting the pretrained model parameters allows the new model to learn the task-specific features more effectively from the new dataset. To enable the use of the original ResNet-18 model for the purposes of this study, the structure is slightly modified. Instead of a one-hot output with the original size 1000 associated with IMAGENET1k, our model uses three fully connected layers with sizes of 8, 4, and 1, with Rectified Linear Unit (ReLU) and batch normalization layers between each two. This allows our model to output a single value that represents the prediction for the mass fraction of the attached mortar. Given the small learning rate adopted for model training (0.0001), the transferred model is not frozen during retraining. Furthermore, during model training, the training images are augmented with image jittering (e.g., random rotation, flipping, etc.). Doing so allows an improved data variation, which contributes to enhancing the model robustness with a fixed number of training images. Readers seeking additional explanations on CNN, transfer learning, and image augmentation are referred to a previous publication (Y. Song et al., 2020).

3.3.5. Rietveld based reconstruction of attached mortar

The powder of AM obtained from each group resulting from mechanical detaching was further analyzed using XRPD. The reconstruction of AM volume and carbonation degree for every group of samples is performed from a novel mineralogical model introduced. Weighted percentages of crystalline minerals resulting from Rietveld QPA provide essential "fingerprint" data for the average mineral composition across multiple samples, as described in Sections 2.2.1 & 2.2.2. The model incorporates the weight percentages of identified crystalline phases ($Wt_{(i)}$), normalized to unity, and uses tabulated densities (g/mm^3) from literature for silicates, carbonates, and synthetic cement product phases (Balonis & Glasser, 2009) as parameters in Equation (3). Each parameter is a weighted mean based on the QPA-Rietveld percentages. Subsequently, the ratio of AM mass (g) measured after the detachment procedure is introduced to estimate AM Volume coverage in mm^3, as described in **Equation (10)**.

$$AM\ Volume\ (mm^3) = \frac{AM_{(g)}}{\rho_{pseudo}\ (g/cm^3)} \quad \textbf{(10)}$$

Where AM is the mass of powder obtained from each group, ρ_{pseudo} is the weighted mean parameter of tabulated density of mineral as described in **1.3.1**.

The volume (%) of attached mortar in RAs groups can be obtained by combining AM Volume (mm^3) data from QPA-Rietveld with IAM results (Section 2.2.1). Despite some deviations from the theoretical description, the presence of 10 individual RAs exemplars in each group corrects the overall data, yielding average values for Total Area in mm^2 (8) used to calculate the sample average radius from **Equation (11)**:

$$RA\ radius = \sqrt{\frac{Total\ Area\ (mm^2)}{4\pi}} \quad \textbf{(11)}$$

and then a measurement of the volume is easily obtained with **(12)**:

$$RAs\ volume = \left(\frac{4}{3}\right)\pi\ *\ (RA\ radius)^3 \quad \textbf{(12)}$$

The final volume (%) of AM which covers the RAs surface (3DC%) is then obtained as **(13)**:

$$3DC\% = \frac{AM\ volume(mm^3)}{RAs\ volume\ (mm^3)} * 100 \quad \textbf{(13)}$$

In conclusion the final database (See Section 3.4 and Supplementary Materials) consists for each group of a calculated average total volume of the RAs (mm^3) resulting from combined IAM and QPA-Rietveld.

3.4 – Results and discussion

3.4.1. ImageJ analysis and GMM clustering

Following the IAM method, the starting dataset of 300 RA is divided into three subgroups (**SUPPLEMENTARY TABLE X & TABLE XI & TABLE XII**), primarily as a result of the GMM clustering procedure used (**Figure 28a**). The quantile-quantile plot (Q-Q plot) in **Figure 28b** shows a linear trend by dispersing the quantile distribution among the beginning data with the predicted mixture distribution reflecting the model's effectiveness in fitting after 10,000 iterations. Following the first IAM quantitative analysis, a first batch of 100 individual samples provided SC% values of 0. As a result, they were categorized as

clean RAs (C-RA) and aren't shown in plots. Following that, the GMM model's implementation produced a first Normal Distribution that described a population of unique RAs with a mean value of 47 SC% that were ascribed to the M-RA group. The model simultaneously fits a second Normal Distribution with a mean of 67 SC% which is then classified as D-RA (**SUPPLEMETARY TABLE XIII & TABLE XIV & TABLE XV**)

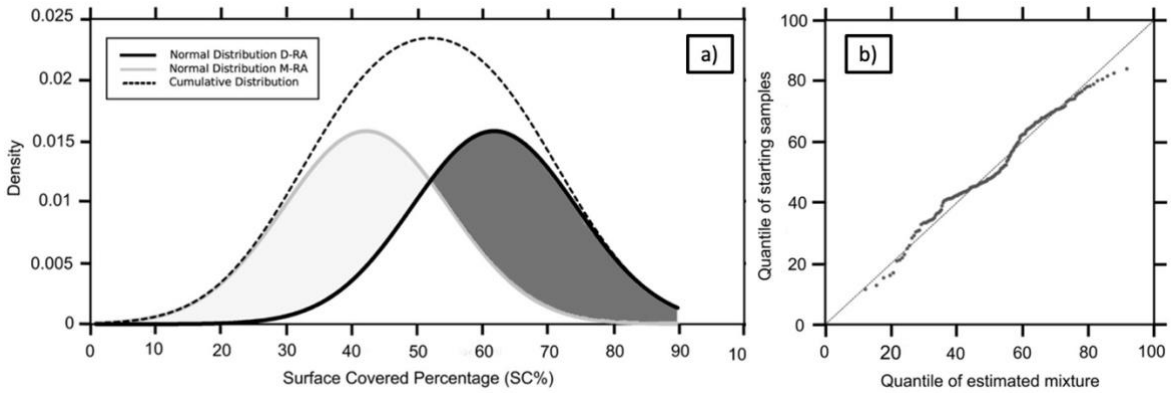

Figure 28. *Clustering of samples from (a) Gaussian Mixture Model, dark-grey line stands for D-RA and light-grey for M-RA, dotted line stands for the Cumulative Distribution calculated. (b) Q-Q plot of the quantiles from original samples vs the estimated mixture distribution.*

Eventually, the initial RAs samples are separated into three groups called C-RA, M-RA, and D-RA based on comparable AM content levels. In order to group 300 individual RAs analyzed samples into 30 groups with similar SC% values, 10 singular clasts were used (**Figure 29**).

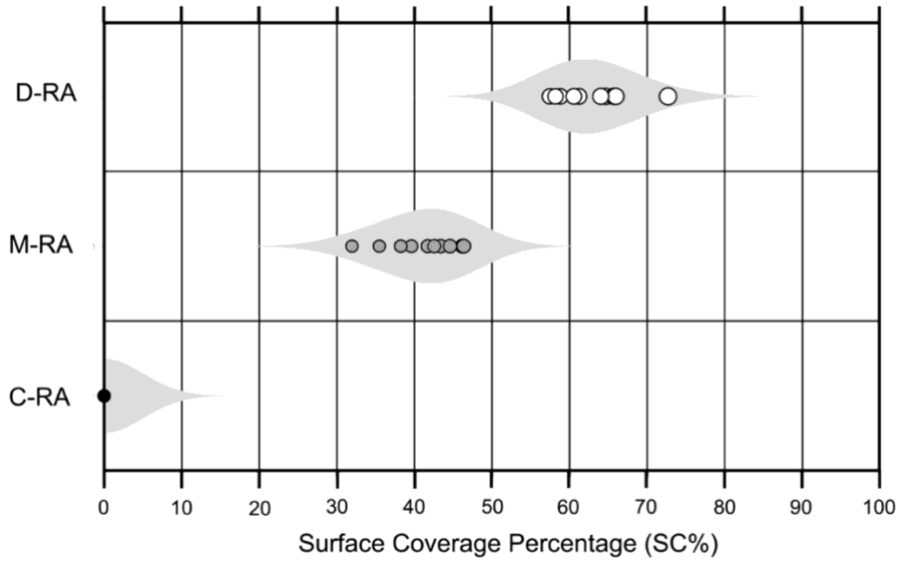

Figure 29. *Violin plot distribution of the 30 groups resulting from the GMM divided into C-MA, M-RA and D-RA.*

In total, there are ten groups in each of the three major categories (C from 1 to 10, M from 1 to 10, and D from 1 to 10). The division of the RAs into three distinct macro-groups (C, M, and D) is consistent with earlier research (J. Kim, 2022; G. Liu et al., 2022; Mazhoud et al., 2022) within: mortar-free RAs (C-RA) being similar to natural aggregates, mortar-covered RAs (M-RA) which only has partial areas of surface AM, and mortar-based RAs (D-RA) which is primarily comparable to pure hydrated cement paste.

3.4.2. Detaching attached mortar by mechanical treatment

Following the mechanical treatment based on rotational milling and sieving tests the following values are obtained for the sub-groups composed of 10 individual RAs merged from the IAM and GMM clustering technique (**Table 1** and complete set on **SUPPLEMETARY TABLE XVI & TABLE XVII & TABLE XVIII**). The powder amount mechanically detached and collected from each group represents an accurate measurement of average AM content, presented as AM mass ratio (%). The results obtained for the samples belonging to the C-RA category mainly confirm the IAM procedure's findings that AM is not present in C-RA groups. In fact, no powder was found within the aforementioned specimens following the detaching procedure. After the same treatment, the M-RA category displaying an intermediate AM content exhibiting an average RAs total mass of 7.11 g and of 0.25 g of pure AM, which is equivalent to a mean AM mass ratio of 3.51 wt.%. Finally, for the D-RA category, which according to GMM has the greatest AM content, an average total mass of 5.31 g and of 0.54 g of pure AM is reported, which is equivalent to a mean percentage of detached powder of 10.11 wt.%. The average density of the surface layer of the AM is 1.8-2.2 g/cm^3 due to the high inherent porosity of the dried cement paste, whereas the value for the natural mineral pieces of aggregates embedded is around 2.8-3.0 g/cm^3 (Bai et al., 2020; Xiao et al., 2006).

Sub-Group (from 1 to 10)	Average RA Tot. mass (g)	Average AM mass (g)	Average NA Weight (g)	Average AM mass ratio (%)
C-RA	5.63	0	5.63	0
M-RA	7.11	0.25	6.86	3.51
D-RA	5.31	0.54	4.77	10.47

***Table 1**. Results of Mechanical Treatments conducted on M-RA and D-RA.*

3.4.3. XRPD powder analysis and QPA-Rietveld

The XRPD pattern collected involved the subgroup M-RA and D-RA, being in total composed of 20 distinct samples of AM powders removed after the mechanical treatment among 10 individual RAs within each group. From peak positions are identified the occurrence of residual cement minerals and other secondary crystalline phases (vaterite, aragonite, ettringite, AFm phases, namely the calcium aluminate ferrite hydrates both tri- and mono-substituted) which represent the hydration and carbonatation products of the cement paste. The occurrence of feldspars and quartz likely stands for micro-aggregates powder embedded inside the AM. The presence of calcite can be present either as micro-aggregate (primary), or more important as a main carbonatation product (secondary) together with vaterite and aragonite. The occurrence of both primary and secondary calcite is revealed by the asymmetry of the main peak of calcite (at 29.6° 2θ) which was modeled using two types of calcites with different crystallite sizes: a type-1 calcite with an average crystallite size of 80 nm and a type-2 calcite with a value of 25 nm (**Figure 30**). The formation of bimodal crystallite size of calcite (the secondary with 25 nm), and of the $CaCO_3$ polymorphs (vaterite and aragonite), can be due to different cement type used, CO_2 partial pressure, or the carbonatation of different hydrated products, namely C-S-H, ettringite, or AFm (Auroy et al., 2018; Goñi et al., 2002; Y. Li et al., 2020). The anhydrous cement phases (C_3S, C_2S, C_4AF, C_3A) represent unreacted crustal of cement paste, which are always found together with the hydration product inside the matrix. Following QPA-Rietveld each identified mineralogical phase is quantified (wt. %) in every sample analyzed (see Supplementary Materials for the complete list).

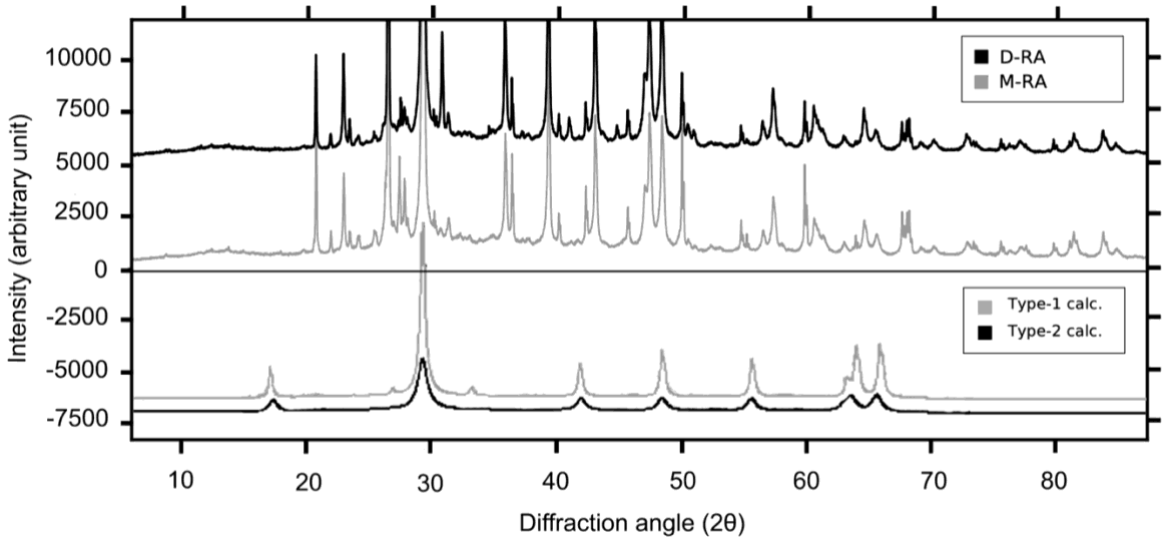

***Figure 30**. XRPD pattern of D-RA compared to M-RA and bimodal crystallite site of two types of calcites identified.*

3.4.5. QPA-Rietveld based model reconstruction of attached mortar and carbonation degree

To generate a mineralogical model and to obtain the volumetric crystalline assemblage (mm^3) of the studied AM powders, bulk tabulated density parameters from mineralogical components discovered using XRPD are encompassed (**SUPPLEMENTARY TABLE XIX & TABLE XX & TABLE XXI**). From the solutions of equation (3), AM volumes for M-RA are determined to be around 50 and 125 mm^3, whereas AM volumes for D-RA are found between 125 and 300 mm^3. Thus, the outcomes of equation (5)'s image analysis total volume reconstruction demonstrate that the mean total RA volumes for M-RA and D-RA are 470 mm^3 and 418 mm^3, respectively. Ultimately, using equation (6), it is possible to obtain information that falls within a wide range of AM volume ratio (3DC%) values, enabling comparison of the extent of AM reconstructed from the model with the entire RAs volume calculated for each sample under consideration. The comparison of the 3DC% volume coverage with the AM mass ratio (wt. %) obtained for the same samples after mechanical detaching shows a good linear correlation (R = 0.94), and almost all the values are contained inside the standard deviation of the dataset (**Figure 31**).

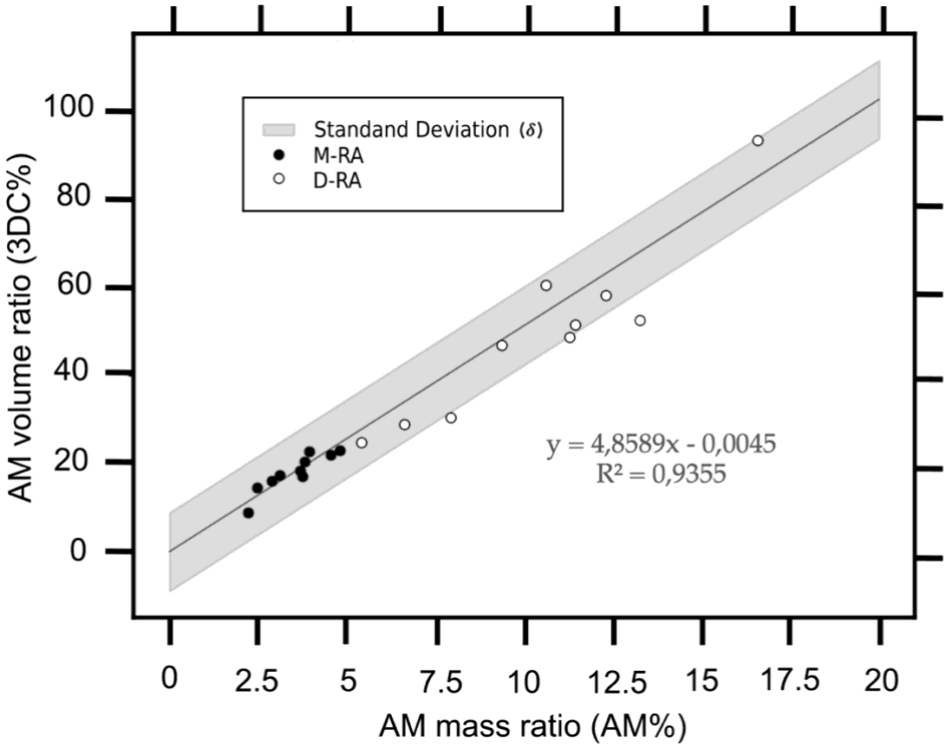

Figure 31. *Relation between calculated AM volume ratio (3DC%) obtained from a QPA-Rietveld based model and the values of AM mass ratio (AM%) from the mechanical detaching from the surface of RA.*

This investigation demonstrates that the microscopical assemblage acquired from XRPD QPA-Rietveld may be utilized to rebuild the volume of AM covering the surface of RAs throughout a whole range of values (from 9 to 95%). A substantial boundary separation between the two GMM-generated subgroups is still there after charting the findings. A first compact cluster of scatter data related to M-RA exhibit an estimated volume coverage ratio ranging from 9% to 23%, while a second, more scattered group of samples associated to the D-RA ranges from 25% to 95%. Furthermore, using the same model it was possible to determine and provide an indication on the level of carbonation of the AM cement paste. From the QPA-Rietveld fitting model of the bimodal crystallite size of calcite (25 nm) and the $CaCO_3$ polymorphs (vaterite and aragonite) we obtained quantitative information on the wt.% of carbonation products for each sample. The results of computing the Carbonation volume ratio (CARB%) of the AM using the total sum of weights (%) of carbonation products after XRPD studies are shown (**Figure 32**).

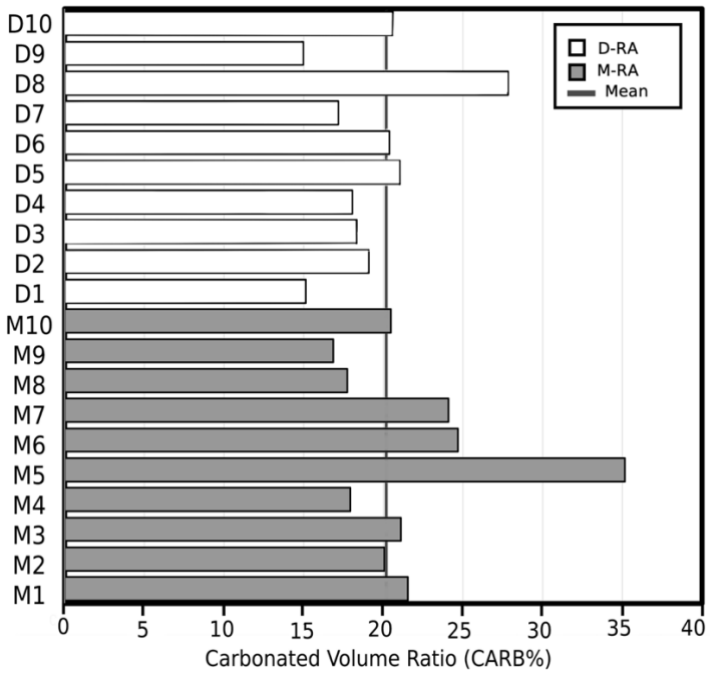

Figure 32. *Results of the estimation of the carbonation volume (%) of the attached mortar within the samples.*

The values are obtained employing again the **Equation (10)**, based on the mineralogical model proposed in **Equation (2)**. The fraction of AM that is carbonated among the two subgroups is essentially uniform, having a mean value throughout the whole range of 20.61%. This can be explained by the homogenous source of waste stream taken as a sample in the present study. Instead, due to various aging, environmental circumstances during

disposal, and the initial composition of the cement used, the carbonation level of the residual paste attached may vary substantially.

3.4.6 Computer-vision-based prediction of attached mortar

To enable a high-throughput classification of the recycled aggregate, a deep learning model is developed and trained to predict the mass fraction of the attached mortar based on the sole input of the photo of individual aggregate particles. In the context of our study, it is worth noting that, although predicting a 3D-based concept (i.e., mass fraction of the attached mortar) from 2D data (i.e., photo of the recycled aggregate) may not immediately appear intuitive. However, it is not uncommon for latent correlations to underlie the feasibility of such a 2D-to-3D mapping. Most likely, the aggregate samples of similar mortar attachments tend to exhibit comparable 2D appearances—for instance, an aggregate with even, brownish color is more likely to be coated with a thick layer of mortar than that showing a mix of different colors. Other examples include but are not limited to aggregate size, surface texture, and origin. The model is trained using 80% of the images collected in this study. Upon completion of the model training, the accuracy of the model was tested based on the remaining 20% of images. This evaluation of the test set images offers insight into the model's effectiveness in predicting the AM of new aggregate samples that were not previously included in the model's training phase. In **Figure 33** is displayed the evolution of the model accuracy on both training and test sets over the 100 training epochs (i.e., 100 iterations of model training).

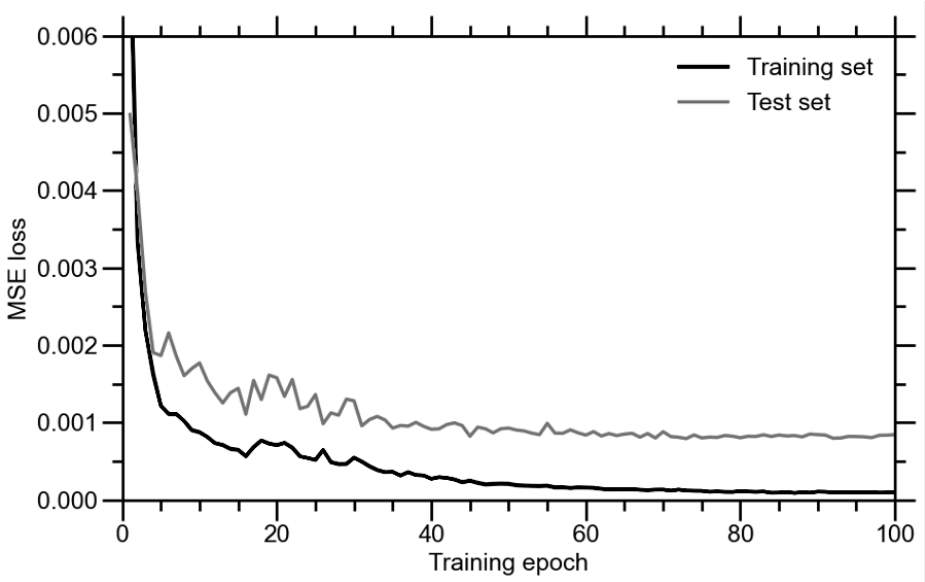

***Figure 33**. Evolution of mean squared error (MSE) loss of the model with the increase of training epoch, based on both training and test sets.*

As a common practice, the model accuracy in this plot is indicated by the mean squared error (MSE) loss, where lower loss means higher prediction accuracy. The model loss here indicates the improvement of the model accuracy as a function of the training iterations. It can be seen that, as the training proceeds, the model loss decreases exponentially and plateaus at around 60 epochs. After that, model performance gradually converges to a steady stage where a small divergence between training and test sets is observed. This low level of overfit is deemed to be acceptable considering the limited size of the training dataset.

As an assessment of the model's performance after the training, **Figure 33** shows its predictions for both the training and test samples. Here, the presence of vertical patterns in the plot is attributed to the fact that, during the mechanical test (refer to Section 2.2.3), each of the ground truth values is obtained as the mass fraction averaged over the 10 samples of the same set. In terms of the model prediction for the training samples, we note that the scatters are distributed tightly along the line of equality, indicating that the model can fit the training samples well. At different levels of the mortar fraction along the x-axis, the predicted values vary within a certain range. In addition to the variation of the aggregate appearance, this is also related to the noise in the dataset, for example, it is difficult to obtain an ideal focus for the whole aggregate particle consistently for each sample under the stereological microscope. Nevertheless, with the sole input of the 2D aggregate image, it is encouraging that the model can yield fairly accurate predictions for most of the training samples, especially given that the prediction target depends on the aggregate volume in 3D. Regarding the prediction for the test samples, the results indicate that the model can still yield reasonably accurate predictions, where the root mean square error (RMSE) on the test set samples is merely 2.8%. Regarding the model accuracy, **Figure 34** indicates that the model exhibits fairly high accuracy on the samples within the C-RA and M-RA groups, as well as most of the samples in the D-RA group up to about 10%. To assess the model's robustness more comprehensively, we present the distribution of prediction errors (i.e., predictions minus true values) for the test set samples in **Figure 35**. The analysis reveals that the distribution of the prediction errors is roughly symmetric, with approximately 40% of the test samples falling within a deviation of ±1%. This observation indicates no significant bias in the model's predictions on the test set, underscoring the robustness of its predictive capabilities. From **Figure 34**, it can be also seen that the predicted values are somewhat capped at about 10%, indicating that the model does not generalize well for aggregates that are heavily coated with the mortar. This should be attributed to the fact that there are limited samples with very high fractions of the attached mortar within the present dataset. Thus, the model is not sufficiently trained to extrapolate beyond the aggregates containing more than

10% of the attached mortar. In addition, it is also possible that aggregates appear very similar after reaching a certain fraction of attached mortar (such as color tone and surface texture). In such a case, it becomes intrinsically challenging to predict the samples of very high AM% regardless of processing methods.

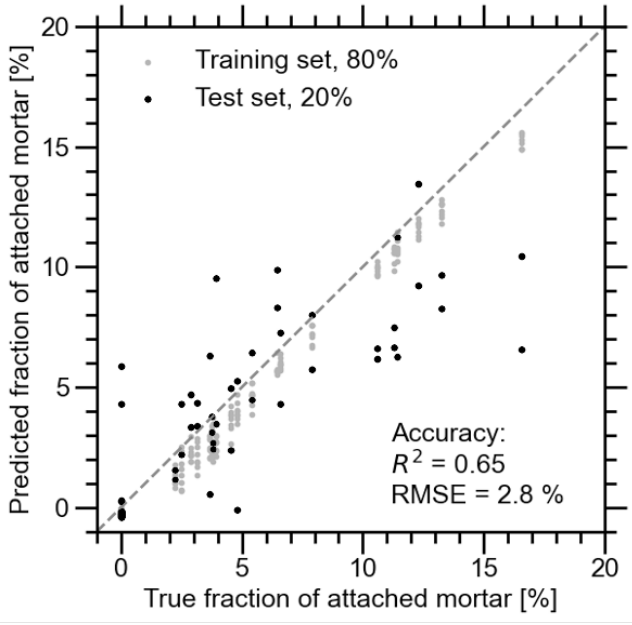

Figure 34. *Prediction of the mass fraction of the attached mortar for the different samples in the recycled aggregate dataset. The blue scatters correspond to the 80% samples in the training set and the 20% samples in the test set, respectively.*

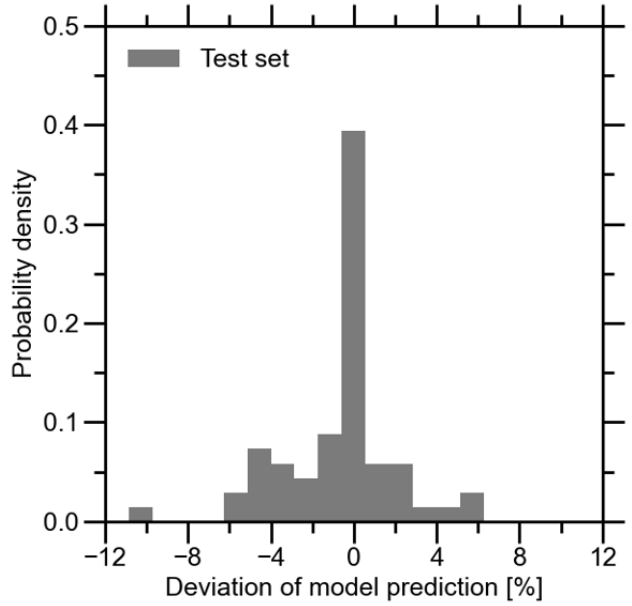

Figure 35*. Distribution of the prediction error for the test set samples. Here, the deviation of model prediction is defined as the difference in the mass fraction of the attached mortar (i.e., prediction – true).*

3.4.7. Empowering the high-throughput screening of recycled aggregates with artificial intelligence

Based on the results presented in **Sec. 3.6**, we now discuss the potential of using our deep learning model to enable the high-throughput classification of recycled aggregates. We first note that the trained model exhibits fairly accurate predictions on the recycled aggregate dataset curated in this study. This is not only observed from the samples used for training the model, but also for most of the test set samples that are never involved with the model training. To this end, the results presented in **Figure 34.** Prediction of the mass fraction of the attached mortar for the different samples in the recycled aggregate dataset. The blue scatters correspond to the 80% samples in the training set and the 20% samples in the test set, respectively. are further analyzed to obtain a confusion matrix to reflect the model performance in differentiating the three classes of recycled aggregates with different AM amounts—namely, Low: <2%, Medium: 2-to-5.1%, and High: >5.1%, as shown in **Table 2**. Note that, to obtain a fair assessment of the model accuracy on predicting samples that are not seen during training, all the results presented in Table 2 are solely based on the test set samples and intersection over union (IoU) is considered as the metric for classification accuracy.

Confusion matrix		Predicted AM%			IoU accuracy [%]
		C-RA	M-RA	D-RA	
True AM%	Low (<2.0%)	18	1	1	75
	Medium (2.0-5.1%)	4	13	3	57
	High (>5.1%)	0	2	18	75

Table 2. *Confusion matrix of the deep learning model for classifying the recycled aggregate samples in the test set (i.e., 20% of the samples at each AM% level), along with the intersection over union (IoU) accuracy.*

Considering the noise in the dataset and the intrinsic difficulty in inferring the mass fraction of the attached mortar based on 2D images, the deep learning model offers a desirable classification accuracy. In comparison, the model performs best in detecting the C-RA and D-RA, where only 2 out of 20 samples in both of those groups are misclassified. Furthermore, no aggregate from the D-RA group is misclassified into the C-RA group. In comparison, the model exhibits inferior accuracy in recognizing the samples in the M-RA

group. With the IoU accuracy almost 20% lower than the other two classes, 20% and 15% of the M-RA samples are predicted to be C-RA and D-RA, respectively. This can be attributed to two reasons. Firstly, the averaged AM% values for each set of samples may not accurately capture the variation of attached mortar in the individual samples under each set. Secondly, the variation in model predictions leads to confusion due to the gradual transition in appearance between C-RA, M-RA, and D-RA, which is exacerbated by the much smaller band of values occupied by the category. Despite the above-mentioned challenges faced by the model prediction, we highlight several significant advantages of our proposed computer-vision-based model in addressing the critical requirement for rapid classification in high throughput screening of recycled aggregates.

1. By leveraging the deep learning, we are able to provide instantaneous predictions of the AM% for a given aggregate image. Notably, as a regression model, it demonstrates commendable accuracy, yielding reliable inferences of the AM mass ratio (%) within a range of up to 10%.
2. Meanwhile, when converting the predicted values into aggregate classes, our model exhibits an impressive 90% recall rate in accurately predicting the C-RA and D-RA aggregate categories.
3. An additional strength lies in the fully automatic training process of the deep learning model, eliminating the need for manual judgments such as determining color thresholds for specific image datasets.

3.4.8. Enhancing RA recycling by deep learning and mineralogical models

In addition to classifying the waste according to the predicted AM fraction using deep learning, another step is done to increase the likelihood of recycling and reusing CDW in new construction materials. While determining the best strategies to recover CDW from old concrete, the AM content is not the only factor to consider.

1. The mineralogical composition of the AM can vary abundantly, being primarily affected by the degree of carbonation of the layer itself due to various aging, environmental circumstances during disposal, and the initial composition of the cement used. The final result is a variety of raw material byproducts with various chemical and physical characteristics, depending on the degree of carbonation.
2. After using the QPA-Rietveld mineralogical model and utilizing the methodological technique based on GMM clustering of samples and mechanical detachment of AM,

the best suited methods to reuse the CDW can be established in customized application. This step could represent the final stage of a decision-making process in terms of choosing a technological and organizational solution in the field of concrete waste management (Sobotka & Sagan, 2021). This data structure can be combined and integrated with actual project workflows, including time, cost, and other supply chain indicators that aid in informed decision-making (Sivashanmugam et al., 2023).

3. If the optimum way to reuse C-RA is always to employ them as brand-new aggregates in fresh concrete, suggesting a similar procedure for M-RA and D-RA could be not advantageous. The two parameters that needs to be taken into account simultaneously are the AM content and the carbonation degree of the connected residual cement paste (**Figure 36**).
4. The materials classified as M-RA can be categorized as natural aggregates with less than 25% volume ratio of cement paste connected (Figure 9), and the reuse as RA can be determined depending on the AM's degree of carbonation. If the materials present a low-carbonation of the AM the best solution is to reuse them as RA after removing mechanically, chemically or thermally the old interfacial transition zone layer (Ouyang et al., 2020; R. Wang et al., 2020). Instead, a positive interaction forms when the components are utilized inside fresh cement paste if the AM layer has a high carbonation degree (Stefaniuk et al., 2023). The carbonation process led to the formation of silica gel which transforms the materials in a pozzolanic source, giving to the new cement matrix a recovery of latent performances of the available cement phases (Lu et al., 2019; R. Wang et al., 2020).
5. The D-RA class display a volume of AM that is never suitable for use as new aggregates in concrete, superior to 25% volume ratio (Figure 9). Once more, if the materials exhibit a modest degree of carbonation, they can be used as by-products of raw-mix materials for the clinker production since they are a good supply of carbonate and silico aluminate to be used in the kiln (De Schepper et al., 2013). Instead, if they exhibit a high carbonation level, they once more constitute a reliable supply of pozzolanic materials and can be then included as supplemental cementitious materials in a mixture with new clinker (Moreno-Juez et al., 2021;Stefaniuk et al., 2023).

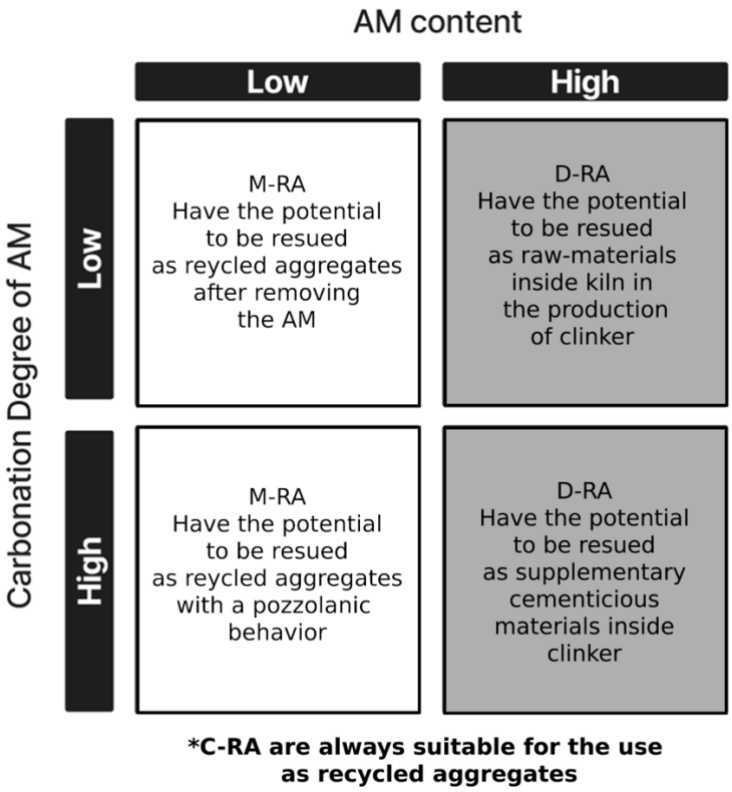

Figure 36. *Schematic description for the best suited methods to reuse the CDW can be established in customized application.*

3.5. Conclusions

The approach based on IAM, machine learning and mineralogical laboratory methods to determine the residual AM volume and to estimate the carbonation degree led to the following conclusions:

1. Although the use of IAM to estimate the amount of AM on the surface of RA seems to be a trustworthy way to quantify the AM content, it is nevertheless susceptible to inaccuracies from human sources. The improvement made from the computer-vision-based model gives less uncertainty and higher accuracy in predicting the AM content on surface of RA.
2. By leveraging the deep learning, we are able to provide instantaneous qualitative predictions of the AM content for a given aggregate image. Notably, as a regression model, it demonstrates commendable accuracy, yielding reliable inferences of the AM mass ratio (%) within a short range of values.
3. Our model shows an impressive 90% recall rate in correctly predicting the C-RA materials and D-RA aggregate categories when converting the predicted values into aggregate classes. This result shows that a portion of high-quality secondary raw

materials (C-RA) can be extracted from the CDW unsorted waste stream using an optical-based sorting plant that employs artificial intelligence. These RAs can be fully reused in the production of concrete without compromising the overall engineering properties due to the presence of residual AM, making them perfectly comparable to those derived from nature's resources.

4. The mineralogical model introduced to reconstruct the volume of attached mortar paste on the surface of RA from XRPD and Rietveld refinement displayed a strong correlation (R^2 0.94) with the measured attached mortar mass, representing a valid and viable method to estimate this parameter.
5. By using the same model, it is possible to obtain an indication of the degree of carbonation of the connected residual cement paste. Even though this data is less precise and sensitive than other known analytical technique and methods currently available, it may nevertheless be more usefully utilized for a fast evaluation and categorization of the secondary materials.
6. Different potential final uses for the CDW are discussed, depending on the AM concentration and cement paste carbonation level, it is not possible to rely solely on one of them in order to achieve the effective reuse of these materials. Because both of these factors are significant to define tailored reuse of RA, toward the sustainable development of the building material sector.

It is worth mentioning that despite more testing is required to better calibrate the procedure with industrial operating conditions, such as high fluxes of simultaneous materials to be analyzed, dry and wet conditions and RGB camera settings, the technology proposed has the potential to be scaled in large-scale optical sorting plants for CDW. It is essential to validate all these results in the real-world application.

The future objective of this research is to establish an extensive laboratory characterization of AM on CDW sorted materials for verifying the accuracy of the prediction’s outcomes, as well as to conduct continuous test on the reuse of these secondary raw-materials in different building materials applications based on the mineralogical method proposed.

4. Multi-scale X-ray techniques for assessing recycled concrete aggregates: from XRPD analysis of leftover cement in recycled aggregates to micro-CT imaging of concrete microstructure

Abstract

The proportion of leftover cement paste to natural sand and gravel is a significant element for the quality of recycled aggregates. Various strategies are being used in laboratory to obtain this information from chemical (acid dissolution, water absorption) to physical approaches (mechanical separation, thermal desegregation), as well as spectroscopic and microscopy analyses. Most of these procedures are time consuming and often do not provide a direct measure in this regard. Using a novel mineralogical model based on X-ray Powder Diffraction and Rietveld quantitative phase analysis the same measure is conducted. The results are compared with those obtained from a multi-scale investigation (microscopy, X-ray computed tomography, mechanical testing) applied to the concrete specimens containing the same products. The results display a relationship between the leftover cement paste and numerous features and properties of the concrete, ranging from the microstructure to the hydration products developed and also, eventually, to the mechanical performance.

Keywords: recycled concrete aggregates, attached mortar, CDW, X-ray diffraction, microstructure.

The data contained in this chapter are part of a Full-Length Article submitted in Development in the Built Environment, Elsevier (29th November 2024):

Multi-scale X-ray techniques for assessing recycled concrete aggregates: from XRPD analysis of leftover cement in recycled aggregates to micro-CT imaging of concrete microstructure

A. Bisciotti[a,*], L. Mancini[b] , A. Viani[c], V. Zalar Serjun[b], A. Mladenovic[b], G. Cruciani[a]

[a] *Department of Physics and Earth Science, University of Ferrara, Via Saragat 1, 44122 Ferrara, Italy.*
[b] *Slovenian National Building and Civil Engineering Institute - ZAG, Dimičeva ulica 12, 1000 Ljubljana, Slovenia.*
[c] *University of Modena and Reggio Emilia, Department of Chemical and Geological Sciences, Via Campi 103, 41125 Modena, Italy.*

4.1. Introduction

Construction and demolition waste (CDW) is one of the main categories of waste produced globally, so, its recycling in a circular economy to produce new building materials has become crucial (J. Li et al., 2023; Su et al., 2024). Recycled aggregates (RAs), which are produced from CDW, might potentially cut down the total environmental effect of concrete production downsizing the mining of natural resources from aggregate quarries and pits (Dinh et al., 2022; Nilimaa, 2023). It is commonly acknowledged that RAs derived from the comminution of CDW are potential substitute of natural aggregates (NAs) in construction projects (Althoey et al., 2023; Karlsson et al., 2021). At the same time, the current use of these secondary raw materials is mostly devoted to sub-bases and bases of pavements of roads and highways, where they are employed in unbound layers and low-grade concretes (Zhang et al., 2020). The lack in the adoption of the RAs in high-grade applications (i.e., structural concrete) comes from the composite nature, and high heterogeneity of these secondary raw-materials, resulting in uneven interactions with cementitious binders (Djerbi, 2018). In fact, when directly produced from CDW crushed concrete, RAs are typically composed of the original NAs and of a variable amount of leftover cement paste (AM) clinging to the surface (de Juan & Gutiérrez, 2009). The final properties of recycled aggregate concrete, where RAs are used instead of natural counterparts, are adversely impacted by the amount of AM (Bai et al., 2020; J. Kim, 2022; Seo & Choi, 2014). This characteristic is considered as the primary obstacle that prevents the use of RAs in new structural high-grade concrete (Tam et al., 2021; Verian et al., 2018). Compared to natural rocks, the AM increases the average porosity and reduces the bulk density of such aggregates, which is a major reason for the observed declining trend on the fresh-mixing properties (Deng et al., 2023; Faleschini et al., 2014; B. Li et al., 2021), mechanical performances (Piccinali et al., 2022; B. Wang et al., 2021), and durability of recycled aggregate concrete (Guo et al., 2018), affecting the confidence of the stakeholders in adopting RAs. The content of AM within RAs is known to vary depending on the average RAs diameter size, crushing methods, ageing and original strength grade of the AM, thus affecting the final properties of concrete with a variable and unpredictable order of magnitude (Chen et al., 2024). The evaluation and characterization of the AM content appears then as a mandatory step to monitoring the quality of RAs, and shall become a mandatory requirement prior to batching plant. Despite of this requirement, an internationally standardized procedure has not been established yet, whereas different methods have been proposed, as summarized in (Braymand et al., 2016). Various

methodologies are now being utilized to obtain this information (dos Santos Macedo et al., 2019; Zhao et al., 2013), ranging from the chemical (acid dissolution, water absorption) to the physical approaches (mechanical separation, thermal desegregation) as well as spectroscopic and microscopic analysis (Ulsen et al., 2022). Many of these procedures are time-consuming and not-suitable for routine quality monitoring, while others fail to offer a clear, straightforward information for this purpose (Rangel et al., 2019). The acid leaching approach, for example, could overestimate the cement paste content when recycled aggregates contain limestone, or many other acid-soluble rocks/minerals. Microscope investigation is typically highly operator dependent. The water absorption value is affected by cement paste porosity. Whereas methods based on the chemical composition (i.e., X-ray fluorescence) are yet not able to distinguish AM from limestone content (Angulo et al., 2009). In this scenario, X-ray Powder Diffraction (XRPD), which is nowadays largely employed in the cement and construction sector, may offer a valuable alternative solution (Snellings, 2016). This method has grown beyond its roots in the world of laboratory research and is regarded as one of the most powerful industrial process-control tools in the field of building materials and minerals (Meier et al., 2012). XRPD opens enormous possibilities for *in-situ* monitoring of process and quality control, even in the field of continuous on-line measurements during industrial production (Dhanjal et al., 2006; Gugin et al., 2024). In this field, additional techniques can be also combined with XRPD to enhance material classification (Bortolotti et al., 2019; Secchi et al., 2018). Bisciotti et al., 2024, first introduced the measurement and quantification of AM using XRPD, also exploring the potential industrial upscaling through artificial intelligence and automated in-line sorting of RAs. The estimation is based on a mineralogical model in which parameters are obtained from XRPD quantitative phase analysis by the Rietveld method. The result reflects the crystalline assemblage in RAs, providing a snapshot of the overall mineralogical composition. In terms of the speed of acquisition, the introduction of ultra-fast silicon-based linear and two-dimensional detectors gives up to 150-fold speed increase (Anderson et al., 2015). A scan that once required three hours to collect data can now be completed in less than two minutes, with some advanced settings achieving results in just a few seconds (D O'Flynn et al., 2013). The Rietveld approach which is the bottleneck of the method proposed can also be automated to speed up the methodology and reduce human mistakes using artificial intelligence algorithm (Feng et al., 2019; H. Kim & Yoon, 2024). The whole process from sample preparation to the Rietveld calculations can be implemented in less than 30 minutes. Due to the completely automated operation principle, no additional personnel is required and the results are user independent (Walenta & Füllmann, 2004). With

the aim of testing the aforementioned method and validate a possible testing protocol, different samples from coarse, fine and ultra-fine RAs are substituted to NAs in a fixed proportion into the concrete mix-design. The samples are previously analyzed through XRPD adopting the mineralogical model for the AM measure. Setting a fixed concrete formulation—where the cement type, water-to-cement ratio, and mixing and curing procedures are kept constant—allows for more accurate tracking of the microscopic features that emerge from RAs usage. This consistency helps highlighting the effects of the AM itself on the microstructure, enabling a straightforward comparison between the obtained values and concrete properties such as porosity, bond strength, and aggregate-paste interface. For this purpose, the investigation of the concrete microstructure has been conducted adopting lab-based X-ray computed tomography (X-ray micro-CT) in conjunction with optical microscopy (OM) and scanning electron microscopy (SEM). A detailed review of X-ray micro-CT application to cement and concrete materials can be found in da Silva, 2018. This technique allows the microstructural characterization of a large range of materials in the three-dimensional (3D) domain with a non-destructive approach (Baker et al., 2012), XRPD and micro-CT have also been used in conjunction for quality monitoring although being very challenging (Artioli et al., 2010; Korolkovas, 2022). Eventually, quantitative data gathered from multi-scale analyses—including pore count, size, geometry, and connectivity—and concrete mechanical testing are compared with AM measurements obtained from the novel XRPD-based methodology. Most of the explored macro and microscopical features from different concrete samples exhibit linear trends with the AM values, representing a preliminary validation of the proposed methodology. Furthermore, a general worsening for most of them is reported and described when increasing AM values are found. Nevertheless, the results expand the existing understanding of D-ITZ developing from RAs interaction with the fresh cement paste at the microstructural level (de Almeida Ferreira et al., 2024). Therefore, if we recognize the AM content as a primary feature to address RAs quality monitoring, the proposed method offers a novel and effective approach for rapid screening, highlighting its practical relevance in concrete production.

4.2 – Materials

4.2.1. Natural and Recycled aggregates

The NAs used are sand and gravel from the River Po (Italy), which are described based on UNI EN 932-3:2022. The gradation of the materials is shown in **Figure 37**. The starting

CDW contains more than 90% of structural concrete (> 40 MPa, 28 days compressional strength), the crushed concrete RAs are obtained from the demolition of a structure originally composed of white cement. The materials are collected from the stock piles in accordance with standard UNE-EN 932-1 (1998). After dry sieving (UNI EN 933-1, 2012) the size distributions obtained are used to replace NAs in the mix-design (**Table 3**) maintaining the final granulometric curve unaltered.

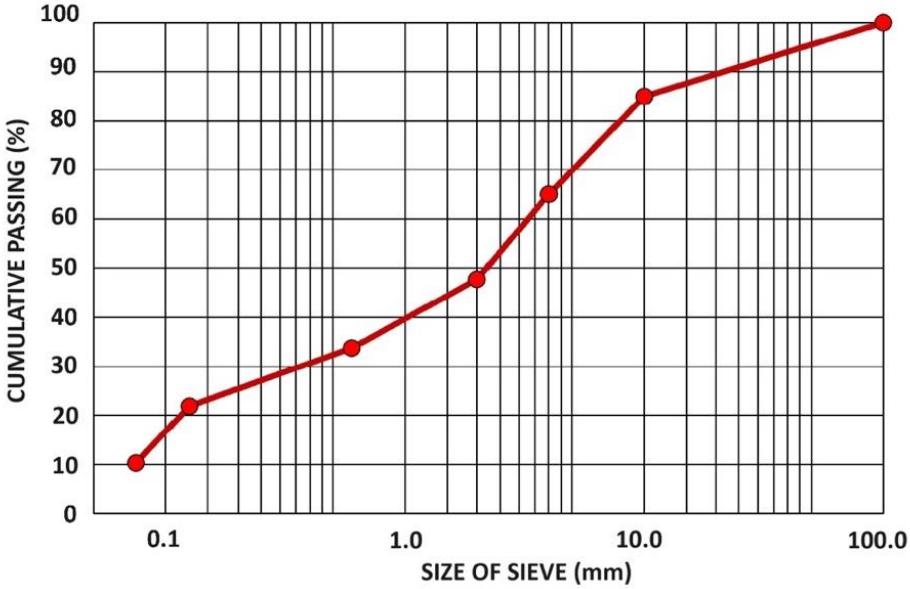

Figure 37. *Gradation curve of the natural aggregate.*

4.2.2. Concrete specimen preparation

The mix-design of the concrete is done according to the British Department of the Environment (DOE) standard method (Teychenne et al., 1997), which targeted a compressive strength of 25 MPa on the 28th day. Type CEM I Portland cement 52.5 R is used, having a sharp different color from the residual white cement paste clinging to the RAs. River Po (Italy) sand and gravel are used both as fine and coarse NAs. Besides the reference concrete (named NAC) made of only NAs, there are notably other three types of mixtures prepared by replacing the NAs with three individual classes of RAs having different diameter sizes: 10 - 4 mm (CRA), 4 - 0.6 mm (FRA), and 0.6-0 mm (UFRA), although coming from the same original source. The replacement percentage of RAs is calculated based on the total weight of the aggregate content, substituting entirely the corresponding size fraction from the mix-design results. The mix-design for all the specimens is presented in **Table 3**. The water-binder ratio is kept at 0.58 in all the mixtures. No chemical admixtures are used.

	Material content (kg/m3)						
Mixture	**Cement**	**NA**	**CRA**	**FRA**	**UFRA**	**Water**	**W/C**
NAC	313.64	1822.68	-	-	-	181.68	0.58
CR104	313.64	1184.80	637.88	-	-	181.68	0.58
CR406	313.64	1251.51	-	571.17	-	181.68	0.58
CR060	313.64	1209.05	-	-	613.64	181.68	0.58

Table 3. *Material content within the concrete specimen accordingly to the mix-design obtained with British DOE Standard Method.*

4.3. Methods

4.3.1 Testing protocol

The samples of RAs analyzed, divided into the aforementioned classes (CRA, FRA, UFRA), are obtained in the lab using a quartering method according to UNE-EN 932–2, 2000. Starting from each RAs mound, a 10% weight of the material content is collected and shredded into fine powder using a jaw-crusher and afterwards a mechanical press. The fine powders obtained are directly analyzed through XRPD. From the results employing Rietveld quantitative phase analysis, the wt. (%) of the different crystalline constituents of the RAs is used to reconstruct the AM content accordingly to the method proposed in Bisciotti et al., 2024. Subsequently, all the concrete mixtures designed have been produced accordingly to UNI EN 206:2021. The specimens are casted in laboratory condition and demolded at 24 ± 2 hours after mixing, and then fully submerged in water at a temperature of 25 ± 2 °C until the age of testing. The determination of the flexural and compressive strength is done after 7, 28 and 90 days of curing. Following a first investigation with OM and SEM, the concrete samples are subjected to X-ray micro-CT analysis. Different microstructural characteristics of the concrete specimens are quantified from the 3D tomographic reconstruction and from further image analysis process. The obtained results are compared and discussed. **Figure 38** schematically depicts the testing protocol.

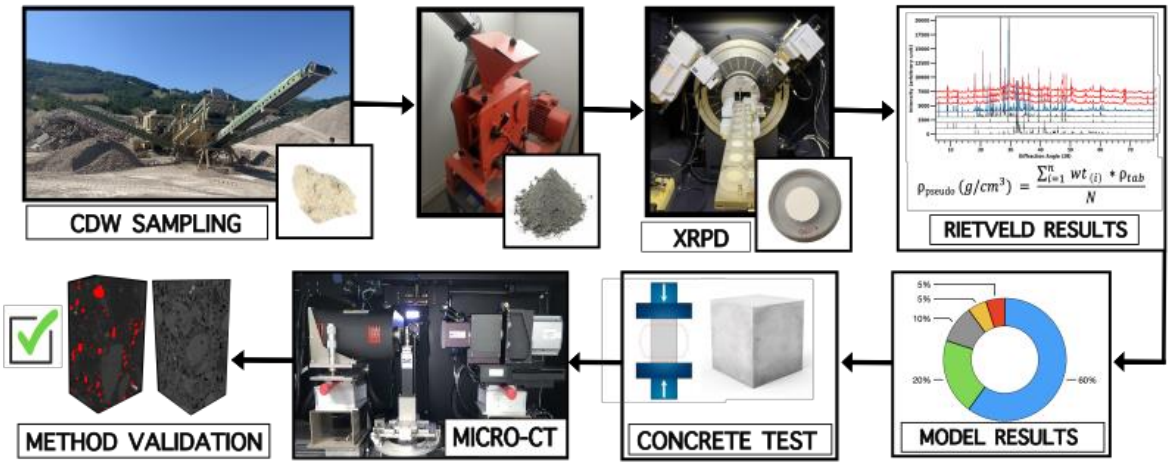

Figure 38. *Testing protocol for attached mortar paste monitoring and validation from the concrete microstructure.*

4.3.2. Raw materials analyses and mineralogical model

Using a Bruker D8 Advance Da Vinci diffractometer at room temperature, the XRPD patterns were collected in the 2θ range of 5-90° at the Department of Physics and Earth Science of the University of Ferrara. The phase identification was carried out with DIFFRACT.EVA suite utilizing the Powder Diffraction File (PDF-2) database maintained by the International Centre for Diffraction Data (ICDD). An accurate quantitative phase analysis (QPA) was then performed by the Rietveld profile fitting method applied to the X-ray diffraction patterns, using the Bruker TOPAS 5.0 software. The results provided a direct volume quantification for the natural fragments dispersed in the RAs, the residual clinker minerals, the hydration phases and of the carbonation products resulting from the latter. Four main classes of crystalline micro-constituents are defined for the RAs materials as follows:

- Rock-forming minerals (RFM) related to the NAs original fraction (quartz, feldspars, chlorite etc.).
- Unreacted-cement (UC) for the anhydrous clinker phases (alite C_3S, belite C_2S, aluminate C_3A – calcium aluminoferrite C_4AF is not present here due to the white cement composition).
- Hydrated-cement (HC) for the hydration products (ettringite AFt, portlandite CH and AFm phases, namely the hydrated calcium aluminates based on the hydrocalumite-like structure). For the C-S-H gel component, a tobermorite-like structure was used (), and a crystallite size of 1.5 nm was fixed to obtain a profile fitting that follows the amorphous content.
- Carbonated-cement (CC) for the calcite polymorphs (calcite, vaterite, aragonite).

During the Rietveld calculation, the individual peak shape functions of the crystalline constituents were summed and combined with a background function. The background was modeled using a two-term Chebyshev polynomial equation over the entire 2θ range to maintain a linear profile. This approach enabled the visualization and quantification of the C-S-H semi-amorphous peak. The weight percentages (wt.%) of the other crystalline phases were determined based on their peak positions and relative intensities. The goodness of fit was evaluated using the Residual Weighted Profile (Rwp) value and visually assessed by plotting the difference between observed and calculated data on the same scale.

4.3.3. Microstructural investigation of concrete

To undertake the microstructure examination, concrete sections embedded in epoxy resin from various specimens were observed using OM and SEM. The SEM device employed is a JEOL JSM-IT500 with an EDS detector and a BSE backscattered electron detector. The acquisitions were carried out in low-vacuum mode, allowing imaging and analysis of uncoated materials with a gun voltage of 15.0 kV. Concrete specimens of 10x10x60 mm were cut and imaged using X-ray micro-CT. The micro-CT analyses have been performed using a Zeiss XRadia's MicroXCT-400 instrument available at the Materials Department of ZAG (Slovenia) with the following operating parameters: voltage = 80 kV, source power = 10 W, LE2 filtering, source-to-sample distance = 52.5 mm, and source-to-detector distance = 150 mm. For each sample, a series of 1600 radiographs (projections) were acquired over a total angle of 360º, with an exposure time per projection of 3 seconds and an effective pixel size of 17.6 µm. The tomographic reconstruction was performed using the XRM Zeiss reconstruction software. This software also allows to apply a beam hardening correction to the images. The resulting reconstructed axial slices are in 16-bit TIFF format.The processing and analysis of the reconstructed 3D data has been performed using the DragonFly software (version 2022.2, free license for academic users) by ORS (Canada). The quantitative parameters extracted from the volumetric images have been selected with an emphasis on the pore system including porosity (volume %), pore size distribution, pore spatial distribution and connectivity. After an optimization procedure, the following multi-stage protocol was adopted: (1) For all imaged specimens, the original reconstructed slices have been converted to 16-bit raw format, using the Fiji software (Schneider et al., 2012), in the same interval of gray levels intensities in order to compare the gray level values assigned to pores (the darkest areas), silica mineral particles (the brightest areas), and cement matrix (the areas with intermediate intensity). (2) From the overall reconstructed volumes, the

background areas have been removed after defining a Volume of Interest (VOI) from the concrete specimens which is made out of cropped rectangular prisms. For each imaged a VOI composed of (365 x 390 x 830) voxels (corresponding to ca. 6.40 x 6.85 x 15 mm^3) was selected. The VOI must include all relevant morphological features of interest, such as the old and new cement matrix, pores and D-ITZ, being at the same time a representative elementary volume (REV). Due to the inclusion of aggregate particles, concrete specimens have usually high pore volume variations and low connectivity within similar VOI (Yio et al., 2017). Therefore, the REV assessment was undertaken by evaluating pores dispersion using the bounding box approach (Al-Raoush & Papadopoulos, 2010; Lanzafame et al., 2018). (3) The sample microstructure is composed of different phases of interest having broad compositions variability identified after the raw materials analyses (See Sec. 2.3.1). The main feature of interest is the porosity distribution. The 3D images were preprocessed with a grayscale-to-grayscale filter to reduce the noise and enhance its edges. A median filter has been afterwards adopted together with an unsharp filter to enhance the contrast and resolution of very fine pores. The resulting image was then segmented to obtain the binary distribution for the objects of interest. We adopted a semi-automated threshold-based segmentation process to optimally identify the pores by applying the 3D Otsu method (Otsu, 1979). The pores touching the edges of the ROI's prism were excluded from the analysis in order to conduct a study only on the inner representative features. Quantitative analysis was carried out on this preprocessed image. For a meaningful description of the VOI, pores with volume less than 8 voxels have been excluded from the quantitative analysis. (4) After the segmentation procedure it has been possible to calculate the volume (%) of pores and to determine their spatial 3D distribution within the cement matrix as well as the main properties of interest such as geometrical features and connectivity. All this information has been obtained after completing a skeletonization of the pore phase using the tool available in the Dragonfly software. This method allows to extract the "spine" of a 3D object generating a node at each pore location and node-to-node branches. Analyzing the skeleton morphology allows for a simpler 3D depiction of the pore network, providing quantitative data such as the number of nodes and the branch distribution (Zandomeneghi et al., 2010).
(5) Numerous statistical attributes were computed for each individual pore, in addition to their volume percentage (total porosity). These parameters were chosen after a review of the literature and variables found in studies on the porosity of bricks and other building materials. Among them, six parameters have been selected for characterizing the microstructure of the investigated concrete samples, namely: pores volume, aspect ratio,

sphericity and mean Feret diameter as well as skeleton Euclidean length and number of skeleton branches.

4.4. Results

4.4.1. X-ray powder diffraction and Rietveld refinement

The XRPD pattern collected from the CRA, FRA and UFRA samples provides a unique 'fingerprint' information on the crystalline constituents from the bulk RAs assemblage (**Figure 39**). The results of the QPA applied to the X-ray diffraction patterns of the RAs are shown in **Table 4.**

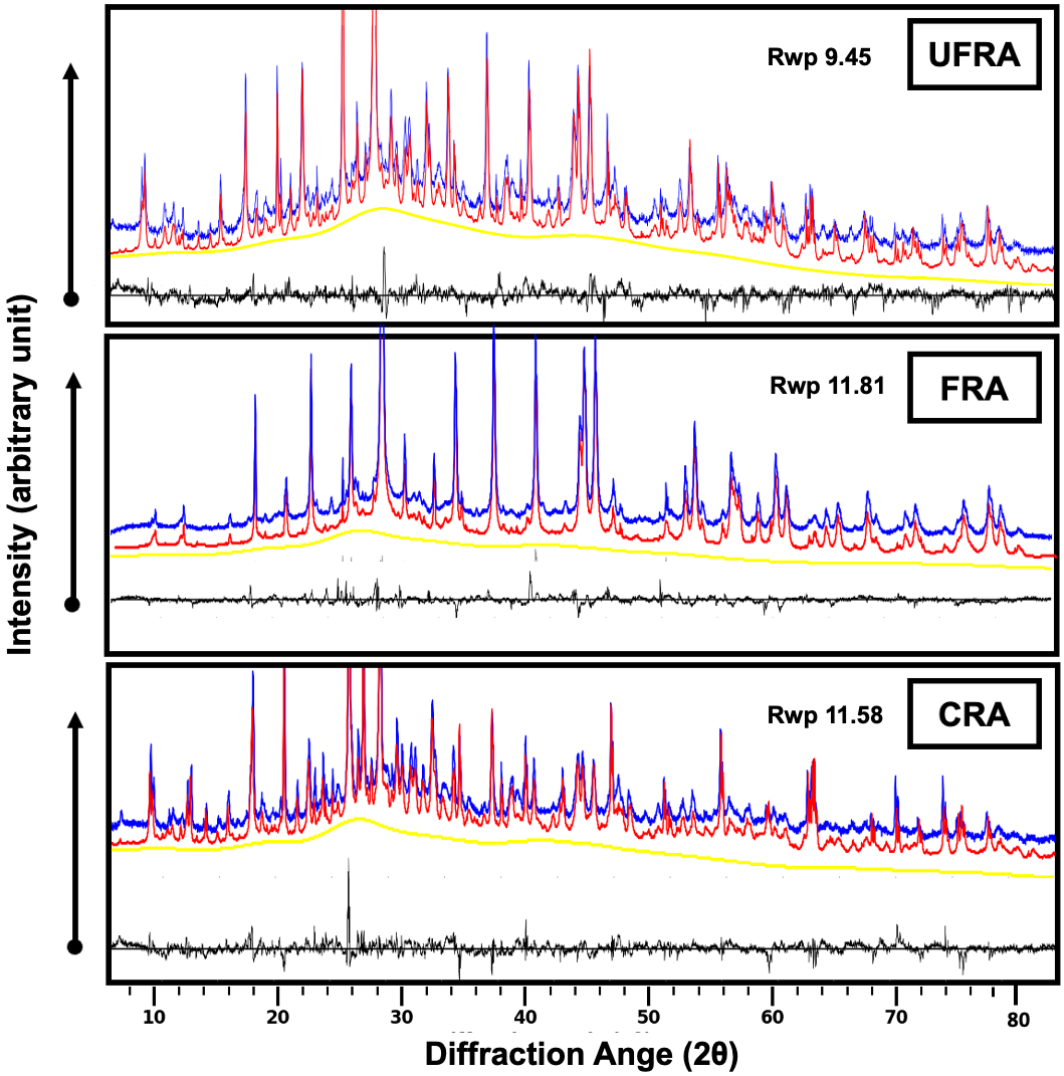

Figure 39. *XRPD diffraction pattern for the coarse recycled aggregates (CRA), fine recycled aggregates (FRA), and ultra-fine recycled aggregates (UFRA). The blue profile is for the measured patterns, the red profile is for the Rietvield calculations and the yellow for the C-S-H semi amorphous profile.*

From the peak positions, the occurrence of residual cement minerals (C_3S, C_2S, C_3A) and other secondary crystalline phases which represent the hydration and carbonation products of the AM, were identified. The C_3S phase used is the monoclinic form (M3), based on the CIF file determined in De La Torre et al., 2002. The C_2S employed is in the *alpha* form having a hexagonal structure (Mumme et al., 1995). C_3A is instead in the cubic space accordingly to de Andrade Gobbo et al., 2004. The profile shape for the C-S-H amorphous phase is very similar between the samples, and comes from the CIF file of hillebrandite, a crystalline natural analogous of C-S-H, based on Dai & Post, 1995). By setting the crystallite size below 5 nm the C-S-H semi-amorphous structure was model. Beside AFt (ettringite), two main AFm phases are identified. AFm (1) in Table 2, refers to the emi-carbo aluminate form and AFm (2) to the mono-carbo aluminate one (Renaudin et al., 1999). The minerals accounting for RFM are mainly silicates and carbonates. Hence, the occurrence of feldspars, quartz, dolomite, iron-minerals (hematite and goethite) likely pertain to the original NAs counterpart fragments. Hornblende as well, is a common mineral often associated with volcanic and metamorphic rocks. Other phyllosilicate minerals (muscovite and chlorite) could mainly result from the fine-NAs originally used, or occasionally resulting from soil mixing during disposal of the CDW. Calcite is therefore present either as aggregate (primary), or more important as a main carbonation product (secondary) together with vaterite and aragonite. Both primary (type-1) and secondary (type-2) calcite are revealed by the shape of main peak at 29.6° 2θ. The coexistence of two calcite types was modeled using two structures having different crystallite sizes: a type-1 calcite with an average crystallite size above 80 nm and a type-2 calcite with a value of 25-35 nm.

Mineral phases	**UFRA**	**FRA**	**CRA**
Calcite type-1	23.91	53.08	55.16
Quartz	7.14	3.54	9.29
Albite	0.96	0	1.88
Orthoclase	0.94	1.52	1.37
Chlorite	0	0.43	0.39
Muscovite	2.8	1.27	2.16
Dolomite	3.61	1.13	2.28
Lizardite	0.12	0	0.02
Goethite	0.18	0.04	0.03
Hematite	0.17	0.1	0.02
Horneblende	0	0.2	0.34
Kaolinite	1.35	0	0.45
Tricalcium Silicate C_3S (M3)	3.74	0.23	0.19

Dicalcium Silicate C_2S	2.21	0.52	0.6
Gypsum	0.13	0.4	0.36
C_3A	0.15	0.04	0.05
C-S-H	43.31	34.92	24.35
Ettringite (AFt)	2.27	0.54	0.18
AFm (1)	1.35	0.61	0.63
AFm (2)	0.24	0	0.03
Portlandite	1.95	0.84	0.2
Calcite type-2	3.06	0.4	0
Vaterite	0.41	0.21	0.02

Table 5. *Rietveld quantitative phase analysis of the studied RA samples (UFRA, FRA, CRA) with the wt.% of mineral phases identified and classified as unreacted cement (UC), hydrated cement (HC), carbonated cement (CC) and rock forming minerals (RFM).*

4.4.2. Mineralogical model

The results of the XRPD Rietveld quantitative phase analysis were used to reconstruct the volume of RFM, UC, HC and CC for the different RAs used. To reconstruct the volume for the different RAs under analysis an equivalent sphere was calculated for the three groups. The CRA have an equivalent volume of 1436.02 mm3, the FRA of 50.94 mm3 and the UFRA 0.11 mm^3. The partial steps of calculation for the mass content and relative volumes can be found in **Table 6**.

	Wt. (%) from Rietveld			**Reconstructed volume (mm^3)**		
RAs type	***CRA***	***FRA***	***UFRA***	***CRA***	***FRA***	***UFRA***
RFM	73.39	61.31	41.18	10.5E4	3123	4.65
UC	1.20	1.19	6.23	0.1E4	60.62	0.70
HC	25.41	37.12	49.53	3.6E4	1890	5.60
CC	0.00	0.40	3.06	0.00	20.37	0.35

Table 6. *Results of the calculated mass and reconstructed volume from the XRPD mineralogical model QPA-based of different RAs.*

The results of the XRPD Rietveld quantitative phase analysis were used to obtain the volume of RFM, UC, HC and CC for the different RAs used. The results show that CRA have the higher volume fraction of RFM (%) related to the NAs counterpart (73%), whereas for the FRA and UFRA the values are progressively decreasing (respectively 61 and 41%). The opposite trend is found for the HC (%) volumes, which account for 25% in the CRA, 37.5%

in FRA and 50% in UFRA. A similar trend is found for the UC%. The CC (%) is eventually very similar within all the different samples, accounting for only few points percentage. The sum of the mentioned components, without the RFM (%) content, contributes to the total LCP (%) content, which is found to be 59% in UFRA, 39% in FRA and 27% in CRA in **Figure 40**.

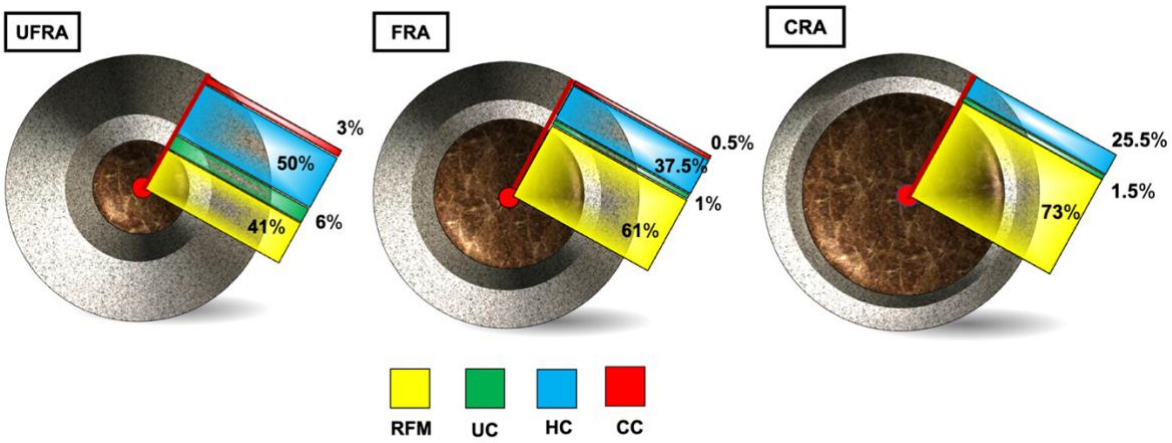

***Figure 40**. Pie charts of the RAs reconstruction according to the mineralogical model.*

4.4.3. Concrete sections microscopy

The petrography of sand and gravel of the Po' river, following OM analysis is provided in **TABLE XXII** of the Supplementary Materials. The properties of the concrete samples, such as the cement matrix, aggregates, and D-ITZ surroundings, were also captured and outlined using OM (**Figure 41**). The new cement paste is gray, while the old AM is made with white cement, making it easy to distinguish RAs clasts from their natural counterparts. Comparing the reference sample NAC with the other recycled aggregate concrete samples it is possible to highlight a different distribution of grains. In fact, NAs tend to be more rounded than RAs, which could directly affect packing distributions and, consequently, the final properties of the concrete. (Q. Liu et al., 2024; Ren et al., 2024). Also, it is evident that the amount and distribution of AM is uneven within RAs, some grains are fully covered whereas other are only partially surrounded (i.e., sample RC104). This condition is a direct consequence of the crushing process of the original source of concrete-CDW (Y. Chen et al., 2024) and could significantly affect the accuracy of other testing approaches. While XRPD analyzes bulk samples, microscopy and SEM provide estimates of AM in individual grains. As a result, these methods may not yield a representative view of the overall clast distribution, if the AM content is unevenly distributed.

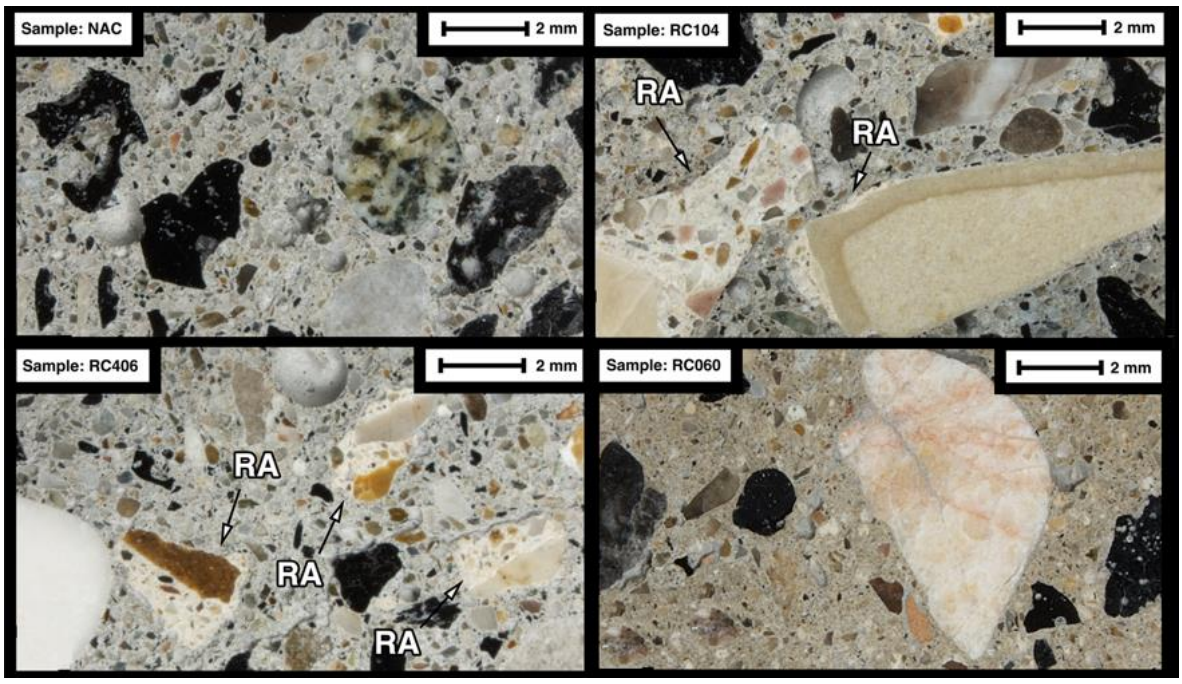

Figure 41. *Optical microscopy images of the concrete specimen sections.*

Direct imaging of hydraulic cement products by SEM analysis yields a more complete picture of both bulk and surface phase compositions of the cement matrix. Characteristic features such as crystal shape, occurrence within the micro-structure, and semi-quantitative point analysis have all been employed in the phase identification and in the morphological descriptions. Following the SEM analysis of the reference concrete sample NAC (**Figure 42a**), the refence Portland Cement hydrated paste composition is measured providing a description of the C-S-H amorphous phase being the Ca/Si molar ratio measured at 2.15 when the Ca/Si molar ratio is usually comprised from 1.0 to 2.3 (Nonat, 2004; Richardson, 1999). From the analysis of Sample RC104 it is clearly observable the presence of RAs with the distinct presence of AM (**Figure 42b**). From the morphology of the grain and point analyses on the surrounding area, it is reported the clear presence of unreacted C3S grains (**Figure 42c**). Furthermore, ettringite crystals (called e) are found within the CEM matrix. In the sample RC406 (**Figure 42d**), it is still possible to observed the presence of RAs with a considerable amount of AM within the cement matrix. The composition of the AM is usually enriched in Ca compared to the standard C-S-H ratio of Ca/Si. The rim of the AM analyzed from BSE images shows a micrometric (less than 5 μm) front, lighter in color, mainly composed of Ca, which can be described as part of the ITZ (**Figure 42e**). Last image, (**Figure 42f**) comes from sample RC060 where three RA (0.60 – 0 mm) are shown and apparently being almost completely composed of AM on the outer surface. Precedent literature already indicates that the AM is usually higher within smaller diameters RAs (Bai

et al., 2020). The presence of unreacted cement grains, mostly C3S crystals, is widespread in the new CEM paste matrix mostly in the surrounding areas of RAs. The overall distribution of unreacted products is here higher than how reported in the previous samples.

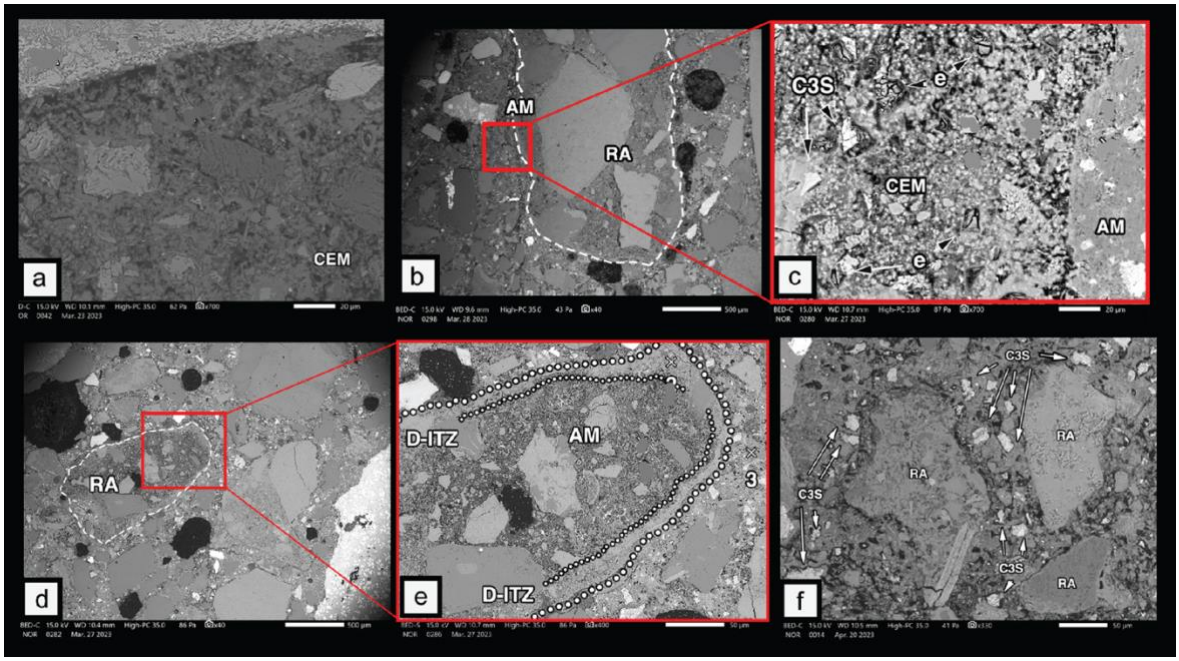

Figure 42. *SEM images of studied samples and BSE chemical semi-quantitative results from the point analyses.*

4.4.4. X-ray computed microtomography results

Based on the reconstruction of the micro-CT images (**Figure 43**), a sequence of image processing operations was performed to quantify the sample's main features of interest.

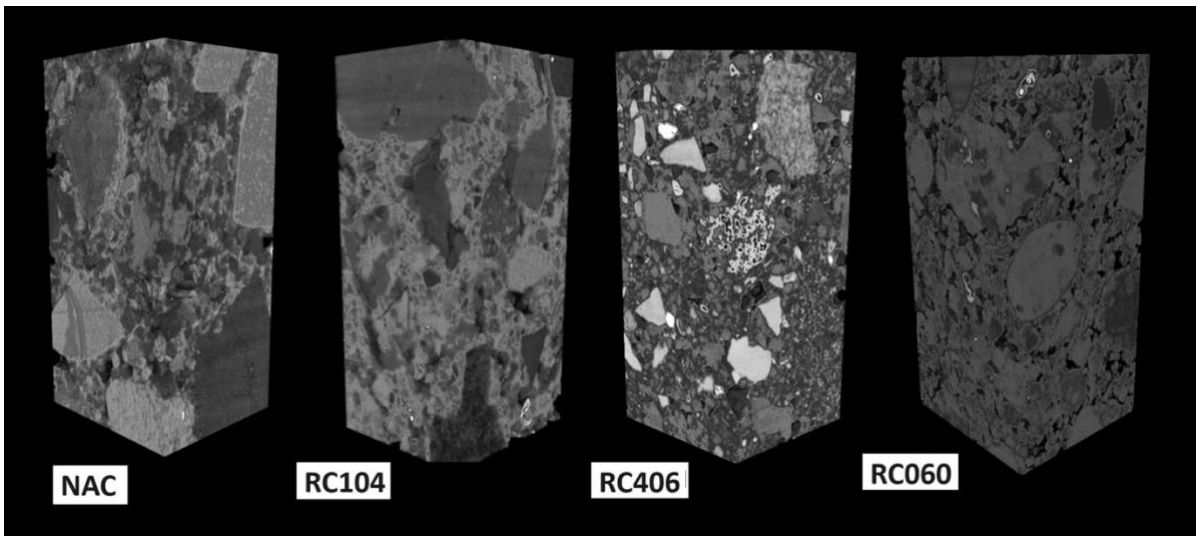

Figure 43. *3D rendering of the investigated volume of interest (10 x 10 x 60) mm for different concrete specimens.*

The characteristic diameter of the RAs utilized (CRA, FRA and UFRA) is found to have a direct influence in shaping the porosity developed inside the cement matrix (**Figure 44**). Both total porosity (%) and pores volume (mm^3), which is a measure of the average volume for the whole porosity distribution, decline linearly when RAs of smaller size are replaced in the reference mix-design.

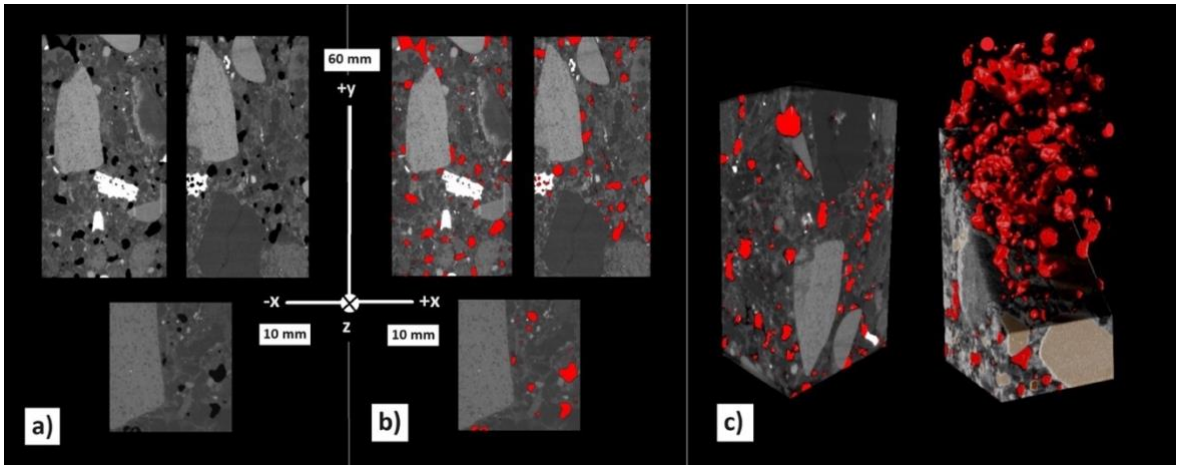

Figure 44. *Results of image processing and analysis for the reference sample NAC. a) Reconstructed slices in the main axial directions, b) the same slices after processing and segmentation, c) 3D total porosity distribution.*

For the porous phase, diameters, volumes, surface areas, and sphericities of pores have been obtained, along with color-coded visualizations according to pore attributes. Numerous statistical attributes were computed for each individual pore, as shown in **Table 7**, in addition to their volume percentage (total porosity). The geometry of pores changes with the use of different RAs, the aspect ratio is higher for the RC060 (0.70) and steadily decreases until it reaches the NAC reference sample (0.64). The sphericity of the pores, which indicates the general geometry, exhibits the maximum value (0.94) in the NAC sample before steadily declining to the RC060 (0.91). The mean Feret diameter yields a mean value of the pore's diameter, the metric shows that from the RC060 (0.06 mm) to the NAC sample (0.11 mm) the value double.

Samples	*Total porosity (%)*	*Pores volume (mm^3)*	*Pores aspect ratio*	*Pores sphericity*	*Mean Feret diameter (mm)*	*Skeleton Euclidean Length (mm)*	*Connected skeleton branches count*
NAC	5.4	0.008	0.64	0.94	0.11	0.18	6918
RC104	5.6	0.007	0.66	0.93	0.11	0.18	5989
RC406	6.7	0.004	0.66	0.93	0.10	0.17	8225
RC060	7.8	0.002	0.70	0.91	0.06	0.11	80640

***Table 7**. Mean values of the variables obtained from the multi-ROI analysis used to describe the pore distribution for the different samples.*

Furthermore, the score plot of the entire data distribution for the pores' volume displays some other interesting features (**Figure 45**). While the NAC reference concrete has a conventional porosity distribution, with the prevalence of pores larger than 0.5 mm^3, all the other concrete specimens containing RAs exhibit a somewhat opposite trend. In these samples are prevailing finer pores with a maximum volume of 0.005 mm^3, which are not found in the reference concrete. It is worth mentioning the trend involving the fraction of the smallest pores within the recycled concrete themselves (p. < 0.005 mm^3), whose contribution linearly increases with the inclusion of smaller-sized RA, from CR104 (around 350 counts) to CR060 (around 450 counts).

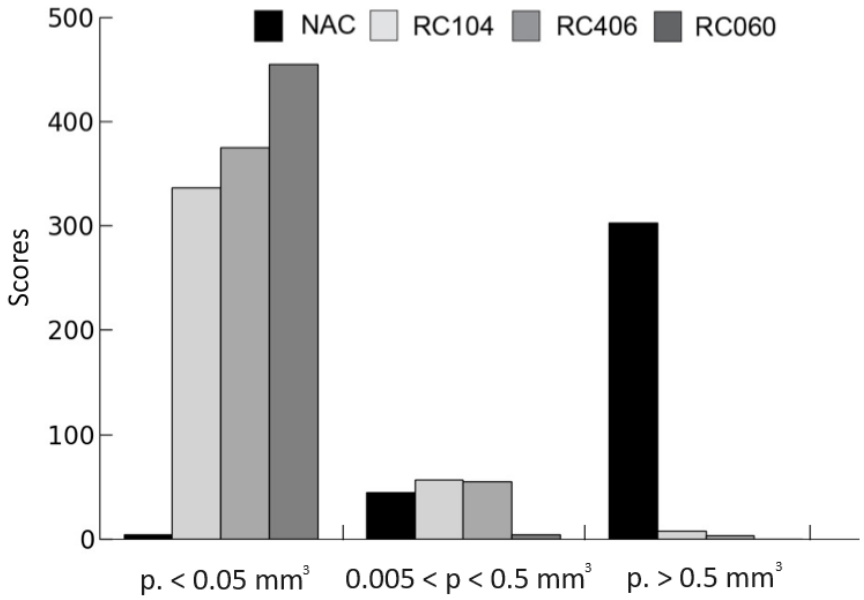

***Figure 45**. Bar charts plot of the pore (p) volume (mm^3) distribution within the studied samples.*

Another significant information obtained from the micro-CT analysis involves the evaluation of the skeleton Euclidean length values and connectivity density (**Table 7**), which characterizes the extension and number of possible paths that connect node-to-node and node-to-end branches measured from a dense graph of the individual pores. From the skeleton Euclidean length (mm) the maximum distance in the porosity network is found in the reference natural aggregates concrete (NAC), the same measure is slowly decreasing with introduction of smaller diameters RAs. The count of skeleton branches, with length between 0 and 0.2 mm, displays even broader differences. RC060 has more than 80,000 local pores connection (**Figure 46**). Comparing the other samples, we can observe that the order of magnitude is in the scale of 10 times higher. In this regard, it is also interesting to point out that sample RC104 has less pore's skeleton branches than the reference sample NAC.

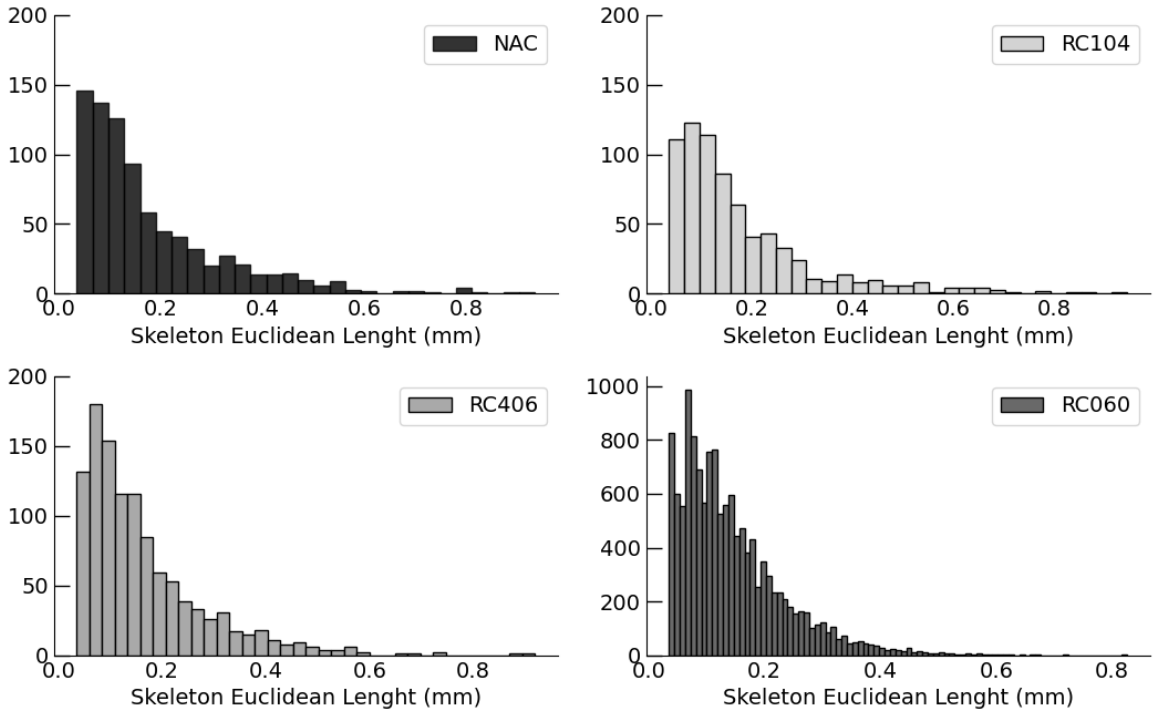

Figure 46. *Skeleton Euclidean length (mm) bar charts for the different specimens*

4.4.5. Mechanical testing

The mechanical test results for the analyzed concrete specimens show a non-uniform pattern that explains the positive or negative impact of replacing NA with RAs in regular mix-design. As prior work has already shown (B. Wang et al., 2021), there are significant variations between coarse (4 - 10 mm in size) and fine (below 4 mm in size) RAs utilization. Following 28 days of curing, the use of fine RAs, as observed for samples RC060 and RC406 lead to a decrease of 38% and 27%, respectively, in comparison to the reference concrete mechanical strength. In contrast, the use of coarse RAs, as in sample RC104, allowed to achieve a mechanical strength 7% higher than for the reference NAC sample (**Figure 47**). The observed reduction of mechanical properties at 90 days of curing for recycled aggregate concrete samples can be due to the aggregate-cement paste weakening caused by moisture absorption from the AM that affects the bond strength, as reported previously (Etxeberria et al., 2007; Poon et al., 2004). This condition represents a substantial threat for the durability and safety of constructions that encompass RAs (J.C. Liu et al., 2023).

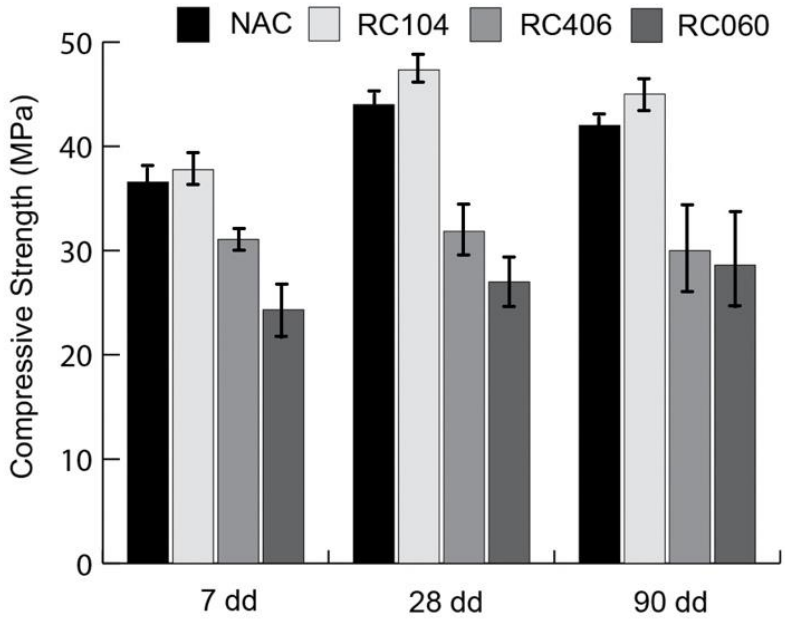

Figure 47. *Bar chart of the compressive strength after 7, 28 and 90 dd of curing.*

4.5. Discussion

4.5.1. Raw materials analyses and mineralogical model

Following the mineralogical model utilized the values pertaining to the four main RA's variables has been determined (**Figure 40**), providing a concise quantitative description of the secondary raw-materials used in the concrete admixture. The model applied to the three types of RAs (CRA, FRA, and UFRA) provides a direct description of the crystalline mineralogical assemblage and how it varied between the different samples. As a result, the RAs may be easily described using only four parameters of importance, which allow for the volumetric reconstruction of the features of interest based on the main groups of crystalline phases. The RFM value represents the volumetric reconstruction for the group of minerals attributed to the original aggregate embedded in the RAs. These fragments, mainly composed of silicate minerals, are primarily responsible for the positive contribution to the final mechanical performance of concrete. It is possible to state that the higher the volume of RFM found in the RA, the higher is the quality of this secondary raw-materials. Indeed, the NA are generally obtained from the rocks having compressive strength higher than 50 MPa, while the recycled aggregates are obtained by the crushing of concretes which have compressive strength lower than 50 MPa. The anhydrous cement phases (UC) are clinker compounds that have not fully reacted during the hydration process. Together with the HC

and CC, they substantially contribute to the overall volume of the AM (%). The presence of UC inside the cement paste is not unusual (Bergold et al., 2013; Jansen et al., 2018) whereas the complete transformation of the starting clinker phases into C-S-H gel is not commonly observed. The compounds counted as HC are ettringite, portlandite and AFm phases. Although the C-S-H gel is the major product of the cement hydration process due to its poorly-crystalline nature it is typically included in the XRD amorphous fraction, which can be also measured using an internal standard (Aranda et al., 2012). The values of CC (%) which represent an indication on the degree of carbonation of the AM resulting from the ageing process. Taking into account that the samples of RAs have been collected from the same environmental condition of disposal and are originated from the same source of the parental concrete are found to be similar. At the same time UFRA display higher values, and this could result from the higher specific surface of the latter. In the studied RAs it is found that the content of AM increases exponentially with the decrease of the diameters. In agreement with most of previous literature data (de Juan & Gutiérrez, 2009; Mazhoud et al., 2022).

4.5.2. Concrete microstructure investigation

The microstructure examination obtained through OM and SEM allowed to understand the main macroscopical and microscopical features of the NAs and RAs. The presence of unreacted clinker minerals in the proximity of RAs, observed by SEM analyses, mainly indicates that the latter interacted with the fresh cement paste, absorbing part of the mixed water, locally affecting the process of hydration. Another well-known consequence of RAs usage is the formation of D-ITZ layers, which has been also observed. Eventually, the thickness of the D-ITZ layers is found to be in the range of 20 - 100 μm, as already described from previous literature (Fang et al., 2023; S. Zhang et al., 2023), therefore the pixel size resolution for the micro-CT analysis was set below this value. The total porosity inside the different concrete specimens soars with the substitution of RAs, and it also increases with the reduction of the RAs' mean diameter (see total porosity (%) in **Table 7**). In detail, all of the RC specimens developed a capillary porosity (volume size < 0.05 mm^3), which is not seen in the reference NAC sample (**Figure 48**). Taking into account the size of the pores, using the mean Feret diameter (**Table 7**), the average radius of the pores is almost two times higher in the NAC sample (0.11 mm) compared to the RC specimens (0.06 mm). The number of small pores increases as the size of RAs decreases, peaking in the RC060 sample and diminishing through the RC406 and RC104 specimens.

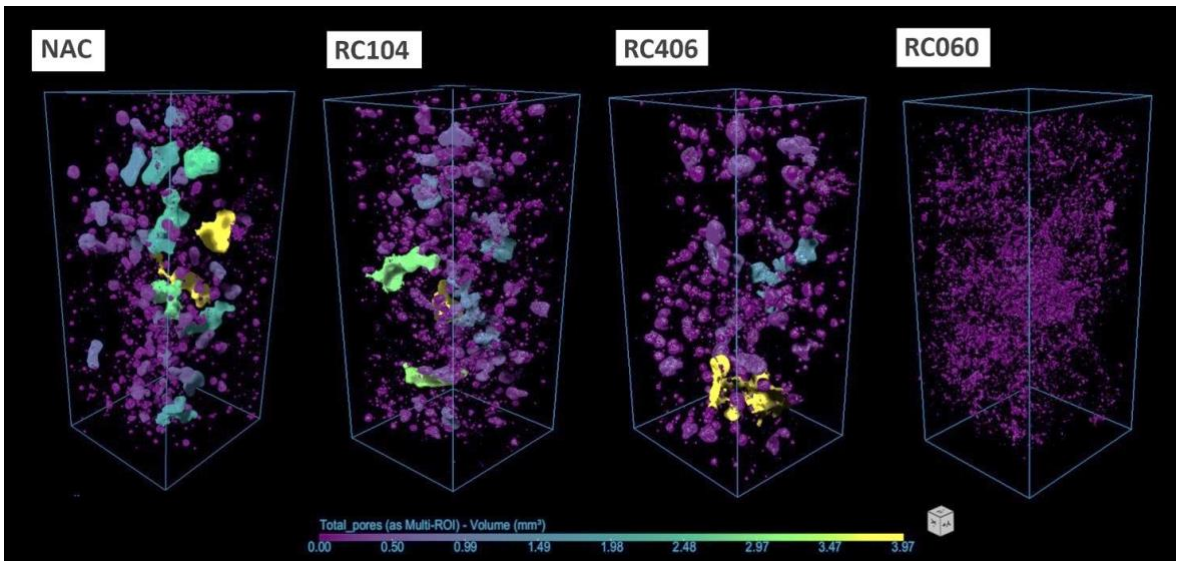

Figure 48. *3D rendering showing the pores size distribution (color-coded) within the studied samples resulting from X-ray micro-CT data.*

The geometry of the pores described from their aspect ratio and sphericity values (**Table 7**) indicates that the use of finer RAs leads to the formation of more equidimensional pores (similar max/min axis) even if less spherical. Larger pores, albeit less uniform, are primarily found in NAC and are caused by entrapped air voids, which range in size from 50 to 300 μm, created during compaction and mixing stages (W. Chen et al., 2023). On the other hand, in the presence of RAs, widespread capillary pores are formed, which are more uniform and usually range in size from 10 nm to 10 μm. These pores are developed when the fresh cement paste and the AM interact (Sáez del Bosque et al., 2017; Zhan et al., 2020). Their development results from the local absorption of the available binding water by the AM, as already proposed previously (Erdem et al., 2018). The pore skeletonization evidenced a correlation in the formation of a tight network of capillary pores and the decreasing in the RAs diameters. The information from the skeleton Euclidean length (mm) represents another key description of the pore distribution in the cement matrix. The use of small diameter RAs causes the length of local-scale connections within the pores to decrease, as shown by the color visualization (**Figure 49**). Eventually, with adoption and subsequent reduction of RAs size, the capillary pores formed are smaller, more frequent, and widespread, resulting in the increase of pore's density connectivity (**Table 7**). This latter circumstance has a large impact on the overall microstructure of the concrete, representing diffused voids and unbound areas formed in the surroundings of RAs, specifically in the proximity of AM. It is therefore possible to conclude that the described capillary porosity is effectively part of the D-ITZ layers.

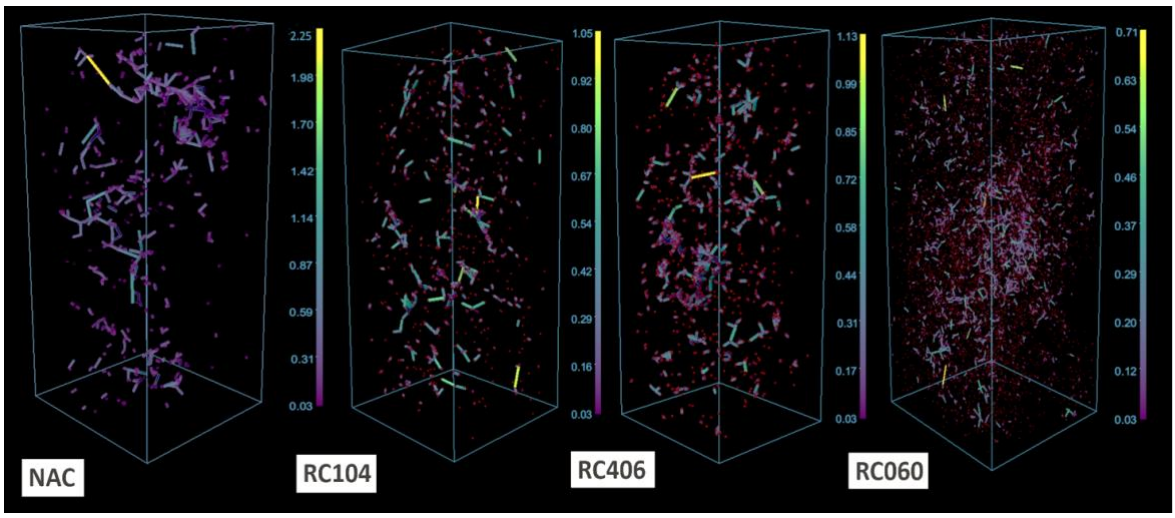

Figure 49. *Skeleton data with the color visualization of Euclidean length (mm) for the studied samples.*

4.5.3. From the mineralogical model to the concrete properties

The non-destructive microstructural characterization in the 3D domain described above, provided a further validation of the method proposed in Bisciotti et al., 2024. In the studied samples the content of AM increased constantly with the decrease of the RAs' diameters, in agreement with previous studies (R. Singh et al., 2022). The exponential soar in the AM content going from CRA and FRA (respectively 27 and 39%) until UFRA (59 %) has been also reported previously in the literature (Ulsen et al., 2022). This condition represents one of the main burdens in reusing fine RAs, limiting the full-scale circularity of all the CDW fractions. Remarkably, all the quantitative information regarding concrete porosity were found to correlate with the AM values obtain from the aforementioned methodology (**Figure 50**). The pore's number, volume, geometry and network of pores are directly shaped by the RAs usage and especially by the AM content. Although a limited number of specimens under discussion the strong linear relations (R^2 from 0.69 to 0.92) are clearly highlighted, also supported by the macroscopical mechanical properties of the samples (**Figure 47**). Notably, more than nine different microstructural parameters are found to strictly follow these trends. In agreement with such trends, the order of magnitude in the parameters found for the RC060 sample's microstructure (pores volume, aspect ratio etc.), supports the evidence that the content of AM in the UFRA could be actually four times higher than in CRA and FRA, as confirmed by the XRPD mineralogical model. This last evidence could be also supported by the results of the mechanical properties, where the RC060 showed a significant worsening compared to RC104 and RC406 (**Figure 50**). As previously discussed, the developing of this capillary porosity reflects the formation of D-ITZ layers, where the micro-cracks are

known to be preferentially generated under loading (Xiong et al., 2016). Eventually, the macroscopic characteristics of concrete, like mechanical performance, are affected by the pore's types and their distribution, and therefore also directly by the AM content (Kumar Mehta & Monteiro, 2006).

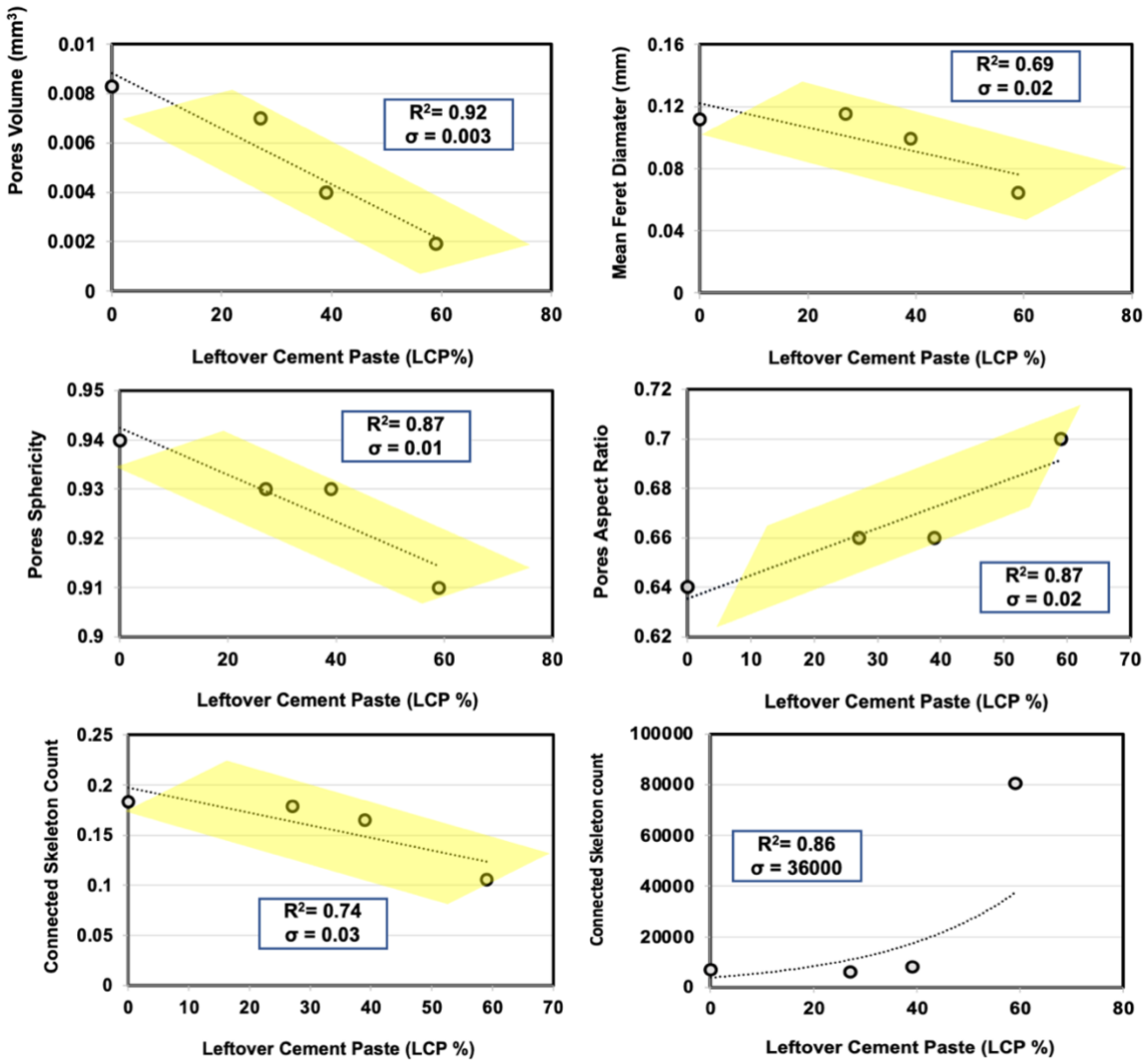

***Figure 50**. Scatter plots with the comparison from the concrete microstructure features and the attached mortar content (AM %) from the mineralogical model.*

4.6. Conclusions

The evaluation and characterization of the AM content appears as a mandatory step to assess the quality of RAs. The method adopted and discussed in the present research, based on XRPD and Rietveld refinement, represents a valid protocol to the accurate determination of this feature. The main outcomes can be summarized as follows:

• A straightforward reconstruction of the volume of AM is obtained for RAs of different diameters based on XRPD and Rietveld quantitative phase analysis. Other information on

the RAs like - degree of carbonation, residual clinker minerals and NAs' mineralogical composition – can be easily implemented in the method by modifying Equation (1).

- The results of the XRPD mineralogical model are in general consistent with earlier research, which found that the quantity of AM volume increases as RA's characteristic size decreases, with an exponential increase in RAs with a diameter below 0.6 mm.
- The AM content on the RAs appears to have a direct impact on the establishment of a capillary porosity (<0.005 mm^3 in volume) distribution inside the concrete specimens. Other variables, like pores volume, geometry, sphericity and connectivity are also found to be directly affected by the AM content. A good linear correlation (R2 from 0.80 to 0.99) links the AM content with all the available porosity's variables.
- The capillary-porosity reflects the formation of the D-ITZ layers, mainly resulting from the process of water and moist absorption by the AM, which gives a general worsening of the concrete properties and of the mechanical performances at the different curing ages.

In conclusion, the AM values obtained through the aforementioned method, are corroborated by the evidences emerged from the investigation on the concrete microstructure. Besides concrete production, the method can be further developed to trace back the ageing of the CDW, disposal condition and also to obtain information on the different types of leftover cement found (Type I, II, III, IV etc. according to UNI EN 197-1:2000). Representing useful information to define treatments methods to improve RAs' properties and/or to define the best operating condition to recycle these materials (Semugaza et al., 2023).

5. Conclusions and future perspectives

The world we live in is rapidly changing, and the majority of these changes are interconnected. Western civilization's progress has brought both wellness and negative impacts to many people, some of whom have yet to be born. If we are now called to respond to these changes, it means that we must develop new paradigms to replace ones that are no longer viable. On the 21st of October 2024 we had celebrated 200 years since the release of the Portland Cement patent, by Joseph Aspdin back in 1824. Today's cement production still bears a striking resemblance to the old-fashioned methods of the Victorian era, heavily reliant on coal, mining, and pollution-intensive industries. However, if we consider the world itself, technological advancements have surged significantly over the same period, to cite one the recent developing of computer science and artificial intelligence. After 200 years, the time for change is now, and it must be accomplished within the next 20 to 30 years if we want to effectively address the global environmental crisis. The construction sector, mainly through cement and concrete production, contributes significantly to the consumption of non-renewable mineral raw materials and to the greenhouse gasses emission. Indeed, much is happening at this very moment, as the building materials sector collaborates with academia to move beyond traditional paradigms and reshape this essential industry. For example, transitioning from a linear economy to a circular one represents a significant leap toward more sustainable development, as discussed at the core of this doctoral thesis focused on sorting and recycling of Construction and Demolition Waste (CDW). The achieving of a circular construction sector would represent a shift towards minimizing CDW production and embracing end-of-life materials reuse, limiting the consumption of nonrenewable raw materials, particularly from mining and quarry. Failure to fully recycle CDW poses significant risks related to its disposal in landfills. As discussed in Chapter 2 of this doctoral thesis, when CDW is landfilled, rainwater, surface water, or groundwater may come into contact with the waste, leading to the leaching of hazardous elements such as Cr, Cu, Ni, Pb, and V. This contamination represents a potential threat to the environment (Saca et al., 2017) highlighting the need to assess the environmental risks associated with CDW and its pollutant release potential (Diotti et al., 2020). Standardized leaching tests, while effective, require several days of laboratory work, making real-time, on-site risk assessment of incoming CDW impractical. To address this challenge, this thesis presents an artificial neural network model capable of predicting key leachate concentrations directly from the bulk chemical composition of CDW. This tool offers a practical solution for improving CDW management. Given that leaching behavior varies significantly depending on the bulk

chemical composition and source of CDW, machine learning models provide a valuable means for predicting contaminant release and assessing environmental hazards. Traditional demolition methods, which often result in massive amounts of waste being sent to landfills, are increasingly being replaced by selective deconstruction (Coelho & De Brito, 2011). Whereas the concept of urban mining has gained significant attention within the circular economy movement in construction (van den Berg et al., 2020). Rather than relying on new raw materials extracted from the earth, urban mining involves reclaiming resources from existing structures and infrastructure. To make this approach more efficient, construction sites are increasingly incorporating on-site sorting and recycling facilities, including also the most advanced technological tools from computer vision to robotics (Z. Wang et al., 2020; W. Xiao et al., 2020). By separating materials at the source, these facilities improve recovery rates and reduce the costs associated with transporting mixed waste and with further separation of heterogeneous agglomerates to centralized recycling facilities. In this doctoral thesis, a significant advancement in the recycling and circular utilization of CDW has been presented and analyzed in Chapter 3. A critical focus has been the estimation of attached mortar (AM) on the surface of recycled aggregates (RAs), a pivotal step in promoting the upcycling of RAs. This approach aims to transition their use from low-value applications, such as road base and subbase layers, to higher-value applications like structural concrete (e.g., the EU funded "CDW Circle" project - LIFE22-ENV-IT-LIFE-CDW-CIRCLE/101113587) and artificial stones to fill wire mesh gabions (the "ECO-STONEFILL" project – presented and under evaluation from the EC). This shift is particularly important given that concrete is the second most consumed material worldwide, surpassed only by drinking water, while the demand for road infrastructure may eventually plateau. Moreover, the thesis explores various potential end uses for CDW, determined by the AM content and the degree of cement paste carbonation. A comprehensive strategy, rather than reliance on a single approach, is essential for the effective reuse of these materials from the stakeholder. Consumer and industry awareness is also growing, as both end-users and professionals become more informed about the benefits of more sustainable materials through the adoption of material's certification like Environmental Product Declarations (EPDs). EPDs provide transparent, standardized information on the environmental impact of products throughout their lifecycle. EPDs are based on ISO standards and include data on aspects such as resource use, energy consumption, and emissions, allowing architects, builders, and other stakeholders to make more informed, sustainable choices. By quantifying the environmental performance of materials, EPDs facilitate comparisons and contribute to certifications like LEED (Leadership in Energy and Environmental Design) and BREEAM

(Building Research Establishment Environmental Assessment Method), promoting eco-friendly practices and advancing the transition toward a circular economy in construction. These certifications are also becoming highly valuable in the marketplace, as they are associated with quality, environmental stewardship, and social responsibility. In turn, this demand drives companies to adopt more sustainable practices to remain competitive and relevant in an increasingly eco-conscious market. This shift is driving more companies to prioritize sustainability in their operations, as the financial incentives align with reduced environmental impact and long-term resource efficiency. Moreover, new business models often driven by start-ups are emerging within the construction industry that align with circular economy goals. Regulations and policies worldwide are also propelling the construction sector towards a circular economy. The European Union, for example, has implemented several policies to promote sustainable construction practices. Similar efforts are underway in other regions, with tax incentives and environmental regulations encouraging the use of recycled and biobased materials. Italy's recent End-of-Waste legislation (D.M. n. 127/2024) provides a clear framework for when CDW can be considered as no longer waste, outlining quality standards and contamination limits along with recycling protocols. The introduction of ML algorithms and AI, holds the promise of addressing various challenges in waste management and driving significant advancements in this field, as discussed. Indeed, ML offers the opportunity for real-time monitoring and predictive analytics base on large data, allowing authorities to respond to waste creation and disposal concerns proactively (Hossain et al., 2017; Imam et al., 2024). The testing in the field of CDW provide a faster and efficient method to achieve End-of-Waste certifications with important practical implications in the management of waste and recycling materials (Ershadi et al., 2023). Following End-of-Waste classification secondary raw materials have the potential to drive circularity in the construction sector; however, significant challenges remain to be addressed. Technical and confidence barriers remain, mostly due to poor sorting of RAs and high heterogeneity of these products being the main limitations. Following the results present in **Chapter 4,** the AM content is found to have a linear direct relation with the development of multiple microstructural features inside the concrete specimens (pores density, pores volume, shape, connectivity). The capillary-porosity reflects the formation of the D-ITZ layers, mainly resulting from the process of water absorption by the AM, which gives a general worsening of the concrete properties and of the mechanical performances at the different curing ages. This condition could substantially affect the durability, safety and stability of buildings and infrastructures. Therefore, the evaluation and monitoring of the AM content shall become a mandatory step to assess the quality of RAs, becoming a

mandatory requirement prior to batching plant. Despite of this evidence, an internationally standardized procedure has not been established yet, whereas different methods have been proposed, as summarized in (Braymand et al., 2016). This doctoral thesis mainly revolves around the use of X-ray Powder Diffraction (XRPD) and its well-established combination with the Rietveld method for quantitative phase analysis (QPA), which is nowadays more and more widespread in the cement and construction sector, mainly due to his reliability and speed (Snellings, 2016). XRPD opens enormous possibilities for *in-situ* monitoring of process and quality control, even in the field of continuous on-line measurements during industrial production (Dhanjal et al., 2006; Gugin et al., 2024). The approach presented based on XRPD and pseudo-density parameters represent an innovative protocol to test this feature. The Rietveld approach which is the bottleneck of the method proposed can also be automated to speed up the methodology and reduce human mistakes using artificial intelligence algorithm to improve the automation level of Rietveld refinement (Feng et al., 2019). A similar approach has been already tested in aluminium batch electrolytes (Knorr & Kelaart, 2009). A future developing of the present research could in fact become the developing of AI-based Rietveld refinement of recycled materials. A similar application holds significant potential to revolutionize the recycling of CDW. AI-driven algorithms could enhance the precision and efficiency of phase identification, quantification, and structural parameter refinement by automating complex, time-consuming steps. Machine learning models trained on extensive diffraction datasets could predict optimal starting parameters, identify subtle peak overlaps, and refine structural models with minimal user intervention. Furthermore, integration with big data analytics and cloud computing could facilitate real-time, high-throughput analysis of CDW from different geographical areas of the world, paving the way for more tailored reused application. Lastly, the so-called p_{pseudo} represents mainly a tool to transform the weighted percentage of mineralogical QPA into a volume reconstruction, without considering any physical constrain and amorphous content. This parameter enables the rapid classification of RAs materials, both pre- and post-recycling treatments, which has proven to be useful to model and describe various engineering properties and macroscopic features, like the AM content. Still, a lot needs to be done to increase the screening and separation processes for CDW. Advanced sorting plant, that employs technological devices like optical cameras, hyper-spectral imaging (HSI) or laser-induced breakdown spectroscopy (LIBS), are just a few and most of the recycling processes still rely mostly on crushing and sieving. The adoption of such advanced optical sorting equipment would be an important step in CDW management and further development could be achieved in the future by implementing in-line XRPD in CDW sorting

plants. An XRPD scan that once required three hours to collect data can now be completed in less than two minutes, with some advanced settings achieving results in just a few seconds (D O'Flynn et al., 2013). Through rapid and real-time diffraction measurements would be possible not only to distinguish between bricks, ceramics, concrete and natural stones within the CDW, but also to provide a material characterization that could lead to a more accurate sorting process compared to traditional methods such as manual sorting or standard RGB sensors. The End-of-Waste perspectives of these products would not only be considered within recycled aggregates for concrete production but also to develop a full-cycle circularity in the construction sector encompassing also masonry production and other significant building materials industries (gypsum boards, tiles, asphalts etc.). Despite the challenges, ongoing research and innovation are expected to drive further advances in the next years. New materials, digital tools, and recycling techniques are continuously emerging, offering potential solutions to current limitations. As the construction sector continues to evolve, the circular economy promises to play a critical role in creating a more sustainable, resource-efficient future. As a key enabler, technological progress not only provides solutions to mitigate climate change, but also provides humanity with the means to adapt to challenges while preserving ecosystems for future generations.

6. Supplementary Materials

TABLE I. XRF composition of CDW major and trace elements

	No mixed samples													
Sample	BR1	BR2	BR3	BR4	BR5	BR6	BR7	LF1	PO1	TL1	TL2	GR1	RF1	CON
SiO_2 (wt%)	43,8	49,4	46,3	52,7	50,4	49,4	49,0	46,3	51,1	48,1	16,8	52,1	47,7	11,7
TiO_2	0,52	0,6	0,59	0,57	0,64	0,58	0,58	0,52	0,26	0,57	0,12	0,4	0,6	0,09
Al_2O_3	13,1	13,6	13,4	13,7	14,7	13,4	13,3	10,3	19,5	13,9	2,12	13,2	13,5	1,96
Fe_2O_3	3,92	4,65	4,71	4,47	5,23	4,16	4,6	3,74	0,57	3,16	1,31	0,77	4,48	0,99
MnO	0,11	0,11	0,15	0,11	0,12	0,1	0,12	0,04	0,00	0,19	0,03	0,01	0,12	0,06
MgO	3,52	4,09	2,27	4,19	5,07	4,19	4,24	5,77	0,28	2,15	6,42	0,46	2,92	0,81
CaO	8,20	9,93	11,7	11,1	9,69	9,00	10,8	13,1	0,77	6,95	33,4	7,46	12,2	42,2
Na_2O	1,25	1,18	0,94	1,54	1,22	1,17	1,03	1,09	2,39	1,62	0,52	3,23	1,11	0,30
K_2O	1,82	2,59	2,49	2,39	2,54	2,38	2,39	2,15	1,17	2,56	0,50	2,00	2,26	0,33
P_2O_5	0,13	0,12	0,09	0,22	0,14	0,15	0,12	0,12	0,03	0,09	0,05	0,1	0,11	0,07
Total	83,5	91,6	86,7	95,6	94,6	89,5	92,9	89,2	76,1	81,3	91,1	84,4	91,6	93,1
LOI	7,09	5,28	4,06	4,66	4,89	4,95	6,71	6,02	0,00	1,97	29,8	4,64	6,63	34,6
Ba (ppm)	403	474	436	495	483	433	518	306	2253	831	110	367	717	545
Co	25	25	21	23	26	19	21	13	9	101	17	6	20	12
Cr	163	160	111	175	212	180	167	116	53	188	148	89	129	30
Cu	32	41	46	37	48	33	38	22	18	33	11	14	36	21
Ga	14	15	14	13	14	12	13	9	22	20	3	20	15	1
Ni	160	141	76	130	166	130	144	57	16	90	204	16	91	30
Sc	9	12	13	12	13	13	14	8	4	11	n.d.	3	9	n.d.
V	104	101	115	83	109	100	102	111	32	93	24	41	129	41
Zn	116	100	99	94	103	83	88	99	1901	1238	25	73	138	30

TABLE II. XRF composition of CDW (1:1) mixed samples

	Samples mixed with concrete (mix ratio 1:1)												
Sample	BR1	BR2	BR3	BR4	BR5	BR6	BR7	LF1	PO1	TL1	TL2	GR1	RF1
SiO_2 (wt%)	33,2	33,7	33,4	34,2	33,3	34,3	33,1	32,7	40,2	36,3	16,2	37,7	32,8
TiO_2	0,38	0,39	0,40	0,36	0,40	0,39	0,37	0,35	0,23	0,41	0,12	0,29	0,39
Al_2O_3	9,07	8,56	8,89	8,25	8,88	8,64	8,30	6,92	13,90	9,70	2,31	9,01	8,49
Fe_2O_3	2,94	3,11	3,29	2,90	3,33	2,90	3,05	2,67	0,93	2,51	1,30	1,02	3,02
MnO	0,10	0,09	0,12	0,09	0,10	0,09	0,10	0,05	0,03	0,15	0,05	0,04	0,10
MgO	2,60	2,70	1,77	2,65	3,14	2,80	2,74	3,72	0,64	1,78	4,13	0,73	2,06
CaO	28,6	29,0	30,4	29,4	28,7	28,6	29,4	31,0	24,1	27,9	42,7	28,0	30,3
Na_2O	0,93	0,81	0,71	0,97	0,81	0,83	0,72	0,78	1,74	1,17	0,47	2,10	0,77
K_2O	1,30	1,61	1,63	1,44	1,53	1,52	1,48	1,40	0,96	1,77	0,47	1,38	1,43
P_2O_5	0,12	0,10	0,09	0,15	0,11	0,12	0,10	0,10	0,06	0,09	0,07	0,10	0,10
Total	79,2	80,1	80,7	80,4	80,3	80,3	79,4	79,7	82,8	81,7	67,8	80,4	79,4
LOI	20,8	19,9	19,3	19,6	19,7	19,8	20,7	20,3	17,3	18,3	32,2	19,6	20,6
Ba (ppm)	474	510	491	520	514	489	532	426	1399	688	328	456	631
Co	19	19	17	18	19	16	17	12	11	57	15	9	16
Cr	96	95	71	102	121	105	99	73	41	109	89	60	79
Cu	27	31	34	29	35	27	30	22	20	27	16	18	28
Ga	7	8	8	7	7	6	7	5	11	11	2	10	8
Ni	95	86	53	80	98	80	87	44	23	60	117	23	61
Sc	n.d.	n.d.	n.d.	n.d.	n.d.	n.d.	n.d.	n.d.	n.d.	n.d.	n.d.	n.d.	n.d.
V	72	71	78	62	75	70	71	76	36	67	32	41	85
Zn	73	65	64	62	66	57	59	64	966	634	28	51	84

TABLE III. Leaching results of ICP-MS analysis on CDW samples

	No mixed samples													
Sample	BR1	BR2	BR3	BR4	BR5	BR6	BR7	LF1	PO1	TL1	TL2	GR1	RF1	CON
Na (mg/L)	6,69	46,3	10,5	7,68	26,0	5,85	4,24	48,9	2,66	7,69	31,2	10,4	10,2	21,8
Mg	19,2	7,83	4,73	5,56	16,92	10,72	3,63	59,6	0,67	0,04	0,02	0,44	12,26	0,00
K	6,29	47,4	10,0	11,0	40,9	11,8	6,55	35,2	0,17	7,90	14,4	4,70	8,97	46,4
Ca	609	44,8	47,4	25,8	569	230	22,35	493	5,58	112	32,4	23,3	137	115
Li	0,218	0,066	0,087	0,056	0,115	0,040	0,050	0,115	0,011	0,193	0,013	0,071	0,037	0,024
B	0,378	4,506	3,706	0,157	1,695	0,346	0,135	0,543	0,073	0,203	0,005	0,120	0,332	0,002
Al	0,1	0,01	0,04	0,04	0,02	0,05	0,12	0,03	0,31	1,49	2,35	0,16	0,08	3,4
P	n.d.	n.d.	n.d.	0,018	0,038	n.d.	0,027	0,010	0,001	0,009	0,020	0,001	0,003	0,012
Sc	0,003	0,000	0,000	0,000	0,002	0,001	0,000	0,002	0,000	0,001	0,000	0,000	0,001	0,000
Ti	0,282	0,023	0,023	0,012	0,257	0,108	0,011	0,242	0,006	0,063	0,057	0,012	0,069	0,007
Ba	0,003	0,021	0,020	0,016	0,025	0,031	0,005	0,035	0,019	0,033	0,099	0,015	0,031	0,267
V	0,014	0,120	0,126	0,081	0,063	0,049	0,073	0,005	0,004	0,096	0,002	0,039	0,109	0,001
Cr	0,015	0,096	0,136	0,009	0,011	0,043	0,023	0,274	0,000	0,131	0,076	0,016	0,049	0,104
Fe	0,2	0,010	0,013	0,01	0,14	0,06	0,01	0,130	0,02	0,03	0,03	0,018	0,04	0,0
Co	0,001	n.d.	n.d.	0,002	0,000	n.d.	n.d.	n.d.	0,008	n.d.	n.d.	0,000	0,001	0,000
Ni	0,023	0,001	0,004	0,010	0,002	0,004	0,008	0,000	0,005	n.d.	0,001	0,001	0,011	0,000
Cu	0,001	0,001	0,003	0,005	0,007	0,001	0,013	n.d.	n.d.	n.d.	n.d.	0,003	0,007	0,001
Ga	0,001	0,000	0,000	0,000	0,000	0,000	0,001	0,000	0,000	0,002	0,005	0,001	0,001	0,006
As	0,002	0,011	0,002	0,013	0,007	0,008	0,014	0,001	0,001	0,001	0,000	0,001	0,007	n.d.
Se	0,003	0,003	0,008	0,001	0,062	0,003	0,000	0,041	n.d.	0,000	0,001	0,000	0,005	0,001
Rb	0,018	0,080	0,036	0,015	0,068	0,024	0,009	0,168	0,001	0,026	0,018	0,007	0,038	0,128
Sr	0,8	0,28	0,22	0,13	1,51	1,10	0,12	1,49	0,02	0,55	3,70	0,12	0,59	2,0
Mo	0,002	0,010	0,007	0,002	0,043	0,003	0,002	0,088	0,002	0,008	0,003	0,018	0,011	0,003

TABLE IV. Leaching results of ICP-MS analysis on CDW (1:1) mixed samples

	Samples mixed with concrete (mix ratio 1:1)												
Sample	BR1	BR2	BR3	BR4	BR5	BR6	BR7	LF1	PO1	TL1	TL2	GR1	RF
Na (mg/L)	16,0	39,6	14,5	14,3	23,0	12,9	9,8	15,6	33,2	11,9	14,2	14,7	26,0
Mg	0,23	0,01	0,01	0,01	0,03	0,02	0,01	0,00	0,07	0,00	0,02	0,00	0,00
K	24,2	56,3	22,3	25,4	43,6	23,9	16,3	23,3	39,4	21,5	20,0	27,2	27,4
Ca	651	66,2	88,2	54,2	313	159	87,4	107,1	347	115	127	109	126
Li	0,081	0,039	0,052	0,039	0,050	0,028	0,023	0,034	0,094	0,037	0,029	0,061	0,046
B	0,004	0,121	0,091	0,027	0,014	0,004	0,023	0,074	0,001	0,019	0,003	0,009	0,024
Al	0,3	0,75	1,54	2,05	0,67	1,21	1,55	0,71	2,28	2,30	2,23	2,7	1,36
P	0,026	0,001	0,006	0,043	0,029	0,094	0,045	0,016	0,016	0,014	0,016	0,028	0,057
Sc	0,002	0,001	0,000	0,000	0,001	0,001	0,000	0,001	0,000	0,000	0,000	0,000	0,000
Ti	0,309	0,055	0,029	0,045	0,160	0,077	0,045	0,144	0,028	0,023	0,013	0,029	0,057
Ba	0,052	0,040	0,056	0,067	0,043	0,049	0,046	0,052	0,106	0,119	0,164	0,084	0,039
V	0,064	0,063	0,025	0,013	0,052	0,019	0,025	0,010	0,003	0,010	0,002	0,007	0,044
Cr	0,061	0,083	0,108	0,053	0,064	0,064	0,050	0,174	0,051	0,107	0,090	0,059	0,054
Fe	0,2	0,026	0,014	0,02	0,08	0,04	0,02	0,073	0,017	0,01	0,01	0,0	0,03
Co	0,000	n.d.	n.d.	0,001	0,000	0,000	0,000	0,000	0,001	0,000	0,000	0,000	0,000
Ni	0,003	n.d.	n.d.	0,002	0,000	0,000	0,002	0,000	0,000	0,000	0,000	0,000	0,001
Cu	0,009	0,001	0,002	0,017	0,009	0,007	0,020	0,002	0,002	0,002	0,002	0,005	0,007
Ga	0,002	0,003	0,003	0,004	0,002	0,003	0,003	0,002	0,003	0,004	0,005	0,004	0,003
As	n.d.	n.d.	n.d.	n.d.	n.d.	n.d.	n.d.	0,000	n.d.	n.d.	0,000	n.d.	0,000
Se	n.d.	n.d.	0,000	n.d.	0,030	n.d.	n.d.	0,018	0,000	0,001	0,001	0,000	0,002
Rb	0,053	0,103	0,060	0,046	0,084	0,045	0,024	0,110	0,044	0,070	0,050	0,046	0,048
Sr	2,3	0,64	0,70	0,73	1,30	1,01	0,59	1,41	0,74	1,05	2,14	0,8	0,65
Mo	0,002	0,005	0,003	0,002	0,014	0,002	0,001	0,032	0,002	0,005	0,003	0,012	0,004

TABLE V. Leaching results of IC analysis on CDW and (1:1) mixed samples

No mixed samples														
Sample	BR1	BR2	BR3	BR4	BR5	BR6	BR7	LF1	PO1	TL1	TL2	GR1	RF1	CON
Cl (mg/L)	1,61	41,8	5,33	1,74	22,8	1,30	1,36	42,0	n.d.	n.d.	n.d.	n.d.	n.d.	4,41
NO_3	1,97	106	4,77	n.d.	112	3,55	2,70	120	n.d.	6,59	41,7	2,84	8,99	1,75
SO_4	1481	137	156	29,2	1323	720	10,5	1419	1,1	106	42,0	48,7	392	26,6
Samples mixed with concrete (mix ratio 1:1)														
Sample	BR1	BR2	BR3	BR4	BR5	BR6	BR7	LF1	PO1	TL1	TL2	GR1	RF1	
Cl (mg/L)	2,81	24,8	4,44	3,00	14,7	2,25	2,14	25,1	1,83	3,41	11,4	2,65	6,25	
NO_3	0,86	55,6	2,87	1,01	51,3	1,42	1,35	58,8	0,62	3,06	23,1	1,57	4,97	
SO_4	1918	207	161	120	836	313	98	901	63,3	65,2	48,7	98,8	247	

TABLE VI. Calculated Cf and Cd for CDW

No mixed samples														
Sample	BR1	BR2	BR3	BR4	BR5	BR6	BR7	LF1	PO1	TL1	TL2	GR1	RF1	CON
C_f (Cr)	0,20	1,23	1,74	0,12	0,14	0,56	0,29	3,52	0,01	1,68	0,97	0,21	0,63	1,33
C_f (Ni)	0,31	0,01	0,06	0,13	0,03	0,06	0,11	0,01	0,07	-	0,01	0,02	0,14	0,00
C_f (Cu)	0,02	0,02	0,08	0,15	0,21	0,04	0,37	-	-	-	-	0,10	0,20	0,04
C_f (V)	0,43	3,65	3,81	2,44	1,91	1,49	2,22	0,16	0,11	2,91	0,05	1,19	3,30	0,03
C_d	0,24	1,23	1,42	0,71	0,57	0,54	0,75	0,92	0,05	1,15	0,26	0,38	1,07	0,35

TABLE VII. Calculated Cf and Cd for CDW (1:1) mixed samples

Samples mixed with concrete (mix ratio 1:1)													
Sample	BR1	BR2	BR3	BR4	BR5	BR6	BR7	LF1	PO1	TL1	TL2	GR1	RF1
C_f (Cr)	0,78	1,07	1,39	0,67	0,82	0,82	0,64	2,24	0,66	1,37	1,15	0,75	0,70
C_f (Ni)	0,05	-	-	0,02	0,00	0,00	0,02	0,00	0,00	0,00	0,01	0,00	0,01
C_f (Cu)	0,27	0,04	0,07	0,49	0,25	0,22	0,60	0,06	0,05	0,06	0,04	0,14	0,22
C_f (V)	1,94	1,92	0,75	0,41	1,57	0,58	0,76	0,30	0,10	0,30	0,06	0,20	1,33
C_d	0,76	0,76	0,55	0,40	0,66	0,40	0,51	0,65	0,20	0,43	0,32	0,27	0,56

TABLE VIII. Calculated HQ values for CDW samples

No mixed samples														
Sample	BR1	BR2	BR3	BR4	BR5	BR6	BR7	LF1	PO1	TL1	TL2	GR1	RF1	CON
HQ (Cr)	0,31	1,91	2,72	0,18	0,22	0,87	0,46	5,49	0,01	2,61	1,52	0,32	0,98	2,08
HQ (Ni)	2,29	0,10	0,43	0,98	0,23	0,44	0,79	0,05	0,54	-	0,09	0,12	1,05	0,00
HQ (Cu)	0,01	0,02	0,06	0,10	0,14	0,03	0,25	-	-	-	-	0,07	0,14	0,03
HQ (V)	0,06	0,48	0,50	0,32	0,25	0,20	0,29	0,02	0,01	0,38	0,01	0,16	0,44	0,00
HQ (Co)	0,00	-	-	0,01	0,00	-	-	-	0,03	-	-	0,00	0,00	0,00
HQ (Se)	0,28	0,32	0,79	0,11	6,18	0,27	0,01	4,11	-	0,04	0,07	0,03	0,55	0,10
HQ (Ba)	0,00	0,02	0,02	0,02	0,02	0,03	0,01	0,04	0,02	0,03	0,10	0,01	0,03	0,27
HQ (As)	0,03	0,23	0,03	0,27	0,14	0,16	0,29	0,03	0,02	0,02	0,01	0,02	0,15	-
HQ (Cl)	0,00	0,06	0,01	0,00	0,03	0,00	0,00	0,06	-	-	-	-	-	0,01
HQ (NO_3)	0,04	2,12	0,10	-	2,24	0,07	0,05	2,41	-	0,13	0,83	0,06	0,18	0,03
HQ (SO_4)	1,97	0,18	0,21	0,04	1,76	0,96	0,01	1,89	0,00	0,14	0,06	0,06	0,52	0,04
HQ_m	0,62	0,38	0,59	0,22	1,10	0,35	0,23	1,45	0,08	0,40	0,23	0,10	0,46	0,31

TABLE IX. Calculated HQ values for CDW (1:1) mixed samples

Samples mixed with concrete (mix ratio 1:1)													
Sample	BR1	BR2	BR3	BR4	BR5	BR6	BR7	LF1	PO1	TL1	TL2	GR1	RF1
HQ (Cr)	1,22	1,67	2,16	1,05	1,28	1,28	0,99	3,49	1,02	2,14	1,80	1,17	1,08
HQ (Ni)	0,34	-	-	0,15	0,00	0,01	0,18	0,01	0,00	0,01	0,05	0,03	0,08
HQ (Cu)	0,18	0,03	0,05	0,34	0,17	0,15	0,41	0,04	0,03	0,04	0,03	0,10	0,15
HQ (V)	0,26	0,25	0,10	0,05	0,21	0,08	0,10	0,04	0,01	0,04	0,01	0,03	0,18
HQ (Co)	0,00	-	-	0,00	0,00	0,00	0,00	0,00	0,00	0,00	0,00	0,00	0,00
HQ (Se)	-	-	0,01	-	2,96	-	-	1,77	0,03	0,05	0,07	0,04	0,21
HQ (Ba)	0,05	0,04	0,06	0,07	0,04	0,05	0,05	0,05	0,11	0,12	0,16	0,08	0,04
HQ (As)	-	-	-	-	-	-	-	0,00	-	-	0,00	-	0,01
HQ (Cl)	0,00	0,03	0,01	0,00	0,02	0,00	0,00	0,03	0,00	0,00	0,02	0,00	0,01
HQ (NO_3)	0,02	1,11	0,06	0,02	1,03	0,03	0,03	1,18	0,01	0,06	0,46	0,03	0,10
HQ (SO_4)	2,56	0,28	0,21	0,16	1,11	0,42	0,13	1,20	0,08	0,09	0,06	0,13	0,33
HQ_m	0,58	0,28	0,32	0,23	0,72	0,25	0,23	0,83	0,16	0,31	0,27	0,20	0,26

TABLE X. Original RGB complete dataset of C-RA analyzed through Image Analysis Method

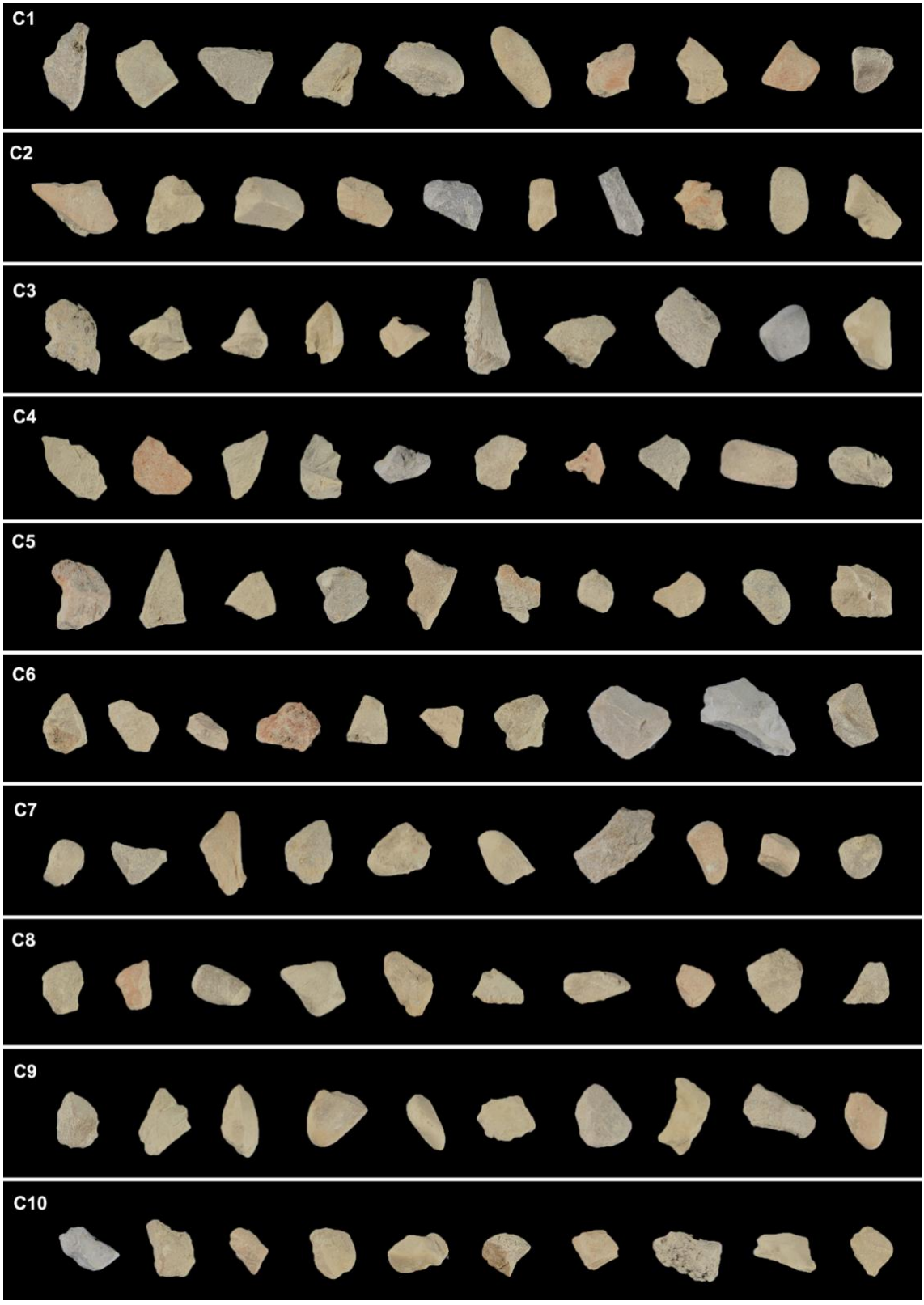

TABLE XI. Original RGB complete dataset of M-RA analyzed through Image Analysis Method

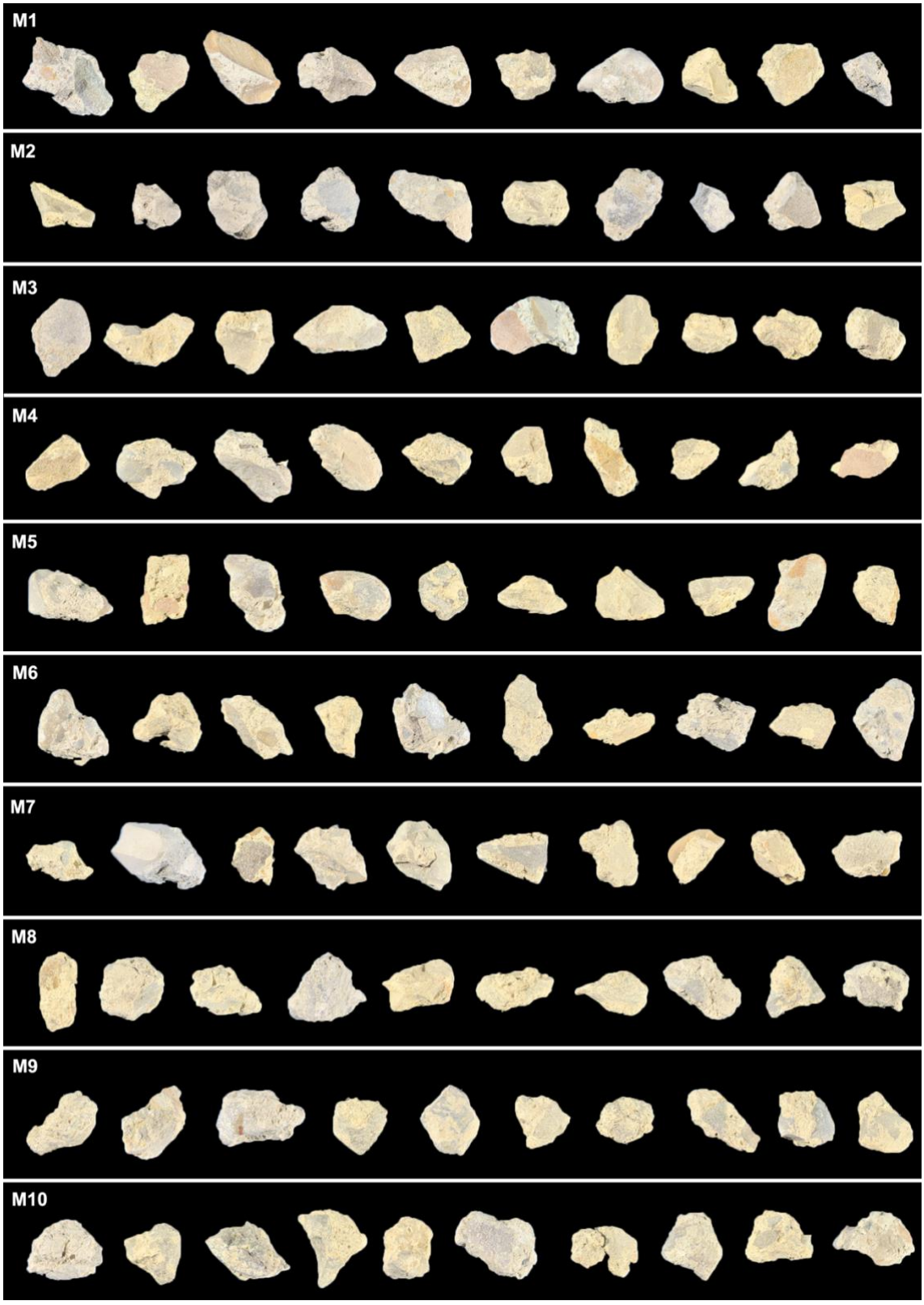

TABLE XII. Original RGB complete dataset of D-RA analyzed through Image Analysis Method

TABLE XIII. Individual values of SC% calculated for the C-RA

	Group of Samples									
Number	**C1**	**C2**	**C3**	**C4**	**C5**	**C6**	**C7**	**C8**	**C9**	**C10**
1	0	0	0	0	0	0	0	0	0	0
2	0	0	0	0	0	0	0	0	0	0
3	0	0	0	0	0	0	0	0	0	0
4	0	0	0	0	0	0	0	0	0	0
5	0	0	0	0	0	0	0	0	0	0
6	0	0	0	0	0	0	0	0	0	0
7	0	0	0	0	0	0	0	0	0	0
8	0	0	0	0	0	0	0	0	0	0
9	0	0	0	0	0	0	0	0	0	0
10	0	0	0	0	0	0	0	0	0	0

TABLE XIV. Individual values of SC% calculated for the M-RA

	Group of Samples									
Number	**M1**	**M2**	**M3**	**M4**	**M5**	**M6**	**M7**	**M8**	**M9**	**M10**
1	37.75	44.59	16.10	25.08	43.01	41.33	43.76	40.55	48.45	41.24
2	45.29	23.02	36.59	12.80	48.39	42.92	47.03	53.68	40.97	45.85
3	28.57	29.23	46.66	36.17	46.25	50.00	30.89	43.85	43.47	20.97
4	34.19	48.70	46.50	49.38	33.95	46.70	41.10	41.66	41.48	42.82
5	55.15	1.82	43.40	41.27	42.12	49.48	41.88	45.16	45.31	51.33
6	46.72	35.07	33.10	59.98	40.69	50.88	34.35	25.92	47.86	45.39
7	59.82	33.25	41.15	15.28	44.87	47.61	42.33	30.41	42.26	48.06
8	37.15	33.33	43.52	88.84	49.60	40.24	47.24	21.85	21.08	55.04
9	44.94	33.85	42.71	41.98	48.00	49.25	45.81	34.78	47.70	49.85
10	44.28	36.58	46.33	11.49	64.68	45.22	43.21	16.88	46.95	45.35

TABLE XV. Individual values of SC% calculated for the D-RA

	Group of Samples									
Number	**D1**	**D2**	**D3**	**D4**	**D5**	**D6**	**D7**	**D8**	**D9**	**D10**
1	60.53	52.20	67.76	53.93	61.46	58.53	58.36	61.78	70.42	66.99
2	79.99	57.47	75.93	75.58	78.01	66.31	70.69	30.66	68.78	66.38
3	51.93	67.81	82.52	80.47	64.33	76.47	39.55	66.42	59.52	67.82
4	72.83	62.51	65.46	77.22	62.40	56.70	66.87	68.37	68.51	66.41
5	71.23	56.97	69.01	83.93	50.22	69.48	56.45	70.77	73.89	52.21
6	70.63	65.19	69.87	44.89	62.24	43.96	51.81	47.71	64.25	75.06
7	78.84	67.80	74.00	45.68	46.57	66.68	62.33	63.77	65.84	59.06
8	81.48	57.41	73.37	61.95	48.90	33.33	71.22	52.32	64.55	51.36
9	37.00	43.50	70.83	69.69	62.69	71.47	54.24	73.71	55.74	69.71
10	42.29	43.71	78.17	64.00	51.22	69.16	73.93	46.31	68.10	65.23

TABLE XVI. Results of mechanical detaching of C-RA

	RAs (g)	AM (g)	NAs (g)	AM (%)
C1	6.51	0	6.51	0
C2	6.01	0	6.01	0
C3	7.46	0	7.46	0
C4	5.2	0	5.2	0
C5	5.21	0	5.21	0
C6	6.07	0	6.07	0
C7	5.67	0	5.67	0
C8	4.55	0	4.55	0
C9	5.45	0	5.45	0
C10	4.15	0	4.15	0

TABLE XVII. Results of mechanical detaching of M-RA

	RAs (g)	AM (g)	NAs (g)	AM (%)
M1	7.29	0.33	6.96	4.53
M2	6.73	0.21	6.52	3.12
M3	7.36	0.27	7.09	3.67
M4	6.966	0.173	6.793	2.48
M5	5.33	0.118	5.212	2.21
M6	6.87	0.33	6.54	4.80
M7	7.66	0.3	7.36	3.92
M8	7.5	0.28	7.22	3.73
M9	7.09	0.27	6.82	3.81
M10	8.35	0.24	8.11	2.87

TABLE XVIII. Results of mechanical detaching of D-RA

	RAs (g)	AM (g)	NAs (g)	AM (%)
D1	4.46	0.51	3.95	11.43
D2	6.722	0.63	6.092	9.37
D3	3.62	0.6	3.02	16.57
D4	5.38	0.57	4.81	10.59
D5	5.73	0.31	5.42	5.41
D6	5.61	0.37	5.24	6.60
D7	5.06	0.4	4.66	7.91
D8	5.89	0.78	5.11	13.24
D9	4.88	0.6	4.28	12.30
D10	5.76	0.65	5.11	11.28

TABLE XIX. Results of Rietveld QPA analysis of M-RA

	M1	M2	M3	M4	M5	M6	M7	M8	M9	M10
Calcite-macro	41.06	48.23	43.85	54.4	36.14	33.36	31.43	46.32	34.44	38.53
Calcite-micro	19.8	17.9	19.27	15.3	32.44	23.33	20.65	16.19	15.18	19.04
Aragonite	0.73	1.15	0.45	0.74	0.94	0.25	2.04	0.89	0.77	0.46
Vaterite	0.52	0.49	0.62	1.3	0.15	0.19	0.46	0.27	0.47	0.31
Quartz	14.16	8.07	10.39	3.51	2.4	9.41	16.14	10.94	13.17	12.81
Albite	6.43	4.69	3.54	1.89	3.92	5.31	6.71	4.47	13.17	4.87
Orthoclase	3.66	4.11	1.4	3.44	0	5.48	0.43	6.09	3.86	3.67
C_3S mono.	0.65	1.59	0.82	0.46	5.77	2.71	7.18	1.97	3.2	2.04
C_3S tricl.	2.21	3.65	6.7	7.04	9.72	6.19	4.27	2.49	2.2	6.38
C_2S	4.83	4.43	6.19	6.16	6.41	7.4	3.43	5.09	6.35	5.77
C_4AF	2.61	2.5	3.74	1.81	1.56	2.67	4.09	2.03	1.76	2.52
Ettringite	0.16	0.16	0.22	0.17	0.18	0.14	0.2	0.17	0.2	0.15
Afm	0.14	0.2	0.24	0	0	0.14	0	0.17	0.22	0.09
Chlorite	2.64	2.71	2.4	3.39	0	2.81	1.91	2.39	4.63	2.98
Muscovite	0.4	0.12	0.17	0.39	0.37	0.61	0.49	0.52	0.38	0.38
Dolomite	0	0	0	0	0	0	0.57	0	0	0

TABLE XX. Results of Rietveld QPA analysis of D-RA

	D1	D2	D3	D4	D5	D6	D7	D8	D9	D10
Calcite-macro	42.78	54.94	30.9	48.29	49.48	55.79	52.77	36.97	46.48	48.29
Calcite-micro	12.9	16.93	18.05	15.22	18.34	18.55	15.27	26.73	13.69	18.55
Aragonite	1.49	1.48	0	2.1	1.46	0.98	1.1	0.47	0.95	0.88
Vaterite	0.2	0.18	0	0.08	0.55	0.37	0.44	0	0.09	0.61
Quartz	12.25	7.74	20.45	9.2	8.32	7.74	11.48	11.49	14.27	9.43
Albite	5.25	1.92	12.55	2.26	2.94	1.88	3.48	6.62	7.67	4
Orthoclase	3.48	2.45	5.22	3.51	1.67	2.31	3.02	3.59	3.81	2.15
C3S_mono	3.51	2.79	2.11	3.45	3.99	0.97	1.53	1.01	1.4	0.76
C3S_Triclinic	6.02	1.18	1.11	0.92	0.28	0.96	1	1.47	1.5	2.53
C2S	5.67	4.94	3.26	7.44	9.49	6.41	5.52	4.24	2.61	3.89
C4AF	3	1.74	2.46	2.34	1.8	1.51	1.42	1.29	1.71	2.54
Ettringite	0.08	0.15	0.16	0.14	0.11	0.14	0.08	0.22	0.28	0.07
Afm	0.15	0.14	0.18	0.11	0.03	0.11	0.12	0.23	0.21	0.28
Chlorite	2.74	3.12	2.64	4.72	1.01	1.97	2.03	3.92	3.92	4
Muscovite	0.3	0.3	0.89	0.21	0.26	0.16	0.23	0.76	0.72	0.42
Dolomite	0	0	0	0	0.27	0.15	0.51	0.99	0.69	1.6

TABLE XXI. Mineral's density used to perform the mineralogical model

Mineral	Density (g/cm^3)	Mineral	Density (g/cm^3)
Calcite-macro	2.711	**C3S_mono**	3.2
Calcite-micro	2.8	**C3S_Triclinic**	3.12
Aragonite	2.95	**C2S**	3.32
Vaterite	2.65	**C4AF**	3.68
Quartz	2.65	**Ettringite**	1.76
Albite	2.62	**Afm**	2.02
Orthoclase	2.56	**Chlorite**	3.3
Dolomite	2.86	**Muscovite**	2.88

TABLE XXII. Lithological description of the NA Po' river and gravel; where Vol. (volcanic rocks), Plu. (plutonic rocks), Pum. (pumice), Lim. (limestone), San. (sandstone), Sil. (siltstone), Che. (chert), Mar. (marlstone), Gne. (gneiss), Qua. (quartzite), Amp. (amphibolite), Qrz. (quartz).

Quantity	**Magmatic rocks**			**Sedimentary rocks**						**Metamorphic rocks**			**Minerals**	
Grains in %	***Vol***	***Plu***	***Pum***	***Lim***	***San***	***Sil***	***Tuf***	***Che***	***Mar***	***Gne***	***Qua***	***Amp***	***Qrz***	***Tot***
NA 4/8 mm	3.1	3.3	-	7.9	32.7	4.9	2.4	2.9	5.3	3.0	3.1	1.3	30.1	100
NA 8/11 mm	2.8	2.4	0.3	7.3	35.9	5.2	1.1	2.1	1.4	4.9	2.8	1.0	32.8	100

References

Abbas, A., Fathifazl, G., Fournier, B., Isgor, O. B., Zavadil, R., Razaqpur, A. G., & Foo, S. (2009). Quantification of the residual mortar content in recycled concrete aggregates by image analysis. *Materials Characterization*, *60*(7), 716–728. https://doi.org/10.1016/j.matchar.2009.01.010

Abdallah, M., Abu Talib, M., Feroz, S., Nasir, Q., Abdalla, H., & Mahfood, B. (2020). Artificial intelligence applications in solid waste management: A systematic research review. In *Waste Management* (Vol. 109, pp. 231–246). Elsevier Ltd. https://doi.org/10.1016/j.wasman.2020.04.057

Abedin Khan, Z., Balunaini, U., & Costa, S. (2024). Environmental feasibility and implications in using recycled construction and demolition waste aggregates in road construction based on leaching and life cycle assessment – A state-of-the-art review. *Cleaner Materials*, *12*. https://doi.org/10.1016/j.clema.2024.100239

Abrahim, G. M. S., & Parker, R. J. (2008). Assessment of heavy metal enrichment factors and the degree of contamination in marine sediments from Tamaki Estuary, Auckland, New Zealand. *Environmental Monitoring and Assessment*, *136*(1–3), 227–238. https://doi.org/10.1007/s10661-007-9678-2

Abzaev, Y., Gnyrya, A., Korobkov, S., Gauss, K., Boyarintsev, A., & Tomrachev, S. (2019). Thermodynamic modeling of Portland cement without mineral additives. *Journal of Physics: Conference Series*, *1145*(1). https://doi.org/10.1088/1742-6596/1145/1/012016

Aitchison, J. (1990). Relative Variation Diagrams for Describing Patterns of Compositional Variability. *Mathematical Geology*, *22*(4), 487–511.

Aitchison, J., & Egozcue, J. J. (2005). Compositional data analysis: Where are we and where should we be heading? *Mathematical Geology*, *37*(7), 829–850. https://doi.org/10.1007/s11004-005-7383-7

Alexandridou, C., Angelopoulos, G. N., & Coutelieris, F. A. (2014). Physical, Chemical and Mineralogical Characterization of Construction and Demolition Waste Produced in Greece. *International Journal of Civil, Environmental, Structural, Construction and Architectural Engineering*, *8*(9). scholar.waset.org/1999.3/9999382

Al-Raoush, R., & Papadopoulos, A. (2010). Representative elementary volume analysis of porous media using X-ray computed tomography. *Powder Technology*, *200*(1–2), 69–77. https://doi.org/10.1016/j.powtec.2010.02.011

Althoey, F., Ansari, W. S., Sufian, M., & Deifalla, A. F. (2023). Advancements in low-carbon concrete as a construction material for the sustainable built environment. *Developments in the Built Environment*, *16*. https://doi.org/10.1016/j.dibe.2023.100284

Amorosi, A. (2012). Chromium and nickel as indicators of source-to-sink sediment transfer in a Holocene alluvial and coastal system (Po Plain, Italy). *Sedimentary Geology*, *280*, 260–269. https://doi.org/10.1016/j.sedgeo.2012.04.011

Anderson, J., Gobbo, L. d. A., & Weeren, H. van. (2015). X-Ray Diffraction: New Eyes on the Process. *IEEE Transactions on Industry Applications*, *51*(1), 20–27. https://doi.org/10.1109/TIA.2014.2350557

Angulo, S. C., Ulsen, C., John, V. M., Kahn, H., & Cincotto, M. A. (2009). Chemical-mineralogical characterization of C&D waste recycled aggregates from São Paulo, Brazil. *Waste Management*, *29*(2), 721–730. https://doi.org/10.1016/j.wasman.2008.07.009

Aranda, M. A. G., De La Torre, Á. G., & León-Reina, L. (2012). Rietveld quantitative phase analysis of OPC clinkers, cements and hydration products. In *Reviews in*

Mineralogy and Geochemistry (Vol. 74, pp. 169–209). https://doi.org/10.2138/rmg.2012.74.5

Ardit, M., Zanelli, C., Conte, S., Molinari, C., Cruciani, G., & Dondi, M. (2022). Ceramisation of hazardous elements: Benefits and pitfalls of the inertisation through silicate ceramics. In *Journal of Hazardous Materials* (Vol. 423). Elsevier B.V. https://doi.org/10.1016/j.jhazmat.2021.126851

Artioli, G., Cerulli, T., Cruciani, G., Dalconi, M. C., Ferrari, G., Parisatto, M., Rack, A., & Tucoulou, R. (2010). X-ray diffraction microtomography (XRD-CT), a novel tool for non-invasive mapping of phase development in cement materials. *Analytical and Bioanalytical Chemistry*, *397*(6), 2131–2136. https://doi.org/10.1007/s00216-010-3649-0

Auroy, M., Poyet, S., Le Bescop, P., Torrenti, J. M., Charpentier, T., Moskura, M., & Bourbon, X. (2018). Comparison between natural and accelerated carbonation (3% CO2): Impact on mineralogy, microstructure, water retention and cracking. *Cement and Concrete Research*, *109*, 64–80. https://doi.org/10.1016/j.cemconres.2018.04.012

Bae, B., Wendusu, Tamura, S., & Imanaka, N. (2016). Novel environmentally friendly inorganic yellow pigments based on gehlenite-type structure. *Ceramics International*, *42*(13), 15104–15106. https://doi.org/10.1016/j.ceramint.2016.06.106

Bai, G., Zhu, C., Liu, C., & Liu, B. (2020a). An evaluation of the recycled aggregate characteristics and the recycled aggregate concrete mechanical properties. In *Construction and Building Materials* (Vol. 240). Elsevier Ltd. https://doi.org/10.1016/j.conbuildmat.2019.117978

Bai, G., Zhu, C., Liu, C., & Liu, B. (2020b). An evaluation of the recycled aggregate characteristics and the recycled aggregate concrete mechanical properties. In *Construction and Building Materials* (Vol. 240). Elsevier Ltd. https://doi.org/10.1016/j.conbuildmat.2019.117978

Baker, D. R., Mancini, L., Polacci, M., Higgins, M. D., Gualda, G. A. R., Hill, R. J., & Rivers, M. L. (2012). An introduction to the application of X-ray microtomography to the three-dimensional study of igneous rocks. In *Lithos* (Vol. 148, pp. 262–276). https://doi.org/10.1016/j.lithos.2012.06.008

Balonis, M., & Glasser, F. P. (2009). The density of cement phases. In *Cement and Concrete Research* (Vol. 39, Issue 9, pp. 733–739). https://doi.org/10.1016/j.cemconres.2009.06.005

Barbudo, A., Ayuso, J., Lozano, A., Cabrera, M., & López-Uceda, A. (2020). Recommendations for the management of construction and demolition waste in treatment plants. *Environmental Science and Pollution Research*, *27*(1), 125–132. https://doi.org/10.1007/s11356-019-05578-0

Barbudo, A., Galvín, A. P., Agrela, F., Ayuso, J., & Jiménez, J. R. (2012). Correlation analysis between sulphate content and leaching of sulphates in recycled aggregates from construction and demolition wastes. *Waste Management*, *32*(6), 1229–1235. https://doi.org/10.1016/j.wasman.2012.02.005

Baudry, J. P., Raftery, A. E., Celeux, G., Lo, K., & Gottardo, R. (2010). Combining mixture components for clustering. *Journal of Computational and Graphical Statistics*, *19*(2), 332–353. https://doi.org/10.1198/jcgs.2010.08111

Belkina, A. C., Ciccolella, C. O., Anno, R., Halpert, R., Spidlen, J., & Snyder-Cappione, J. E. (2019). Automated optimized parameters for T-distributed stochastic neighbor embedding improve visualization and analysis of large datasets. *Nature Communications*, *10*(1). https://doi.org/10.1038/s41467-019-13055-y

Bendixen, M. (2019). Time is running out for sand. *Nature*, *571*, 29–31. https://doi.org/https://doi.org/10.1038/d41586-019-02042-4

Bergold, S. T., Goetz-Neunhoeffer, F., & Neubauer, J. (2013). Quantitative analysis of C-S-H in hydrating alite pastes by in-situ XRD. *Cement and Concrete Research*, *53*, 119–126. https://doi.org/10.1016/j.cemconres.2013.06.001

Best, J. (2019). Anthropogenic stresses on the world's big rivers. In *Nature Geoscience* (Vol. 12, Issue 1, pp. 7–21). Nature Publishing Group. https://doi.org/10.1038/s41561-018-0262-x

Bi, J., Sai, Q., Wang, F., & Chen, Y. (2022). Identification of Working Trucks and Critical Path Nodes for Construction Waste Transportation Based on Electric Waybills: A Case Study of Shenzhen, China. *Journal of Advanced Transportation*, *2022*. https://doi.org/10.1155/2022/7647121

Bianchini, G., di Giuseppe, D., Natali, C., & Beccaluva, L. (2013). Ophiolite inheritance in the Po Plain sediments: Insights on heavy metals distribution and risk assessment. *Ofioliti*, *38*(1), 1–14. https://doi.org/10.4454/ofioliti.v38i1.412

Bianchini, G., Natali, C., Di Giuseppe, D., & Beccaluva, L. (2012). Heavy metals in soils and sedimentary deposits of the Padanian Plain (Ferrara, Northern Italy): Characterisation and biomonitoring. *Journal of Soils and Sediments*, *12*(7), 1145–1153. https://doi.org/10.1007/s11368-012-0538-5

Bianchini, G., Ristovski, I., Milcov, I., Zupac, A., Natali, C., Salani, G. M., Marchina, C., Brombin, V., & Ferraboschi, A. (2020). Chemical characterisation of construction and demolitionwaste in Skopje city and its surroundings (Republic of Macedonia). *Sustainability (Switzerland)*, *12*(5). https://doi.org/10.3390/su12052055

Bisciotti, A., Jiang, D., Song, Y., & Cruciani, G. (2024). Estimating attached mortar paste on the surface of recycled aggregates based on deep learning and mineralogical models. *Cleaner Materials*, *11*, 100215. https://doi.org/10.1016/j.clema.2023.100215

Blezard, R. G. (1998). 1 - The History of Calcareous Cements. In P. C. Hewlett (Ed.), *Lea's Chemistry of Cement and Concrete (Fourth Edition)* (Fourth Edition, pp. 1–23). Butterworth-Heinemann. https://doi.org/https://doi.org/10.1016/B978-075066256-7/50013-8

Bonifazi, G., Palmieri, R., & Serranti, S. (2018). Evaluation of attached mortar on recycled concrete aggregates by hyperspectral imaging. *Construction and Building Materials*, *169*, 835–842. https://doi.org/10.1016/j.conbuildmat.2018.03.048

Bortolotti, M., Lutterotti, L., Borovin, E., & Martorelli, D. (2019). Combined XRD-XRF cluster analysis for automatic chemical and crystallographic surface mappings. *Powder Diffraction*, *34*(S1), S36–S41. https://doi.org/10.1017/S0885715619000216

Bradski, G. (2000). The OpenCV Library. *Dr. Dobb's Journal of Software Tools*.

Braymand, S., Roux, S., Fares, H., Déodonne, K., & Feugeas, F. (2017). Separation and Quantification of Attached Mortar in Recycled Concrete Aggregates. *Waste and Biomass Valorization*, *8*(5), 1393–1407. https://doi.org/10.1007/s12649-016-9771-2

Brinkman, L., & Miller, S. A. (2021). Environmental impacts and environmental justice implications of supplementary cementitious materials for use in concrete. *Environmental Research: Infrastructure and Sustainability*, *1*(2). https://doi.org/10.1088/2634-4505/ac0e86

Butera, S., Christensen, T. H., & Astrup, T. F. (2014). Composition and leaching of construction and demolition waste: Inorganic elements and organic compounds. *Journal of Hazardous Materials*, *276*, 302–311. https://doi.org/10.1016/j.jhazmat.2014.05.033

Butera, S., Trapp, S., Astrup, T. F., & Christensen, T. H. (2015). Soil retention of hexavalent chromium released from construction and demolition waste in a road-base-application scenario. *Journal of Hazardous Materials*, *298*, 361–367. https://doi.org/10.1016/j.jhazmat.2015.06.025

Caro, D., Lodato, C., Damgaard, A., Cristóbal, J., Foster, G., Flachenecker, F., & Tonini, D. (2024). Environmental and socio-economic effects of construction and demolition

waste recycling in the European Union. *Science of the Total Environment*, *908*. https://doi.org/10.1016/j.scitotenv.2023.168295

Chaturvedi, S., & Ochsendorf, J. (2004). Global Environmental Impacts due to Cement and Steel. *Structural Engineering International*, *14*(3), 198–200. https://doi.org/10.2749/101686604777963748

Chen, W., Li, K., Wu, M. M., Liu, D. D., Wang, P., & Liang, Y. (2023). Influence of pore structure characteristics on the gas permeability of concrete. *Journal of Building Engineering*, *79*. https://doi.org/10.1016/j.jobe.2023.107852

Chen, X., Capiau, L., Reynaert, I., Zheng, K., Gruyaert, E., & Li, J. (2022). Comparative study on modelling concrete properties using physical and mechanical properties of recycled coarse aggregate. *Construction and Building Materials*, *345*. https://doi.org/10.1016/j.conbuildmat.2022.128249

Chen, Y., Zhan, B., Hong, L., Guo, B., bian, P., Wang, C., Hong, X., & Yu, Q. (2024). A new perspective on the effect of residual paste content on the properties of recycled fine aggregates. *Journal of Building Engineering*, *94*, 110070. https://doi.org/10.1016/j.jobe.2024.110070

Coelho, A., & De Brito, J. (2011). Economic analysis of conventional versus selective demolition - A case study. *Resources, Conservation and Recycling*, *55*(3), 382–392. https://doi.org/10.1016/j.resconrec.2010.11.003

Colombani, N., Mastrocicco, M., & Dinelli, E. (2015). Trace elements mobility in a saline coastal aquifer of the Po river lowland (Italy). *Journal of Geochemical Exploration*, *159*, 317–328. https://doi.org/10.1016/j.gexplo.2015.10.009

Comas, M., & Thió-Henestrosa, S. (2011). CoDaPack 2.0: a stand-alone, multi-platform compositional software. In J. J. Egozcue, R. Tolosana-Delgado, & M. Ortego (Eds.), *Proceedings of the 4th International Workshop on Compositional Data Analysis*.

Coudray, C., Amant, V., Cantegrit, L., Le Bocq, A., Thery, F., Denot, A., & Eisenlohr, L. (2017). Influence of Crushing Conditions on Recycled Concrete Aggregates (RCA) Leaching Behaviour. *Waste and Biomass Valorization*, *8*(8), 2867–2880. https://doi.org/10.1007/s12649-017-9868-2

Council Directive 75/442 (1975).

D O'Flynn, C B Reid, C Christodoulou, M D Wilson, M C Veale, P Seller, D Hills, H Desai, B Wong, & R Speller. (2013). Explosive detection using pixellated X-ray diffraction (PixD). *Journal of Instrumentation*, *8*(03), P03007. https://doi.org/10.1088/1748-0221/8/03/P03007

da Silva, Í. B. (2018). X-ray Computed Microtomography technique applied for cementitious materials: A review. In *Micron* (Vol. 107, pp. 1–8). Elsevier Ltd. https://doi.org/10.1016/j.micron.2018.01.006

Dai, Y., & Post, J. E. (1995). Crystal structure of hillebrandite: A natural analogue of calcium silicate hydrate (CSH) phases in Portland cement. *American Mineralogist*, *80*(7–8), 841–844. https://doi.org/10.2138/am-1995-7-820

Damgaard, A., Lodato, C., Butera, S., Kamps, M., Corbin, L., Astrup, T., Fruergaard, T., & Tonini, D. (2022). Background data collection and life cycle assessment for construction and demolition waste (CDW) management. *Publications Office of the European Union*. https://doi.org/doi/10.2760/772724

Das, A., Song, Y., Mantellato, S., Wangler, T., Lange, D. A., & Flatt, R. J. (2022). Effect of processing on the air void system of 3D printed concrete. *Cement and Concrete Research*, *156*, 106789. https://doi.org/10.1016/j.cemconres.2022.106789

de Andrade Gobbo, L., Sant'Agostino, L. M., & Garcez, L. R. (2004). C3A polymorphs related to industrial clinker alkalies content. *Cement and Concrete Research*, *34*, 657–664. https://api.semanticscholar.org/CorpusID:96327061

de Jesus, A., & Mendonça, S. (2018). Lost in Transition? Drivers and Barriers in the Eco-innovation Road to the Circular Economy. *Ecological Economics*, *145*, 75–89. https://doi.org/10.1016/j.ecolecon.2017.08.001

de Juan, M. S., & Gutiérrez, P. A. (2009). Study on the influence of attached mortar content on the properties of recycled concrete aggregate. *Construction and Building Materials*, *23*(2), 872–877. https://doi.org/10.1016/j.conbuildmat.2008.04.012

De La Torre, Á. G., Bruque, S., Campo, J., & Aranda, M. A. G. (2002). The superstructure of C3S from synchrotron and neutron powder diffraction and its role in quantitative phase analyses. *Cement and Concrete Research*, *32*(9), 1347–1356. https://doi.org/https://doi.org/10.1016/S0008-8846(02)00796-2

De Schepper, M., De Buysser, K., Van Driessche, I., & De Belie, N. (2013). The regeneration of cement out of Completely Recyclable Concrete: Clinker production evaluation. *Construction and Building Materials*, *38*, 1001–1009. https://doi.org/10.1016/j.conbuildmat.2012.09.061

Deng, X., Li, J., Lu, Z., Zhang, J., Luo, K., Niu, Y., Hu, J., & He, K. (2023). Rheological and early hydration of cementitious material containing recycled concrete powders collected from recycled aggregates. *Construction and Building Materials*, *393*. https://doi.org/10.1016/j.conbuildmat.2023.132108

Dhanjal, S. K., Young, L., & Storer, P. (2006). Automatic control of cement quality using on-line XRD. *IEEE Cement Industry Technical Conference, 2006. Conference Record.*, 17 pp.-. https://doi.org/10.1109/CITCON.2006.1635726

Ding, G. K. C. (2014). 3 - Life cycle assessment (LCA) of sustainable building materials: an overview. In F. Pacheco-Torgal, L. F. Cabeza, J. Labrincha, & A. de Magalhães (Eds.), *Eco-efficient Construction and Building Materials* (pp. 38–62). Woodhead Publishing. https://doi.org/https://doi.org/10.1533/9780857097729.1.38

Dinh, H. L., Liu, J., Ong, D. E. L., & Doh, J. H. (2022). A sustainable solution to excessive river sand mining by utilizing by-products in concrete manufacturing: A state-of-the-art review. *Cleaner Materials*, *6*, 100140. https://doi.org/https://doi.org/10.1016/j.clema.2022.100140

Diotti, A., Galvin, A. P., Piccinali, A., Plizzari, G., & Sorlini, S. (2020). Chemical and leaching behavior of construction and demolition wastes and recycled aggregates. *Sustainability (Switzerland)*, *12*(24), 1–12. https://doi.org/10.3390/su122410326

Diotti, A., Plizzari, G., & Sorlini, S. (2021). Leaching behaviour of construction and demolition wastes and recycled aggregates: Statistical analysis applied to the release of contaminants. *Applied Sciences (Switzerland)*, *11*(14). https://doi.org/10.3390/app11146265

Directive 2008/98/EC (2008).

Djerbi, A. (2018). Effect of recycled coarse aggregate on the new interfacial transition zone concrete. *Construction and Building Materials*, *190*, 1023–1033. https://doi.org/10.1016/j.conbuildmat.2018.09.180

Dong, H., Yoneda, M., & Feng, L. (2021). Risk dynamic evolution index based on fraction transformation and its application to site risk assessment. *Journal of Hazardous Materials*, *412*. https://doi.org/10.1016/j.jhazmat.2021.125210

dos Santos Macedo, R., Ulsen, C., & Mueller, A. (2019). Quantification of residual cement paste on recycled concrete aggregates containing limestone by selective dissolution. *Construction and Building Materials*, *229*. https://doi.org/10.1016/j.conbuildmat.2019.116875

Duquennoi, C., & Martinez, J. (2022). European Union's policymaking on sustainable waste management and circularity in agroecosystems: The potential for innovative interactions between science and decision-making. *Frontiers in Sustainable Food Systems*, *6*, 1–13. https://doi.org/10.3389/fsufs.2022.937802

Dzene, L., Dutournie, P., Brendle, J., Limousy, L., Le Meins, J. M., Michelin, L., Vidal, L., Gree, S., Abdelmoula, M., Martin, C., & Michau, N. (2022). Characterization of Iron-Rich Phyllosilicates Formed at Different Fe/Si Ratios. *Clays and Clay Minerals*, *70*(4), 580–594. https://doi.org/10.1007/s42860-022-00204-6

ECC, E. E. C. (1975). Directive 75/442. *Official Journal of the European Communities*, *194*(39).

Engelsen, C. J., Van Der Sloot, H. A., Wibetoe, G., Justnes, H., Lund, W., & Stoltenberg-Hansson, E. (2010a). Leaching characterisation and geochemical modelling of minor and trace elements released from recycled concrete aggregates. *Cement and Concrete Research*, *40*(12), 1639–1649. https://doi.org/10.1016/j.cemconres.2010.08.001

Engelsen, C. J., Van Der Sloot, H. A., Wibetoe, G., Justnes, H., Lund, W., & Stoltenberg-Hansson, E. (2010b). Leaching characterisation and geochemical modelling of minor and trace elements released from recycled concrete aggregates. *Cement and Concrete Research*, *40*(12), 1639–1649. https://doi.org/10.1016/j.cemconres.2010.08.001

Engelsen, C. J., van der Sloot, H. A., Wibetoe, G., Petkovic, G., Stoltenberg-Hansson, E., & Lund, W. (2009). Release of major elements from recycled concrete aggregates and geochemical modelling. *Cement and Concrete Research*, *39*(5), 446–459. https://doi.org/10.1016/j.cemconres.2009.02.001

Erdem, S., Gürbüz, E., & Uysal, M. (2018). Micro-mechanical analysis and X-ray computed tomography quantification of damage in concrete with industrial by-products and construction waste. *Journal of Cleaner Production*, *189*, 933–940. https://doi.org/10.1016/j.jclepro.2018.04.089

Ershadi, A., Finkel, M., Susset, B., & Grathwohl, P. (2023). Applicability of machine learning models for the assessment of long-term pollutant leaching from solid waste materials. *Waste Management*, *171*, 337–349. https://doi.org/10.1016/j.wasman.2023.09.001

Etxeberria, M., Vázquez, E., Marí, A., & Barra, M. (2007). Influence of amount of recycled coarse aggregates and production process on properties of recycled aggregate concrete. *Cement and Concrete Research*, *37*(5), 735–742. https://doi.org/https://doi.org/10.1016/j.cemconres.2007.02.002

EU Construction & Demolition Waste Management Protocol (2016).

European Commission, E. C., & Directorate-General for Environment. (2017). *Resource efficient use of mixed wastes improving management of construction and demolition waste – Final report*. Publications Office. https://doi.org/doi/10.2779/99903

European List of Waste 2000/532/EC (2000).

EUROSTAT. (2023). *Treatment of waste by waste category, hazardousness and waste management operations*. https://doi.org/https://doi.org/10.2908/ENV_WASTRT

Faleschini, F., Jiménez, C., Barra, M., Aponte, D., Vázquez, E., & Pellegrino, C. (2014). Rheology of fresh concretes with recycled aggregates. *Construction and Building Materials*, *73*, 407–416. https://doi.org/10.1016/j.conbuildmat.2014.09.068

Fan, C. C., Huang, R., Hwang, H., & Chao, S. J. (2016). Properties of concrete incorporating fine recycled aggregates from crushed concrete wastes. *Construction and Building Materials*, *112*, 708–715. https://doi.org/10.1016/j.conbuildmat.2016.02.154

Fang, G., Chen, J., Dong, B., & Liu, B. (2023). Microstructure and micromechanical properties of interfacial transition zone in green recycled aggregate concrete. *Journal of Building Engineering*, *66*. https://doi.org/10.1016/j.jobe.2023.105860

FAO. (2016). *AQUASTAT Main Database (FAO, 2016)*. https://doi.org/http://www.fao.org/nr/water/aquastat/data/query/results.html

Favaretto, P., Hidalgo, G. E. N., Sampaio, C. H., de Almeida Silva, R., & Lermen, R. T. (2017). Characterization and use of construction and demolition waste from South of

Brazil in the production of foamed concrete blocks. *Applied Sciences (Switzerland)*, *7*(10). https://doi.org/10.3390/app7101090

Feng, Z., Hou, Q., Zheng, Y., Ren, W., Ge, J. Y., Li, T., Cheng, C., Lu, W., Cao, S., Zhang, J., & Zhang, T. (2019). Method of artificial intelligence algorithm to improve the automation level of Rietveld refinement. *Computational Materials Science*, *156*, 310–314. https://doi.org/10.1016/j.commatsci.2018.10.006

Frías, M., de la Villa, R. V., Martínez-Ramírez, S., Fernández-Carrasco, L., Villar-Cociña, E., & García-Giménez, R. (2020). Multi-technique characterization of a fine fraction of cdw and assessment of reactivity in a cdw/lime system. *Minerals*, *10*(7), 1–20. https://doi.org/10.3390/min10070590

Frías, M., Martínez-Ramírez, S., de la Villa, R. V., Fernández-Carrasco, L., & García, R. (2021). Reactivity in cement pastes bearing fine fraction concrete and glass from construction and demolition waste: Microstructural analysis of viability. *Cement and Concrete Research*, *148*. https://doi.org/10.1016/j.cemconres.2021.106531

Gagg, C. R. (2014). Cement and concrete as an engineering material: An historic appraisal and case study analysis. *Engineering Failure Analysis*, *40*, 114–140. https://doi.org/10.1016/j.engfailanal.2014.02.004

Galán, B., Viguri, J. R., Cifrian, E., Dosal, E., & Andres, A. (2019). Influence of input streams on the construction and demolition waste (CDW) recycling performance of basic and advanced treatment plants. *Journal of Cleaner Production*, *236*. https://doi.org/10.1016/j.jclepro.2019.06.354

Galderisi, A., Bravo, M., Iezzi, G., Cruciani, G., Paris, E., & Brito, J. de. (2023). Physico-Mechanical Performances of Mortars Prepared with Sorted Earthquake Rubble: The Role of CDW Type and Contained Crystalline Phases. *Materials*, *16*(7). https://doi.org/10.3390/ma16072855

Galderisi, A., Iezzi, G., Bianchini, G., Paris, E., & de Brito, J. (2022). Petrography of construction and demolition waste (CDW) from Abruzzo region (Central Italy). *Waste Management*, *137*, 61–71. https://doi.org/10.1016/j.wasman.2021.10.028

Gálvez-Martos, J. L., Styles, D., Schoenberger, H., & Zeschmar-Lahl, B. (2018a). Construction and demolition waste best management practice in Europe. *Resources, Conservation and Recycling*, *136*, 166–178. https://doi.org/10.1016/j.resconrec.2018.04.016

Gálvez-Martos, J. L., Styles, D., Schoenberger, H., & Zeschmar-Lahl, B. (2018b). Construction and demolition waste best management practice in Europe. *Resources, Conservation and Recycling*, *136*, 166–178. https://doi.org/10.1016/j.resconrec.2018.04.016

Galvín, A. P., Ayuso, J., Agrela, F., Barbudo, A., & Jiménez, J. R. (2013). Analysis of leaching procedures for environmental risk assessment of recycled aggregate use in unpaved roads. *Construction and Building Materials*, *40*, 1207–1214. https://doi.org/10.1016/j.conbuildmat.2011.12.091

Gao, Y., Wang, J., & Xu, X. (2024). Machine learning in construction and demolition waste management: Progress, challenges, and future directions. In *Automation in Construction* (Vol. 162). Elsevier B.V. https://doi.org/10.1016/j.autcon.2024.105380

Gebremariam, A. T., Di Maio, F., Vahidi, A., & Rem, P. (2020). Innovative technologies for recycling End-of-Life concrete waste in the built environment. *Resources, Conservation and Recycling*, *163*. https://doi.org/10.1016/j.resconrec.2020.104911

Geissdoerfer, M., Savaget, P., Bocken, N. M. P., & Hultink, E. J. (2017). The Circular Economy – A new sustainability paradigm? In *Journal of Cleaner Production* (Vol. 143, pp. 757–768). Elsevier Ltd. https://doi.org/10.1016/j.jclepro.2016.12.048

Georget, F., Soja, W., & Scrivener, K. L. (2020). Characteristic lengths of the carbonation front in naturally carbonated cement pastes: Implications for reactive transport

models. *Cement and Concrete Research*, *134*. https://doi.org/10.1016/j.cemconres.2020.106080
Gevrey, M., Dimopoulos, I., & Lek, S. (2003). Review and comparison of methods to study the contribution of variables in artificial neural network models. *Ecological Modelling*, *160*(3), 249–264. https://doi.org/https://doi.org/10.1016/S0304-3800(02)00257-0
Goñi, S., Gaztañaga, M. T., & Guerrero, A. (2002). *Role of cement type on carbonation attack*.
Gonzalez-Corominas, A., Etxeberria, M., & Poon, C. sun. (2017). Influence of the Quality of Recycled Aggregates on the Mechanical and Durability Properties of High Performance Concrete. *Waste and Biomass Valorization*, *8*(5), 1421–1432. https://doi.org/10.1007/s12649-016-9637-7
Gugin, N. Y., Yusenko, K. V, King, A., Meyer, K., Al-Sabbagh, D., Villajos, J. A., & Emmerling, F. (2024). Lighting up industrial mechanochemistry: Real-time in situ monitoring of reactive extrusion using energy-dispersive X-ray diffraction. *Chem*, *10*(11), 3459–3473. https://doi.org/https://doi.org/10.1016/j.chempr.2024.07.033
Guo, H., Shi, C., Guan, X., Zhu, J., Ding, Y., Ling, T. C., Zhang, H., & Wang, Y. (2018). Durability of recycled aggregate concrete – A review. *Cement and Concrete Composites*, *89*, 251–259. https://doi.org/10.1016/j.cemconcomp.2018.03.008
Hakanson, L. (1980). An ecological risk index for aquatic pollution control.a sedimentological approach. *Water Research*, *14*(8), 975–1001. https://doi.org/https://doi.org/10.1016/0043-1354(80)90143-8
He, K., Zhang, X., Ren, S., & Sun, J. (2015). *Deep Residual Learning for Image Recognition*. https://doi.org/https://doi.org/10.48550/arXiv.1512.03385
Hossain, M. U., Wu, Z., & Poon, C. S. (2017). Comparative environmental evaluation of construction waste management through different waste sorting systems in Hong Kong. *Waste Management*, *69*, 325–335. https://doi.org/10.1016/j.wasman.2017.07.043
Hougaard, I.-M. (2023). 'As we exploit the river, we should give something back': A moral ecology of sand extraction. *The Extractive Industries and Society*, *15*, 101301. https://doi.org/https://doi.org/10.1016/j.exis.2023.101301
Hubert, J., Zhao, Z., Michel, F., & Courard, L. (2023). Effect of Crushing Method on the Properties of Produced Recycled Concrete Aggregates. *Buildings*, *13*(9), 2217. https://doi.org/10.3390/buildings13092217
Imam, M., Adam, S., Dev, S., & Nesa, N. (2024). Air quality monitoring using statistical learning models for sustainable environment. *Intelligent Systems with Applications*, *22*. https://doi.org/10.1016/j.iswa.2024.200333
Jansen, D., Naber, C., Ectors, D., Lu, Z., Kong, X. M., Goetz-Neunhoeffer, F., & Neubauer, J. (2018). The early hydration of OPC investigated by in-situ XRD, heat flow calorimetry, pore water analysis and 1H NMR: Learning about adsorbed ions from a complete mass balance approach. *Cement and Concrete Research*, *109*, 230–242. https://doi.org/10.1016/j.cemconres.2018.04.017
Juenger, M. C. G., Snellings, R., & Bernal, S. A. (2019). Supplementary cementitious materials: New sources, characterization, and performance insights. In *Cement and Concrete Research* (Vol. 122, pp. 257–273). Elsevier Ltd. https://doi.org/10.1016/j.cemconres.2019.05.008
Kang, X., Tong, X. yang, Chen, R. peng, & Chen, Y. qing. (2024). Effect of ITZ on chloride ion transport in recycled aggregate concrete: Analytical and numerical studies. *Journal of Building Engineering*, *83*. https://doi.org/10.1016/j.jobe.2024.108443
Karlsson, I., Rootzén, J., Johnsson, F., & Erlandsson, M. (2021). Achieving net-zero carbon emissions in construction supply chains – A multidimensional analysis of

residential building systems. *Developments in the Built Environment*, *8*. https://doi.org/10.1016/j.dibe.2021.100059
Kim, H., & Yoon, J. (2024). Automated Mineral Identification of Pozzolanic Materials Using XRD Patterns. *Journal of Materials in Civil Engineering*, *36*(12). https://doi.org/10.1061/JMCEE7.MTENG-17973
Kim, J. (2022). Influence of quality of recycled aggregates on the mechanical properties of recycled aggregate concretes: An overview. In *Construction and Building Materials* (Vol. 328). Elsevier Ltd. https://doi.org/10.1016/j.conbuildmat.2022.127071
Kirchherr, J., Reike, D., & Hekkert, M. (2017). Conceptualizing the circular economy: An analysis of 114 definitions. In *Resources, Conservation and Recycling* (Vol. 127, pp. 221–232). Elsevier B.V. https://doi.org/10.1016/j.resconrec.2017.09.005
Kiser, B. (2016). Circular economy: Getting the circulation going. *Nature*, *531*(7595), 443–446. https://doi.org/10.1038/531443a
Knorr, K., & Kelaart, C. (2009). Automated analysis of aluminium bath electrolytes by the Rietveld method. *Minerals Engineering*, *22*(5), 434–439. https://doi.org/10.1016/j.mineng.2008.11.002
Komnitsas, K., Zaharaki, D., Vlachou, A., Bartzas, G., & Galetakis, M. (2015). Effect of synthesis parameters on the quality of construction and demolition wastes (CDW) geopolymers. *Advanced Powder Technology*, *26*(2), 368–376. https://doi.org/10.1016/j.apt.2014.11.012
Korolkovas, A. (2022). Fast X-ray diffraction (XRD) tomography for enhanced identification of materials. *Scientific Reports*, *12*(1). https://doi.org/10.1038/s41598-022-23396-2
Kumar Mehta, P., & Monteiro, P. J. M. (2006). *Concrete Microstructure, Properties, and Materials (third edition)*. McGraw-Hill Companies. https://doi.org/10.1036/0071462899
Lakhouit, A., & Shaban, M. (2024). Exploring sustainable solutions with machine learning algorithms: a focus on construction waste management. *Clean Technologies and Environmental Policy*. https://doi.org/10.1007/s10098-024-02925-9
Lanzafame, G., Ferlito, C., & Donato, S. (2018). Combining chemical and X-ray microtomography investigations on crustal xenoliths at Mount Etna: evidence of volcanic gas fluxing. *Annals of Geophysics*, *61*(6). https://doi.org/10.4401/ag-7740
Lau Hiu Hoong, J. D., Lux, J., Mahieux, P. Y., Turcry, P., & Aït-Mokhtar, A. (2020). Determination of the composition of recycled aggregates using a deep learning-based image analysis. *Automation in Construction*, *116*. https://doi.org/10.1016/j.autcon.2020.103204
Lavagna, M., Baldassarri, C., Campioli, A., Giorgi, S., Dalla Valle, A., Castellani, V., & Sala, S. (2018). Benchmarks for environmental impact of housing in Europe: Definition of archetypes and LCA of the residential building stock. *Building and Environment*, *145*, 260–275. https://doi.org/10.1016/j.buildenv.2018.09.008
Li, B., Hou, S., Duan, Z., Li, L., & Guo, W. (2021). Rheological behavior and compressive strength of concrete made with recycled fine aggregate of different size range. *Construction and Building Materials*, *268*. https://doi.org/10.1016/j.conbuildmat.2020.121172
Li, J., Fang, H., Fan, L., Yang, J., Ji, T., & Chen, Q. (2022). RGB-D fusion models for construction and demolition waste detection. *Waste Management*, *139*, 96–104. https://doi.org/10.1016/j.wasman.2021.12.021
Li, J., Zhao, X., Yong, Q., Liang, J., & Wu, H. (2023). Revealing the implicit and explicit attitudes of the public towards recycled aggregate based on psychological experiment. *Developments in the Built Environment*, *16*. https://doi.org/10.1016/j.dibe.2023.100280

Li, Y., Liu, W., Xing, F., Wang, S., Tang, L., Lin, S., & Dong, Z. (2020). Carbonation of the synthetic calcium silicate hydrate (C-S-H) under different concentrations of CO2: Chemical phases analysis and kinetics. *Journal of CO2 Utilization*, *35*, 303–313. https://doi.org/10.1016/j.jcou.2019.10.001

Limbachiya, M. C., Marrocchino, E., & Koulouris, A. (2007). Chemical-mineralogical characterisation of coarse recycled concrete aggregate. *Waste Management*, *27*(2), 201–208. https://doi.org/10.1016/j.wasman.2006.01.005

Liu, G., Li, Q., Song, J., Wang, L., Liu, H., Guo, Y., & Yue, G. (2022). Quantitative analysis of surface attached mortar for recycled coarse aggregate. *Materials*, *15*(1). https://doi.org/10.3390/ma15010257

Liu, J.-C., Hossain, Md. U., Xuan, D., Ali, H. A., Ng, S. T., & Ye, H. (2023). Mechanical and durability performance of sustainable concretes containing conventional and emerging supplementary cementitious materials. *Developments in the Built Environment*, *15*, 100197. https://doi.org/https://doi.org/10.1016/j.dibe.2023.100197

Liu, Q., Cheng, A., Sun, C., Chen, K., Wang, Y., & Li, W. (2024). Effects of aggregate's type and orientation on stress concentration and crack propagation of modeled concrete applied a shear force. *Journal of Building Engineering*, *95*. https://doi.org/10.1016/j.jobe.2024.110340

Liu, Z., Lu, M., Zhang, Y., Zhou, J., & Wang, J. (2022). Identification of heavy metal leaching patterns in municipal solid waste incineration fly ash based on an explainable machine learning approach. *Journal of Environmental Management*, *317*. https://doi.org/10.1016/j.jenvman.2022.115387

López, A., & Lobo, A. (2014). Emissions of C&D refuse in landfills: A European case. *Waste Management*, *34*(8), 1446–1454. https://doi.org/10.1016/j.wasman.2014.04.004

Lu, B., Shi, C., Cao, Z., Guo, M., & Zheng, J. (2019). Effect of carbonated coarse recycled concrete aggregate on the properties and microstructure of recycled concrete. *Journal of Cleaner Production*, *233*, 421–428. https://doi.org/10.1016/j.jclepro.2019.05.350

Lu, W., & Chen, J. (2022). Computer vision for solid waste sorting: A critical review of academic research. *Waste Management*, *142*, 29–43. https://doi.org/10.1016/j.wasman.2022.02.009

Maćkiewicz, A., & Ratajczak, W. (1993). Principal components analysis (PCA). *Computers & Geosciences*, *19*(3), 303–342. https://doi.org/https://doi.org/10.1016/0098-3004(93)90090-R

Maged, A., Elshaboury, N., & Akanbi, L. (2024). Data-driven prediction of construction and demolition waste generation using limited datasets in developing countries: an optimized extreme gradient boosting approach. *Environment, Development and Sustainability*. https://doi.org/10.1007/s10668-024-04814-z

Martín-Morales, M., Zamorano, M., Valverde-Palacios, I., Cuenca-Moyano, G. M., & Sánchez-Roldán, Z. (2013). Quality control of recycled aggregates (RAs) from construction and demolition waste (CDW). In *Handbook of Recycled Concrete and Demolition Waste* (pp. 270–303). Elsevier Inc. https://doi.org/10.1533/9780857096906.2.270

Maslennikova, G. N., Pishch, I. V, & Radion, E. V. (2006). *SCIENCE FOR CERAMICS PRODUCTION CURRENT CLASSIFICATION OF CERAMIC SILICATE PIGMENTS (REVIEW)* (Issue 9).

Mazhoud, B., Sedran, T., Cazacliu, B., Cothenet, A., & Torrenti, J. M. (2022). Influence of residual mortar volume on the properties of recycled concrete aggregates. *Journal of Building Engineering*, *57*. https://doi.org/10.1016/j.jobe.2022.104945

Meier, R., Anderson, J., & Verryn, S. (2012). Industrial X-ray Diffraction Analysis of Building Materials. *Reviews in Mineralogy and Geochemistry*, *74*(1), 147–165. https://doi.org/10.2138/rmg.2012.74.4

Melo, C. C. A., Angélica, R. S., & Paz, S. P. A. (2020). A proposal for rapid grade control of gibbsitic bauxites using multivariate statistics on XRD data. *Minerals Engineering*, *157*. https://doi.org/10.1016/j.mineng.2020.106539

Miller, S. A., Horvath, A., & Monteiro, P. J. M. (2018). Impacts of booming concrete production on water resources worldwide. *Nature Sustainability*, *1*(1), 69–76. https://doi.org/10.1038/s41893-017-0009-5

Mirhadi, B., Mehdikhani, B., & Askari, N. (2012). Effect of zinc oxide on microhardness and sintering behavior of MgO-Al 2O 3-SiO 2 glass-ceramic system. *Solid State Sciences*, *14*(4), 430–434. https://doi.org/10.1016/j.solidstatesciences.2012.01.010

Moreno-Juez, J., Vegas, I. J., Frías Rojas, M., Vigil de la Villa, R., & Guede-Vázquez, E. (2021). Laboratory-scale study and semi-industrial validation of viability of inorganic CDW fine fractions as SCMs in blended cements. *Construction and Building Materials*, *271*. https://doi.org/10.1016/j.conbuildmat.2020.121823

Moreno-Pérez, E., Hernández-Ávila, J., Rangel-Martínez, Y., Cerecedo-Sáenz, E., Arenas-Flores, A., Reyes-Valderrama, M. I., & Salinas-Rodríguez, E. (2018). Chemical and mineralogical characterization of recycled aggregates from construction and demolition waste from Mexico city. *Minerals*, *8*(6). https://doi.org/10.3390/min8060237

Moschen-Schimek, J., Kasper, T., & Huber-Humer, M. (2023). Critical review of the recovery rates of construction and demolition waste in the European Union – An analysis of influencing factors in selected EU countries. *Waste Management*, *167*, 150–164. https://doi.org/10.1016/j.wasman.2023.05.020

Mulder, V. L., Plötze, M., de Bruin, S., Schaepman, M. E., Mavris, C., Kokaly, R. F., & Egli, M. (2013). Quantifying mineral abundances of complex mixtures by coupling spectral deconvolution of SWIR spectra (2.1-2.4 μm) and regression tree analysis. *Geoderma*, *207–208*(1), 279–290. https://doi.org/10.1016/j.geoderma.2013.05.011

Mumme, W. G., Hill, R. J., Bushnell-wye, G., & Segnit, E. R. (1995). *Rietveld crystal structure refinements, crystal chemistry and calculated powder diffraction data for the polymorphs of dicalcium silicate and related phases*. https://api.semanticscholar.org/CorpusID:135973945

Ndahirwa, D., Zmamou, H., Lenormand, H., & Leblanc, N. (2022). The role of supplementary cementitious materials in hydration, durability and shrinkage of cement-based materials, their environmental and economic benefits: A review. In *Cleaner Materials* (Vol. 5). Elsevier Ltd. https://doi.org/10.1016/j.clema.2022.100123

Nežerka, V., Zbíral, T., & Trejbal, J. (2024). Machine-learning-assisted classification of construction and demolition waste fragments using computer vision: Convolution versus extraction of selected features[Formula presented]. *Expert Systems with Applications*, *238*. https://doi.org/10.1016/j.eswa.2023.121568

Nilimaa, J. (2023). Smart materials and technologies for sustainable concrete construction. *Developments in the Built Environment*, *15*. https://doi.org/10.1016/j.dibe.2023.100177

Nonat, A. (2004). The structure and stoichiometry of C-S-H. *Cement and Concrete Research*, *34*(9), 1521–1528. https://doi.org/10.1016/j.cemconres.2004.04.035

OECD, O. for E. C. and D. (2019). *Global Material Resources Outlook to 2060*. OECD. https://doi.org/10.1787/9789264307452-en

Oh, B. K., Choi, S. W., & Park, H. S. (2017). Influence of variations in CO2 emission data upon environmental impact of building construction. *Journal of Cleaner Production*, *140*, 1194–1203. https://doi.org/10.1016/j.jclepro.2016.10.041

Otsu, N. (1979). A Threshold Selection Method from Gray-Level Histograms. *IEIEE TRANSACTIONS ON SYSTEMS, MAN, AND CYBERNETICS*, *9*(1), 62–66.

Ouyang, K., Shi, C., Chu, H., Guo, H., Song, B., Ding, Y., Guan, X., Zhu, J., Zhang, H., Wang, Y., & Zheng, J. (2020). An overview on the efficiency of different

pretreatment techniques for recycled concrete aggregate. In *Journal of Cleaner Production* (Vol. 263). Elsevier Ltd. https://doi.org/10.1016/j.jclepro.2020.121264

Pan, Y., & Zhang, L. (2021). Roles of artificial intelligence in construction engineering and management: A critical review and future trends. *Automation in Construction*, *122*. https://doi.org/10.1016/j.autcon.2020.103517

Paszke, A., Gross, S., Massa, F., Lerer, A., Bradbury, J., Chanan, G., Killeen, T., Lin, Z., Gimelshein, N., Antiga, L., Desmaison, A., Kopf, A., Yang, E., DeVito, Z., Raison, M., Tejani, A., Chilamkurthy, S., Steiner, B., Fang, L., … Chintala, S. (2019). PyTorch: An Imperative Style, High-Performance Deep Learning Library. In H. Wallach, H. Larochelle, A. Beygelzimer, F. d Alché-Buc, E. Fox, & R. Garnett (Eds.), *Advances in Neural Information Processing Systems* (Vol. 32). Curran Associates, Inc. https://proceedings.neurips.cc/paper_files/paper/2019/file/bdbca288fee7f92f2bfa9f7012727740-Paper.pdf

Pedregosa, F., Varoquaux, G., Gramfort, A., Michel, V., Thirion, B., Grisel, O., Blondel, M., Prettenhofer, P., Weiss, R., Dubourg, V., Vaderplas, J., Passos, A., Cournapeau, D., Brucher, M., Perrot, M., & Duchesnay, É. (2011). Scikit-learn: Machine Learning in Python. *Journal of Machine Learning Research*, *12*, 2825–2830. https://doi.org/https://doi.org/10.48550/arXiv.1201.0490

Pedro, D., de Brito, J., & Evangelista, L. (2017). Structural concrete with simultaneous incorporation of fine and coarse recycled concrete aggregates: Mechanical, durability and long-term properties. *Construction and Building Materials*, *154*, 294–309. https://doi.org/10.1016/j.conbuildmat.2017.07.215

Pešta, J., Šerešová, M., & Kočí, V. (2020). Carbon footprint assessment of construction waste packaging using the package-to-product indicator. *Sustainability (Switzerland)*, *12*(23), 1–23. https://doi.org/10.3390/su122310094

Piccinali, A., Diotti, A., Plizzari, G., & Sorlini, S. (2022). Impact of Recycled Aggregate on the Mechanical and Environmental Properties of Concrete: A Review. In *Materials* (Vol. 15, Issue 5). MDPI. https://doi.org/10.3390/ma15051818

Poon, C. S., Shui, Z. H., & Lam, L. (2004). Effect of microstructure of ITZ on compressive strength of concrete prepared with recycled aggregates. *Construction and Building Materials*, *18*(6), 461–468. https://doi.org/10.1016/j.conbuildmat.2004.03.005

Prasad, S., Yadav, K. K., Kumar, S., Gupta, N., Cabral-Pinto, M. M. S., Rezania, S., Radwan, N., & Alam, J. (2021). Chromium contamination and effect on environmental health and its remediation: A sustainable approaches. In *Journal of Environmental Management* (Vol. 285). Academic Press. https://doi.org/10.1016/j.jenvman.2021.112174

Prieto-Espinoza, M., Susset, B., & Grathwohl, P. (2022). Long-Term Leaching Behavior of Organic and Inorganic Pollutants after Wet Processing of Solid Waste Materials. *Materials*, *15*(3). https://doi.org/10.3390/ma15030858

Rangel, C. S., Toledo Filho, R. D., Amario, M., Pepe, M., de Castro Polisseni, G., & Puente de Andrade, G. (2019). Generalized quality control parameter for heterogenous recycled concrete aggregates: A pilot scale case study. *Journal of Cleaner Production*, *208*, 589–601. https://doi.org/10.1016/j.jclepro.2018.10.110

Ren, X., Tang, C., Xie, Y., Long, G., Ma, G., Wang, H., & Tang, Z. (2024). 3D mesoscale study on the effect of ITZ and aggregate properties on the fracture behaviors of concrete based on discrete element method. *Journal of Building Engineering*, *83*. https://doi.org/10.1016/j.jobe.2024.108450

Renaudin, G., Francois, M., & Evrard, O. (1999). Order and disorder in the lamellar hydrated tetracalcium monocarboaluminate compound. *Cement and Concrete Research*, *29*(1), 63–69. https://doi.org/https://doi.org/10.1016/S0008-8846(98)00184-7

Richardson, I. G. (1999). The nature of C-S-H in hardened cements. In *Cement and Concrete Research* (Vol. 29).

Russakovsky, O., Deng, J., Su, H., Krause, J., Satheesh, S., Ma, S., Huang, Z., Karpathy, A., Khosla, A., Bernstein, M., Berg, A. C., & Fei-Fei, L. (2015). ImageNet Large Scale Visual Recognition Challenge. *International Journal of Computer Vision*, *115*(3), 211–252. https://doi.org/10.1007/s11263-015-0816-y

Sabai, S. M. M., Lichtenberg, J. J., Florea, M. V. M., Brouwers, H. J. H., & Lichtenberg, J. J. N. (2016). Construction and Demolition Waste Characteristics in Tanzania. *Journal of the Open University of Tanzania*, *23*(1), 1–19. https://www.ajol.info/index.php/huria/article/view/152721

Saca, N., Dimache, A., Radu, L. R., & Iancu, I. (2017). Leaching behavior of some demolition wastes. *Journal of Material Cycles and Waste Management*, *19*(2), 623–630. https://doi.org/10.1007/s10163-015-0459-7

Sáez del Bosque, I. F., Zhu, W., Howind, T., Matías, A., Sánchez de Rojas, M. I., & Medina, C. (2017). Properties of interfacial transition zones (ITZs) in concrete containing recycled mixed aggregate. *Cement and Concrete Composites*, *81*, 25–34. https://doi.org/10.1016/j.cemconcomp.2017.04.011

Sarc, R., Curtis, A., Kandlbauer, L., Khodier, K., Lorber, K. E., & Pomberger, R. (2019). Digitalisation and intelligent robotics in value chain of circular economy oriented waste management – A review. In *Waste Management* (Vol. 95, pp. 476–492). Elsevier Ltd. https://doi.org/10.1016/j.wasman.2019.06.035

Schneider, C. A., Rasband, W. S., & Eliceiri, K. W. (2012). NIH Image to ImageJ: 25 years of image analysis. In *Nature Methods* (Vol. 9, Issue 7, pp. 671–675). https://doi.org/10.1038/nmeth.2089

Secchi, M., Zanatta, M., Borovin, E., Bortolotti, M., Kumar, A., Giarola, M., Sanson, A., Orberger, B., Daldosso, N., Gialanella, S., Mariotto, G., Montagna, M., & Lutterotti, L. (2018). Mineralogical investigations using XRD, XRF, and Raman spectroscopy in a combined approach. *Journal of Raman Spectroscopy*, *49*(6), 1023–1030. https://doi.org/10.1002/jrs.5386

Seo, D. S., & Choi, H. B. (2014). Effects of the old cement mortar attached to the recycled aggregate surface on the bond characteristics between aggregate and cement mortar. *Construction and Building Materials*, *59*, 72–77. https://doi.org/10.1016/j.conbuildmat.2014.02.047

Serranti, S., Palmieri, R., Bonifazi, G., Gasbarrone, R., Hermant, G., & Bréquel, H. (2023). An Automated Classification of Recycled Aggregates for the Evaluation of Product Standard Compliance. *Sustainability*, *15*(20), 15009. https://doi.org/10.3390/su152015009

Shen, P., Zhang, Y., Jiang, Y., Zhan, B., Lu, J., Zhang, S., Xuan, D., & Poon, C. S. (2022). Phase assemblance evolution during wet carbonation of recycled concrete fines. *Cement and Concrete Research*, *154*. https://doi.org/10.1016/j.cemconres.2022.106733

Silva, R. V., De Brito, J., & Dhir, R. K. (2014). Properties and composition of recycled aggregates from construction and demolition waste suitable for concrete production. *Construction and Building Materials*, *65*, 201–217. https://doi.org/10.1016/j.conbuildmat.2014.04.117

Silva, R. V., De Brito, J., & Dhir, R. K. (2015). The influence of the use of recycled aggregates on the compressive strength of concrete: A review. *European Journal of Environmental and Civil Engineering*, *19*(7), 825–849. https://doi.org/10.1080/19648189.2014.974831

Singh, A. (2015). Survey of Noise in Image and Efficient Technique for Noise Reduction. In *International Journal of Science and Research (IJSR) ISSN*. www.ijsr.net

Singh, R., Nayak, D., Pandey, A., Kumar, R., & Kumar, V. (2022). Effects of recycled fine aggregates on properties of concrete containing natural or recycled coarse aggregates: A comparative study. *Journal of Building Engineering*, *45*. https://doi.org/10.1016/j.jobe.2021.103442

Sivashanmugam, S., Rodriguez, S., Pour Rahimian, F., Elghaish, F., & Dawood, N. (2023). Enhancing information standards for automated construction waste quantification and classification. In *Automation in Construction* (Vol. 152). Elsevier B.V. https://doi.org/10.1016/j.autcon.2023.104898

Skocek, J., Ouzia, A., Vargas Serrano, E., & Pato, N. (2024). Recycled Sand and Aggregates for Structural Concrete: Toward the Industrial Production of High-Quality Recycled Materials with Low Water Absorption. *Sustainability (Switzerland)*, *16*(2). https://doi.org/10.3390/su16020814

Snellings, R. (2016). X-ray powder diffraction applied to cement. In K. Scrivener, R. Snellings, & B. Lothenbach (Eds.), *A Practical Guide to Microstructural Analysis of Cementitious Materials* (2016th ed., Vol. 4, pp. 108–162). CRC Press. https://doi.org/10.1201/b19074

Sobotka, A., & Sagan, J. (2021). Decision support system in management of concrete demolition waste. *Automation in Construction*, *128*. https://doi.org/10.1016/j.autcon.2021.103734

Song, D., Yang, J., Chen, B., Hayat, T., & Alsaedi, A. (2016). Life-cycle environmental impact analysis of a typical cement production chain. *Applied Energy*, *164*, 916–923. https://doi.org/https://doi.org/10.1016/j.apenergy.2015.09.003

Song, Y., Huang, Z., Shen, C., Shi, H., & Lange, D. A. (2020). Deep learning-based automated image segmentation for concrete petrographic analysis. *Cement and Concrete Research*, *135*, 106118. https://doi.org/10.1016/j.cemconres.2020.106118

Song, Y., Lu, X., Wang, K., Ryan, J. V., Smedskjaer, M. M., Vienna, J. D., & Bauchy, M. (2024). Unveiling the effect of composition on nuclear waste immobilization glasses' durability by nonparametric machine learning. *Npj Materials Degradation*, *8*(1). https://doi.org/10.1038/s41529-024-00458-6

Song, Y., Yang, K., Chen, J., Wang, K., Sant, G., & Bauchy, M. (2021). Machine Learning Enables Rapid Screening of Reactive Fly Ashes Based on Their Network Topology. *ACS Sustainable Chemistry and Engineering*, *9*(7), 2639–2650. https://doi.org/10.1021/acssuschemeng.0c06978

Song, Y., Zhang, S., Wang, K., Jin, C., Sant, G., & Bauchy, M. (2022). Interpreting the Strength Activity Index of Fly Ash with Machine Learning. *Advances in Civil Engineering Materials*, *11*(2), 587–602. https://doi.org/10.1520/ACEM20220024

Song, Y., Zhao, Y., Ginella, A., Gallagher, B., & Bauchy, M. (2024). Predicting Rare Earth Elements Concentration in Coal Ashes with Multi-Task Neural Networks. *Materials Horizons*, *6*(11), 1448–1464. https://doi.org/10.21203/rs.3.rs-2172679/v1

Stefaniuk, D., Hajduczek, M., Weaver, J. C., Ulm, F. J., & Masic, A. (2023). Cementing CO2 into C-S-H: A step toward concrete carbon neutrality. *PNAS Nexus*, *2*(3). https://doi.org/10.1093/pnasnexus/pgad052

Stevulova, N., Estokova, A., Holub, M., & Singovszka, E. (2022). 12 - Demolition waste contaminated with asbestos. In F. Pacheco-Torgal, J. O. Falkinham, & J. A. Gałaj (Eds.), *Advances in the Toxicity of Construction and Building Materials* (pp. 261–283). Woodhead Publishing. https://doi.org/https://doi.org/10.1016/B978-0-12-824533-0.00002-5

Strufe, N., Trap, N., & Lauritzen Golder, E. K. (2006). *Kortlaegning af forurenende stoffer i bygge-og anlaegsaffald* (Golder Associates AB, Ed.). Miljøprojekt Nr. 1083.

Su, Y., Xu, Y., Bao, Z., Ng, S. T., & Gao, Q. (2024). Stakeholder interactions of government intervention in construction and demolition waste recycling market: A

game theory approach. *Developments in the Built Environment*, *18*. https://doi.org/10.1016/j.dibe.2024.100391
Susset, B., & Grathwohl, P. (2011). Leaching standards for mineral recycling materials - A harmonized regulatory concept for the upcoming German Recycling Decree. *Waste Management*, *31*(2), 201–214. https://doi.org/10.1016/j.wasman.2010.08.017
Szeliski, R. (2022). *Computer Vision*. Springer International Publishing. https://doi.org/10.1007/978-3-030-34372-9
Tam, V. W. Y., Soomro, M., & Evangelista, A. C. J. (2021). Quality improvement of recycled concrete aggregate by removal of residual mortar: A comprehensive review of approaches adopted. In *Construction and Building Materials* (Vol. 288). Elsevier Ltd. https://doi.org/10.1016/j.conbuildmat.2021.123066
Tang, B., Fan, M., Yang, Z., Sun, Y., & Yuan, L. (2023). A comparison study of aggregate carbonation and concrete carbonation for the enhancement of recycled aggregate pervious concrete. *Construction and Building Materials*, *371*. https://doi.org/10.1016/j.conbuildmat.2023.130797
Teychenne, D. C., Franklin, R. E., Erntroy, H. C., & Building Research Establishment. (1997). *Design of normal concrete mixes*. Building Research Establishment.
Thieffry, P. E., & Nahmias, P. E. (1991). Hastings International and Comparative Law Review The European Community' s Regulation and Control of Waste and the Adoption of Civil Liability Recommended Citation The European Community's Regulation and Control of Waste and the Adoption of Civil Liability. *Hastings International and Comparative Law Review*, *4*(14), 949–970. https://doi.org/https://repository.uchastings.edu/hastings_international_comparative_law_review/vol14/iss4/9
Torres, A., Brandt, J., Lear, K., & Liu, J. (2017). A looming tragedy of the sand commons. In *Science* (Vol. 357, Issue 6355, pp. 970–971). American Association for the Advancement of Science. https://doi.org/10.1126/science.aao0503
Trotta, O., Bonifazi, G., Capobianco, G., & Serranti, S. (2021). Recycling-oriented characterization of post-earthquake building waste by different sensing techniques. *Journal of Imaging*, *7*(9). https://doi.org/10.3390/JIMAGING7090182
Ulsen, C., Contessotto, R., dos Santos Macedo, R., & Kahn, H. (2022). Quantification of the cement paste and phase's association in fine recycled aggregates by SEM-based image analysis. *Construction and Building Materials*, *320*. https://doi.org/10.1016/j.conbuildmat.2021.126206
Ulsen, C., Tseng, E., Angulo, S. C., Landmann, M., Contessotto, R., Balbo, J. T., & Kahn, H. (2019). Concrete aggregates properties crushed by jaw and impact secondary crushing. *Journal of Materials Research and Technology*, *8*(1), 494–502. https://doi.org/10.1016/j.jmrt.2018.04.008
UNEP, U. N. E. P. (2024). *Global Status Report for Buildings and Construction: Beyond foundations - Mainstreaming sustainable solutions to cut emissions from the buildings sector*. United Nations Environment Programme. https://doi.org/10.59117/20.500.11822/45095
USGS, U. S. G. S. (2024). *Mineral commodity summaries 2024*. https://doi.org/10.3133/mcs2024
van den Berg, M., Voordijk, H., & Adriaanse, A. (2020). Recovering building elements for reuse (or not) – Ethnographic insights into selective demolition practices. *Journal of Cleaner Production*, *256*. https://doi.org/10.1016/j.jclepro.2020.120332
Van Der Maaten, L., & Hinton, G. (2008). Visualizing Data using t-SNE. *Journal of Machine Learning Research*, *9*, 2579–2605.
Van Der Maaten, L., & Hinton, G. (2012). Visualizing non-metric similarities in multiple maps. *Machine Learning*, *87*(1), 33–55. https://doi.org/10.1007/s10994-011-5273-4

Van Roijen, E., Sethares, K., Kendall, A., & Miller, S. A. (2024). The climate benefits from cement carbonation are being overestimated. *Nature Communications*, *15*(1). https://doi.org/10.1038/s41467-024-48965-z

Verian, K. P., Ashraf, W., & Cao, Y. (2018). Properties of recycled concrete aggregate and their influence in new concrete production. In *Resources, Conservation and Recycling* (Vol. 133, pp. 30–49). Elsevier B.V. https://doi.org/10.1016/j.resconrec.2018.02.005

Verma, N., Rachamalla, M., Kumar, P. S., & Dua, K. (2023). Assessment and impact of metal toxicity on wildlife and human health. In *Metals in Water* (pp. 93–110). Elsevier. https://doi.org/10.1016/b978-0-323-95919-3.00002-1

Vidak Vasić, M., Muñoz Velasco, P., Bueno-Rodríguez, S., Netinger Grubeša, I., Dondi, M., Pérez Villarejo, L., Eliche-Quesada, D., & Zanelli, C. (2024). State and perspectives of sustainable production of traditional silicate ceramics. In *Open Ceramics* (Vol. 17). Elsevier B.V. https://doi.org/10.1016/j.oceram.2024.100537

Walenta, G., & Füllmann, T. (2004). Advances in quantitative XRD analysis for clinker, cements, and cementitious additions. *Powder Diffraction*, *19*(1), 40–44. https://doi.org/DOI: 10.1154/1.1649328

Wang, B., Yan, L., Fu, Q., & Kasal, B. (2021a). A Comprehensive Review on Recycled Aggregate and Recycled Aggregate Concrete. In *Resources, Conservation and Recycling* (Vol. 171). Elsevier B.V. https://doi.org/10.1016/j.resconrec.2021.105565

Wang, B., Yan, L., Fu, Q., & Kasal, B. (2021b). A Comprehensive Review on Recycled Aggregate and Recycled Aggregate Concrete. In *Resources, Conservation and Recycling* (Vol. 171). Elsevier B.V. https://doi.org/10.1016/j.resconrec.2021.105565

Wang, C., Wu, H., & Li, C. (2022). Hysteresis and damping properties of steel and polypropylene fiber reinforced recycled aggregate concrete under uniaxial low-cycle loadings. *Construction and Building Materials*, *319*. https://doi.org/10.1016/j.conbuildmat.2021.126191

Wang, C., Xiao, J., Liu, W., & Ma, Z. (2022). Unloading and reloading stress-strain relationship of recycled aggregate concrete reinforced with steel/polypropylene fibers under uniaxial low-cycle loadings. *Cement and Concrete Composites*, *131*. https://doi.org/10.1016/j.cemconcomp.2022.104597

Wang, R., Yu, N., & Li, Y. (2020). Methods for improving the microstructure of recycled concrete aggregate: A review. In *Construction and Building Materials* (Vol. 242). Elsevier Ltd. https://doi.org/10.1016/j.conbuildmat.2020.118164

Wang, Y., Liu, J., Zhu, P., Liu, H., Wu, C., & Zhao, J. (2021). Investigation of Adhered Mortar Content on Recycled Aggregate Using Image Analysis Method. *Journal of Materials in Civil Engineering*, *33*(9). https://doi.org/10.1061/(asce)mt.1943-5533.0003864

Wang, Z., Li, H., & Yang, X. (2020). Vision-based robotic system for on-site construction and demolition waste sorting and recycling. *Journal of Building Engineering*, *32*. https://doi.org/10.1016/j.jobe.2020.101769

Wattenberg, M., Viégas, F. B., & Johnson, I. (2016). *How to Use t-SNE Effectively*. https://api.semanticscholar.org/CorpusID:155770513

Wu, T. W., Zhang, H., Peng, W., Lü, F., & He, P. J. (2023). Applications of convolutional neural networks for intelligent waste identification and recycling: A review. In *Resources, Conservation and Recycling* (Vol. 190). Elsevier B.V. https://doi.org/10.1016/j.resconrec.2022.106813

Xi, F., Davis, S. J., Ciais, P., Crawford-Brown, D., Guan, D., Pade, C., Shi, T., Syddall, M., Lv, J., Ji, L., Bing, L., Wang, J., Wei, W., Yang, K. H., Lagerblad, B., Galan, I., Andrade, C., Zhang, Y., & Liu, Z. (2016). Substantial global carbon uptake by cement carbonation. *Nature Geoscience*, *9*(12), 880–883. https://doi.org/10.1038/ngeo2840

Xiao, J. Z., Li, J. B., & Zhang, C. (2006). On relationships between the mechanical properties of recycled aggregate concrete: An overview. *Materials and*

Structures/Materiaux et Constructions, *39*(6), 655–664. https://doi.org/10.1617/s11527-006-9093-0

Xiao, W., Yang, J., Fang, H., Zhuang, J., Ku, Y., & Zhang, X. (2020). Development of an automatic sorting robot for construction and demolition waste. *Clean Technologies and Environmental Policy*, *22*(9), 1829–1841. https://doi.org/10.1007/s10098-020-01922-y

Xiong, Q., Baychev, T. G., & Jivkov, A. P. (2016). Review of pore network modelling of porous media: Experimental characterisations, network constructions and applications to reactive transport. In *Journal of Contaminant Hydrology* (Vol. 192, pp. 101–117). Elsevier B.V. https://doi.org/10.1016/j.jconhyd.2016.07.002

Xu, S., Wang, J., Shou, W., Ngo, T., Sadick, A.-M., & Wang, X. (2021). Computer Vision Techniques in Construction: A Critical Review. *Archives of Computational Methods in Engineering*, *28*(5), 3383–3397. https://doi.org/10.1007/s11831-020-09504-3

Xu, W., Fu, J., Hua, R., & Han, F. (2024). ITZ volume fraction and thermal conductivity of concrete: A unified random packing model for gravels and crushed rocks. *Journal of Building Engineering*, *90*. https://doi.org/10.1016/j.jobe.2024.109457

Yang, J., Du, Q., & Bao, Y. (2011). Concrete with recycled concrete aggregate and crushed clay bricks. *Construction and Building Materials*, *25*(4), 1935–1945. https://doi.org/10.1016/j.conbuildmat.2010.11.063

Yang, M. S., Lai, C. Y., & Lin, C. Y. (2012). A robust em clustering algorithm for Gaussian mixture models. *Pattern Recognition*, *45*(11), 3950–3961. https://doi.org/10.1016/j.patcog.2012.04.031

Yio, M. H. N., Wong, H. S., & Buenfeld, N. R. (2017). Representative elementary volume (REV) of cementitious materials from three-dimensional pore structure analysis. *Cement and Concrete Research*, *102*, 187–202. https://doi.org/10.1016/j.cemconres.2017.09.012

Younis, K. H., & Pilakoutas, K. (2013). Strength prediction model and methods for improving recycled aggregate concrete. *Construction and Building Materials*, *49*, 688–701. https://doi.org/10.1016/j.conbuildmat.2013.09.003

Zandomeneghi, D., Voltolini, M., Mancini, L., Brun, F., Dreossi, D., & Polacci, M. (2010). Quantitative analysis of X-ray microtomography images of geomaterials: Application to volcanic rocks. *Geosphere*, *6*(6), 793–804. https://doi.org/10.1130/GES00561.1

Zhan, B. J., Xuan, D. X., Poon, C. S., & Scrivener, K. L. (2020). Characterization of interfacial transition zone in concrete prepared with carbonated modeled recycled concrete aggregates. *Cement and Concrete Research*, *136*. https://doi.org/10.1016/j.cemconres.2020.106175

Zhang, C., Hu, M., Di Maio, F., Sprecher, B., Yang, X., & Tukker, A. (2022). An overview of the waste hierarchy framework for analyzing the circularity in construction and demolition waste management in Europe. In *Science of the Total Environment* (Vol. 803). Elsevier B.V. https://doi.org/10.1016/j.scitotenv.2021.149892

Zhang, C., Hu, M., Yang, X., Miranda-Xicotencatl, B., Sprecher, B., Di Maio, F., Zhong, X., & Tukker, A. (2020). Upgrading construction and demolition waste management from downcycling to recycling in the Netherlands. *Journal of Cleaner Production*, *266*. https://doi.org/10.1016/j.jclepro.2020.121718

Zhang, C., Ma, L., & Liu, W. (2023). A Machine Learning Approach for Prediction of the Quantity of Mine Waste Rock Drainage in Areas with Spring Freshet. *Minerals*, *13*(3). https://doi.org/10.3390/min13030376

Zhang, H., Xiao, J., Tang, Y., Duan, Z., & Poon, C. sun. (2022). Long-term shrinkage and mechanical properties of fully recycled aggregate concrete: Testing and modelling. *Cement and Concrete Composites*, *130*. https://doi.org/10.1016/j.cemconcomp.2022.104527

Zhang, S., Yuan, Q., Li, Q., Zhang, F., & Xie, Z. (2023). Microstructural characteristics of bonding interfacial transition zone of concrete and magnesium ammonium phosphate cement. *Journal of Building Engineering*, *76*. https://doi.org/10.1016/j.jobe.2023.107208

Zhao, Z., Remond, S., Damidot, D., & Xu, W. (2013). Influence of hardened cement paste content on the water absorption of fine recycled concrete aggregates. *Journal of Sustainable Cement-Based Materials*, *2*(3–4), 186–203. https://doi.org/10.1080/21650373.2013.812942

Zheng, L., Wu, H., Zhang, H., Duan, H., Wang, J., Jiang, W., Dong, B., Liu, G., Zuo, J., & Song, Q. (2017). Characterizing the generation and flows of construction and demolition waste in China. *Construction and Building Materials*, *136*, 405–413. https://doi.org/10.1016/j.conbuildmat.2017.01.055